

# **Modelling the porosity loss in granular iron based permeable reactive barriers**

Dissertation

zur Erlangung des mathematisch-naturwissenschaftlichen

Doktorgrades

“Doctor rerum naturalium“

der Georg-August-Universität Göttingen

im Promotionsprogramm Geoscience

der Georg-August University School of Science (GAUSS)

vorgelegt von

**Huichen Yang**

aus Nanjing, China

Göttingen, 2022

Betreuungsausschuss:

PD Dr. Chicgoua Noubactep

Abteilung Angewandte Geologie, Georg-August-Universität Göttingen

Prof. Dr. Rui Hu

School of Earth Science and Engineering, Hohai University Nanjing

Prof. Dr. Thomas Ptak

Abteilung Angewandte Geologie, Georg-August-Universität Göttingen

Mitglieder der Prüfungskommission:

Referent:

Prof. Dr. Thomas Ptak

Abteilung Angewandte Geologie, Georg-August-Universität Göttingen

Prof. Dr. Rui Hu

School of Earth Science and Engineering, Hohai University Nanjing

Weitere Mitglieder der Prüfungskommission:

PD Dr. Chicgoua Noubactep

Abteilung Angewandte Geologie, Georg-August-Universität Göttingen

Dr. Jannes Kordilla

Abteilung Angewandte Geologie, Georg-August-Universität Göttingen

Prof. Dr. Hans Ruppert

Abteilung Sedimentologie/Umweltgeologie, Georg-August-Universität  
Göttingen

Prof. Dr. Tobias Licha

Institut für Geologie, Mineralogie und Geophysik, Ruhr-Universität Bochum

Tag der mündlichen Prüfung: 09. 11. 2022

## Short summary

The quality of groundwater resources globally has been under serious threat due to their exposure to a broad spectrum of anthropogenic pollutants. Permeable reactive barriers (PRBs) are an innovative technology being used for in-situ remediation of polluted groundwater for the past three decades. Metallic iron ( $\text{Fe}^0$ ) has been presented as the most efficient reactive medium for PRBs, and  $\text{Fe}^0$ -PRBs can eliminate a large variety of both inorganic and organic compounds from aqueous solutions. Although the performance of installed  $\text{Fe}^0$ -PRBs (using granular  $\text{Fe}^0$ ) has been generally satisfactory, there is still uncertainty on how to properly estimate their service life. The long-term porosity loss of a  $\text{Fe}^0$ -PRB is a key factor to determine its service life or its long-term effectiveness. To date, efforts to characterize the long-term porosity loss of  $\text{Fe}^0$ -PRBs have paid little attention to the inherent porosity loss due to the volumetric expansive nature of iron corrosion. The present work is the first attempt to root the estimation of the service life of  $\text{Fe}^0$ -PRBs on the inherent characteristics of  $\text{Fe}^0$  and its corrosion products.

This study presents a review of the  $\text{Fe}^0$ -PRBs literature that reports the porosity loss based on field reports, laboratory column tests, and numerical model studies. Data on reported porosity loss, their estimation methods, and the corresponding geochemical conditions are summarized and analysed. A new mathematical model based on Faraday's Law is established to describe the porosity change caused by iron corrosion products (FeCPs) in a hypothetical  $\text{Fe}^0$ -based PRB through-flowed by deionized water. Moreover, a three-dimensional (3-D) numerical groundwater flow and transport model of a  $\text{Fe}^0$ -PRB was developed to assess how porosity heterogeneity of the barrier medium may affect groundwater flow over time and influence the long-term effectiveness. A 3-D high resolution aquifer outcrop analogue was utilized to implement aquifer heterogeneity. Contaminant plume migration and groundwater residence time were investigated to evaluate the treatment performance of the PRB.

The literature review reveals that the current estimation methods for porosity loss of  $\text{Fe}^0$ -PRBs, which are based on core sample studies and stoichiometric calculations, may significantly underestimate the effect of iron corrosion products. In addition, the Darcy flux has the strongest positive correlation with the long-term porosity loss. The heterogeneity within the aquifer and the barrier should be well studied.

Iron corrosion rates derived from the Faraday's law based mathematical model are up to 7 times larger than the corrosion rate used in previous modeling studies. This suggests that the previous models have underestimated the impact of in-situ generated FeCPs on the porosity

loss. The model simulations demonstrate that volume-expansion by  $\text{Fe}^0$  corrosion products alone can cause to a great extent porosity loss and emphasizes the need for a careful evaluation of the iron corrosion process in individual  $\text{Fe}^0$ -based PRB.

The findings of the 3-D model simulation demonstrate that the heterogeneity of porosity reduction of the barrier medium is an important factor in estimating the long-term performance of a continuous-wall  $\text{Fe}^0$ -PRB. Ignoring the porosity heterogeneity of the barrier medium leads to an underestimation of the by-passing flow by 30%-41% in a ten-year simulation, and of contaminant plume spread over time.

The overall results of this work provide an important contribution and gives practical implications for the future design of  $\text{Fe}^0$ -PRBs. This study developed a new modeling approach to describe the effect of generated iron corrosion products on long-term porosity loss of the PRB system, and a comprehensive 3-D model to simulate the groundwater flow and to assess the long-term effectiveness of the  $\text{Fe}^0$ -PRB. The thesis highlights the potential impact of volume-expansion by  $\text{Fe}^0$  corrosion products, and the porosity heterogeneity of the barrier medium on the longevity estimation of  $\text{Fe}^0$ -PRBs.

## **Acknowledgments**

I would like to express my sincere gratitude to those people, who supported me during the time of my Ph.D.

First and foremost, I record my sincerest gratitude to PD Dr. Chicgoua Noubactep for the excellent research opportunity, the academic supports and the freedom to develop research ideas. I would like to express my profound thanks to PD Dr. Chicgoua Noubactep, Prof. Dr. Rui Hu, Prof. Dr. Thomas Ptak and Prof. Dr. Hans Ruppert for their valuable supervisions, suggestions, and encouragements during the whole period of my Ph.D. study.

I would like to thank my colleagues and friends in the department of Applied Geology at the University of Göttingen, where I spent my last many years for my Master and Ph.D. studies. Among many, I would like to give special thanks to Quan Liu and Pengxiang Qiu for their helps both academically and in daily life.

I would like to express my love to my parents and my girlfriend. I would not have been able to complete my Ph.D. study without their unconditional supports.



# Table of Contents

<b>1. Introduction</b> .....	<b>1</b>
<b>1.1 Background</b> .....	<b>1</b>
1.1.1 Groundwater and its pollution.....	1
1.1.2 Groundwater remediation .....	1
1.1.3 Fe-based permeable reactive barriers (Fe-PRBs) .....	3
<b>1.2 Objectives of the thesis</b> .....	<b>8</b>
<b>1.3 Methodology</b> .....	<b>9</b>
<b>1.4 Structure of the thesis</b> .....	<b>9</b>
<b>Reference</b> .....	<b>10</b>
<b>2. Porosity loss in iron-based permeable reactive barriers: A review</b> .....	<b>19</b>
<b>2.1 Introduction</b> .....	<b>20</b>
<b>2.2 Background</b> .....	<b>22</b>
2.2.1 Contaminant removal mechanism.....	22
2.2.2 Reasons for porosity loss in Fe-based PRBs.....	23
<b>2.3 Field studies of Fe-PRBs</b> .....	<b>24</b>
2.3.1 Porosity loss and estimation methods.....	25
2.3.2 Field Fe-PRBs porosity loss affecting factors .....	28
<b>2.4 Fe-PRB laboratory column tests</b> .....	<b>31</b>
<b>2.5 Numerical model studies on Fe-PRBs</b> .....	<b>37</b>
2.5.1 Simulation methods for porosity loss.....	37
2.5.2 Simulation results of porosity loss .....	39
<b>2.6 Discussion</b> .....	<b>42</b>
<b>2.7 Conclusions and outlook</b> .....	<b>46</b>
<b>References</b> .....	<b>48</b>
<b>3. Modeling porosity loss in Fe-based permeable reactive barriers with Faraday's law</b> .....	<b>57</b>
<b>3.1 Introduction</b> .....	<b>58</b>
<b>3.2 Fundamental of Fe/H<sub>2</sub>O system</b> .....	<b>60</b>
<b>3.3 Modeling porosity loss in Fe-based PRB</b> .....	<b>61</b>
3.3.1 Description of the model based on Faraday's Law .....	61
3.3.2 Calculation of the coefficient of volumetric expansion .....	62
3.3.3 Estimate of growth of corrosion products and passivation .....	63
3.3.4 Estimate of surface area and porosity change .....	64

3.3.5 Model assumptions .....	65
3.3.6 Model calibration.....	65
3.3.7 Model results.....	66
<b>3.4 Implications for the estimation of the durability of Fe-based PRB.....</b>	<b>69</b>
<b>3.5 Comparison of corrosion rates in different studies.....</b>	<b>70</b>
<b>3.6 Considerations on reactive surface area change versus time .....</b>	<b>72</b>
<b>3.7 Comparison of porosity loss in different studies .....</b>	<b>73</b>
<b>3.8. Effect of Fe<sup>0</sup> mixing ratio .....</b>	<b>74</b>
<b>3.9. Conclusion.....</b>	<b>75</b>
<b>Reference: .....</b>	<b>76</b>
<b>4. Numerical case studies on long-term effectiveness of metallic iron based permeable reactive barriers: importance of porosity heterogeneity of the barrier .....</b>	<b>83</b>
<b>4.1 Introduction.....</b>	<b>84</b>
<b>4.2 Numerical modeling and case studies .....</b>	<b>87</b>
4.2.1 Conceptual model .....	87
4.2.2 Numerical modeling approach .....	89
4.2.3 Case studies.....	91
<b>4.3 Results .....</b>	<b>94</b>
4.3.1 Porosity and hydraulic conductivity reduction.....	94
4.3.2 Redistribution of groundwater flow and by-passing.....	97
4.3.3 Contaminant plume migration.....	100
4.3.4 Groundwater residence time .....	101
<b>4.4 Summary and discussion.....</b>	<b>102</b>
<b>4.5 Conclusions .....</b>	<b>105</b>
<b>References.....</b>	<b>106</b>
<b>5. Significance of the study and summary of achieved results.....</b>	<b>111</b>
5.1 Starting point and dynamic literature review .....	111
5.2 Context of the thesis .....	112
5.3 The role of iron corrosion products (FeCPs) .....	112
5.4 Importance of three-dimensional model approach.....	113
5.5 Summary of achieved results.....	114
References.....	116
<b>6. General conclusions and outlook .....</b>	<b>119</b>

## List of Figures

Figure 1.1 The configurations of (a). Funnel and Gate, (b) Continuous Wall PRBs (adapted from ITRC 2005) .....	2
Figure 1.2 Schematic overview of the usage of Fe <sup>0</sup> to transform aqueous trichloroethylene (RCl): (a) a direct reductive transformation by Fe <sup>0</sup> is not possible; (b) only protons (H <sup>+</sup> ) can be reduced by Fe <sup>0</sup> while Fe <sup>2+</sup> , H <sub>2</sub> and some FeCPs (green rusts, magnetite) can act as reducing agents .....	7
Figure 2.1 Contaminant removal mechanisms in Fe <sup>0</sup> -based PRBs. Cont. (Ox) refers to the oxidized form of a contaminant, and Cont. (Red) refers to the corresponding reduced form of a contaminant. ....	23
Figure 2.2 Possible reasons for porosity loss in Fe <sup>0</sup> -based PRBs.....	24
Figure 2.3 Boxplot of reported field Fe <sup>0</sup> -PRBs porosity loss values measured in core samples and estimated from stoichiometric calculations .....	27
Figure 2.4 Scatter plot of Darcy flux versus reported field Fe <sup>0</sup> -PRB porosity loss .....	30
Figure 2.5 Column test porosity loss values and Darcy flux versus column test durations.....	36
Figure 2.6 Boxplots of Fe <sup>0</sup> -PRBs porosity loss values in field reports, column tests, and numerical model simulations .....	43
Figure 3.1 Principle of contaminant removal process in Fe <sup>0</sup> /H <sub>2</sub> O system.....	61
Figure 3.2 Illustration of the reactive zone before (left) and after corrosion of a layer of metallic iron (right) .....	65
Figure 3.3 Corrosion rates versus time (n is the coefficient of passivation) assuming goethite is the corrosion product.....	67
Figure 3.4 Percentage decrease of relative porosity through the formation of goethite over time for different coefficients of passivation (n) .....	68
Figure 3.5 Percentage decrease of relative porosity through the formation of goethite over time for different iron mixing ratios and n = 1 .....	69
Figure 3.6 Percentage decrease of relative porosity over time for different corrosion products (η is the coefficient of volumetric expansion) for n = 1. ....	69
Figure 3.7 Porosity and Fe <sup>0</sup> volume fraction versus time assuming goethite as reaction product .....	70
Figure 3.8 Comparison of corrosion rates with results from Reardon (1995) (n is the coefficient of passivation) assuming goethite as reaction product (a) 0 to 200 days, (b) 200 to 3650 days .....	71
Figure 3.9 Reactive surface area of Fe <sup>0</sup> particles versus time (n is the coefficient of passivation) .....	72
Figure 3.10 Corrosion rate versus reactive surface area with different coefficients of passivation (n).....	73
Figure 4.1 Conceptual model setup. The Fe <sup>0</sup> -PRB is located in the middle of the surrounding	

aquifer and is oriented perpendicular to the main direction of groundwater flow (x axis). The PRB consists of an entrance domain (green area) and an exit domain (blue area). The red block represents the contaminant source. ....	88
Figure 4.2 The 3-D view of the aquifer analogue $\ln(K)$ field. ....	93
Figure 4.3 (a) Relative average porosity reduction and (b) hydraulic conductivity reduction within the PRB entrance domain. The blue line represents the simulation results for case 1 and case 3. The red line represents the simulation results for case 2. The cyan line represents the simulation result for case 4. The average porosity and hydraulic conductivity reductions are identical for case 1 and case 3. ....	95
Figure 4.4 Porosity distribution within the PRB entrance domain and the surrounding aquifer on a portion of a 2D section of the model domain (y-z section, $x=7.25$ m) for all four cases, initial porosity condition and porosity distribution after 5 and 10 years of operation. The red dashed lines represent the border of the PRB. ....	95
Figure 4.5 Porosity and hydraulic conductivity reduction over time within the exit domain.	97
Figure 4.6 Horizontal Darcy flux distribution within the PRB and its surrounding aquifer on a portion of the 2D section of the model domain (y-z section, $x=7.25$ m) for all four cases, initial condition and Darcy flux distribution after 5 and 10 years of operation. The red dotted frame represents the border of the PRB. ....	97
Figure 4.7 Temporal variation of the average Darcy flux within the Fe-PRB during the operation period for the four simulated cases. ....	99
Figure 4.8 Percentage of flow rate loss within Fe-PRB over time for the four simulated cases. .....	99
Figure 4.9 Contaminant plume distribution within the model domain for all cases. The four rows show the simulation results of case 1, case 2, case 3, and case 4, respectively. The first and second columns illustrate the initial contaminant plume and the contaminant plume migration after 10 years of operation, respectively. ....	101
Figure 4.10. The positions of particles on the cross-section of the model domain for case 1 and case 2 within the first 6 days. The first and second columns show the simulation results of case 1 and case 2, respectively. The first row shows the initial positions of the particles. The second, third and fourth rows illustrate the distribution of particles after 2, 4 and 6 days of transport, respectively. Different colours represent different transport velocities of the particles. Since case 1, case 3, and case 4 assumed the same heterogeneous aquifer, the particle tracing results within the first 6 days for three cases are identical. Thus, the results of case 3, and case 4 are not shown. ....	101
Figure 4.11. Average groundwater residence time within the Fe-PRB over time for all cases. .....	102

## List of Tables

Table 1.1 Advantages and limits of the PRB technology .....	3
Table 1.2 Summary of the types of contaminants removed by metallic iron. ....	3
Table 2.1 Summary of field Fe-PRB characteristics, porosity loss and estimation methods based on literature. ....	25
Table 2.2 Summary of iron characteristics, geochemical condition of influent groundwater, porosity loss of field Fe-PRBs, and the correlation coefficients between each factor and porosity loss. ....	29
Table 2.3 Summary of column test settings (including iron characteristics, geochemical condition of influent flow), the reported porosity loss values, and the estimation methods. ....	32
Table 2.4 Summary of solubility constants, and effective rate constants of mineral precipitation within the Fe-PRBs .....	38
Table 2.5 Summary of volumetric expansion coefficients of iron and its main corrosion products (Caré et al., 2013).....	38
Table 2.6 Summary of simulated porosity loss in numerical studies, model characteristics, applied geochemical conditions, and the considered factors for simulated porosity loss including Pearson correlation coefficients of some factors versus porosity losses.....	40
Table 2.7 Experimental corrosion rates of granular iron in Fe-PRBs literature .....	44
Table 2.8 Experimental corrosion rates in mm/y unit.....	44
Table 2.9 Experimental corrosion rates in other research areas.....	45
Table 2.10 Corrosion rates used in Fe-PRBs models.....	45
Table 3.1 Volumetric expansion coefficients of possible corrosion products .....	62
Table 3.2 Porosity loss simulations in different studies.....	73
Table 3.3 Porosity values for different Fe <sup>0</sup> mixing ratios.....	74
Table 4.1 Chemical reactions in a Fe-PRB .....	87
Table 4.2 Simulation strategy.....	92
Table 4.3 General model input parameters .....	93
Table 5.1 Comparison of porosity loss values after 1 year simulation .....	113



# Chapter 1

## 1. Introduction

### 1.1 Background

#### *1.1.1 Groundwater and its pollution*

Groundwater is a limited resource representing a small percentage (0.75%) of the total water on Earth (McLean et al., 2000; Morris et al., 2003). The contribution from groundwater is vital for the life on Earth and for many human sectors such as agriculture, irrigation, urban water supply, industry, electricity production etc. (Thakur et al., 2020). As many as 2.5 billion people depend directly upon aquifers for drinking water supply, and 40% of the world's food is produced by irrigation agriculture which relies on groundwater (Thiruvengkatachari et al., 2008). The GRACE analysis shows that the groundwater extraction rate globally has increased from 312 km<sup>3</sup>/year (1960) to 734 km<sup>3</sup>/year (2000) (Fienen and Arshad, 2016), which indicates our growing dependence on groundwater in past decades. The increased abstraction rate of groundwater has several negative effects such as the lowering of the groundwater table and the subsidence of the land. In many areas, groundwater is highly vulnerable to widespread contamination (harmful elements, toxic organic compounds including biocides, nitrate). There are many reports of serious incidents of groundwater contamination due to accidental spills, or unsatisfactory disposal of industrial chemicals, agricultural practices, mining activities, etc. (Thiruvengkatachari et al., 2008). The quality of groundwater resources globally is under serious threat due to their exposure to a broad spectrum of pollutants.

#### *1.1.2 Groundwater remediation*

Permeable reactive barriers (PRBs) are one of the innovative technologies being used for in-situ remediation of contaminated groundwater (Thakur et al., 2020; Guan et al., 2015; Noubactep, 2015; Totten and Assaf-Anid 2004; Tratnyek et al., 2002; Gillham and O'Hannesin, 1994). The PRB concept is relatively simple and consists of permanent, semi-permanent or replaceable reactive media placed in the subsurface across the flow path of a plume of contaminated groundwater. The contaminated groundwater flows through the reactive media typically under natural gradient, thereby creating a passive treatment system. The contaminants react

with the media leading to either transformation to less harmful compounds or fixation to the reactive materials (Carey et al., 2002; Obiri-Nyarko et al., 2014; Skinner and Schutte, 2006). The PRB is not a barrier to the groundwater, but a barrier to the contaminants. The reactive media of PRBs are designed to be more permeable than the surrounding aquifer so that contaminants can be remediated as groundwater flows through the barrier without significantly altering groundwater hydrogeology (Thiruvengkatachari et al., 2008; McMurthy and Elton, 1985).

The most common design of PRBs used to date are “Funnel and Gate” and “Continuous Wall” reactive barriers (ITRC, 2005; Smith et al., 2003; Thakur et al., 2020). Figure 1.1 illustrates the configurations of two designs. The “Funnel and Gate” PRB comprises impermeable walls, such as sheet piles and slurry walls, which can direct contaminated groundwater to the “Gate” containing reactive media. The “Continuous Wall” PRB transects the contaminant plume with a wall of reactive materials (Smith et al., 2003). The “Continuous Wall” PRBs are favoured in the developing countries with lower GDP due to their lesser installation cost than the “Funnel and Gate” systems (Thakur et al., 2020).

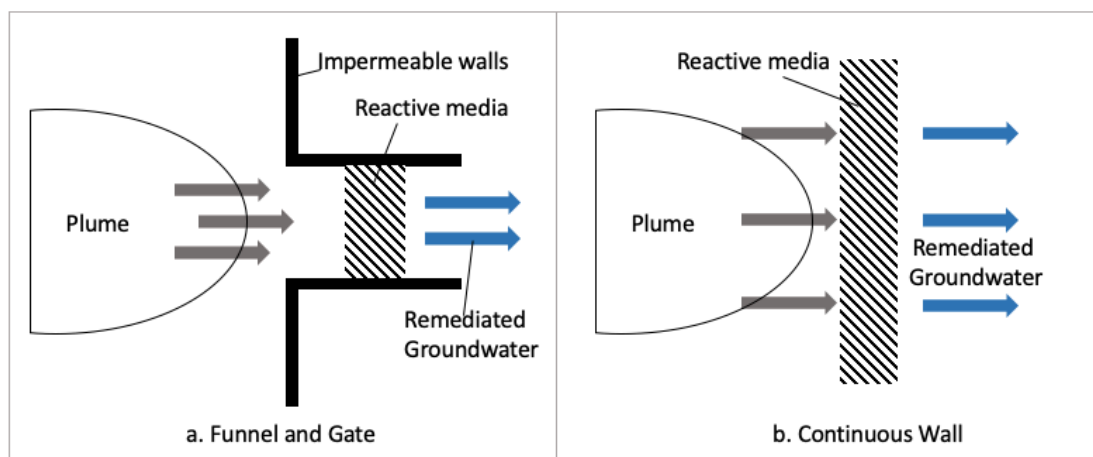


Figure 1.1 The configurations of (a). Funnel and Gate, (b) Continuous Wall PRBs (adapted from ITRC 2005)

The first field PRB studies were conducted at the Canadian Forces Base Borden to remediate groundwater contaminated with chlorinated solvents such as trichloroethylene (TCE), the three isomers of DCE (1,2-cis-, 1,2-trans-, and 1,1,-DCE) and vinyl chloride (VC) (O'Hannesin and Gillham, 1998). After proving to be effective to remediate chlorinated solvents in the groundwater, it has since been followed by a spate of investigations, and the PRB applications were extended to include other contaminants. According to Thakur et al. 2020, there have already been more than fifty review papers and twelve hundred research papers on PRBs (Li et al., 2021; Chen et al., 2019). Table 1.1 summarizes the advantages and limits of the PRB

technology (Carey et al., 2002; Henderson and Demond, 2007; ITRC, 2011; Jirasko, 2012; Obiri-Nyarko et al., 2014; Puls, 2006; Thakur et al., 2020; Warner and Sorel, 2002).

Table 1.1 Advantages and limits of the PRB technology

Advantages
1. Relatively low-cost passive technology, i.e.: low reactive materials cost; low energy cost; little or no disposal costs for treated wastes, and relatively low maintenance and monitoring costs.
2. Allows for treatment of multiple contamination plumes with a wide range of contaminants.
3. The aboveground of the site can be put to profitable use while the treatment is on-going.
4. No cross-media contamination due to the in-situ technique.
5. Only occasional monitoring is required to ensure the proper function of the barrier.
6. No significant disturbance of groundwater hydrogeology.
Limits
1. Only contaminants flowing through the barrier can be treated.
2. Requires proper characterization of the hydrogeological conditions of the aquifer and accurate delineation of the contaminant plume prior to the installation.
3. Restricted to plumes no deeper than 20 m beneath the ground surface.
4. The longevity of barriers remains unknown due to limited field data.
5. Underground structures can present problems in construction and performance.
6. Reactive media may have to be removed or replaced during operation.
7. Long-term monitoring is required.

### 1.1.3 Fe-based permeable reactive barriers (Fe-PRBs)

#### 1.1.3.1 General aspects

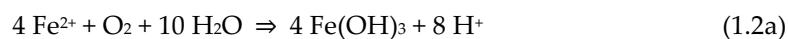
Metallic iron ( $Fe^0$ ), broadly known as zero valent iron (ZVI) is the most frequently used reactive media both in laboratory studies and field applications (Chen et al., 2019; Li et al., 2021; Obiri-Nyarko et al., 2014). Some relevant contaminants reported to be efficiently treated by  $Fe^0$  are summarized in Table 1.2.

Table 1.2 Summary of the types of contaminants removed by metallic iron.

Contaminants	Selected references
Arsenate and arsenite	Neumann et al. (2013); Sun et al. (2014)
Bromate	Xie and Shang (2007)
Chlorinated hydrocarbons (e.g. TCE, PCE, VC and DCE)	O'Hannesin and Gillham (1998); Vogan et al. (1999); ITRC, 2005, 2011; Henderson and Demond (2007); Jeen et al. (2009)
Chromate	Alowitz and Scherer (2002); Feng et al. (2015)
Dyes	Nam and Tratnyek (2000), Konadu-Amoah et al. (2022)

Heavy metals including, but not limited to Cr, Cd, Pd, Cu, U, As	Blowes et al. (1999); Li and Zhang (2007); Ludwig et al. (2009); Scherer et al. (2000); Su and Puls (2001); Su and Puls (2004); Sun et al. (2006); Yang et al. (2007)
Nitrate	Alowitz and Scherer (2002); Wang et al. (2022)
Nitroaromatics	Agrawal and Tratnyek (1996); Keum and Li (2004)
Pesticides (e.g. DDT, DDE and DDD)	Sayles et al. (1997); Yang et al. (2010)
Phenolic compounds	Morales et al. (2002)
Phosphates	Konadu-Amoah et al. (2022)
Selenite	Liang et al. (2013)

The remediation Fe<sup>0</sup>/H<sub>2</sub>O systems have been extensively investigated over last three decades. It is reported that reduction, adsorption, co-precipitation, size-exclusion and microbial activities are the fundamental mechanisms of contaminant removal in Fe<sup>0</sup>-based PRBs (Cundy et al., 2008; Guan et al., 2015; Noubactep, 2015). Since Fe<sup>0</sup> is not stable under oxidizing environmental conditions and the redox couple H<sup>+</sup>/H<sub>2</sub> (E<sub>0</sub>=0.00 V) is higher than that of Fe<sup>II</sup>/Fe<sup>0</sup> (E<sub>0</sub>=-0.44 V) at a<sub>H<sup>+</sup></sub> = 1 (Landolt, 2007), a transfer of electrons from the Fe<sup>0</sup> body (solid state) to the Fe/H<sub>2</sub>O interface occurs whenever a Fe<sup>0</sup> specimen is immersed in an aqueous solution (Hammonds, 1989; Nešić, 2007). Equations 1.1a and 1b show that the oxidative dissolution of Fe<sup>0</sup> by protons (H<sup>+</sup>) from water (H<sub>2</sub>O ⇌ H<sup>+</sup> + OH<sup>-</sup>) forms Fe<sup>2+</sup> and Fe(OH)<sub>2</sub> by increasing the pH. In the presence of dissolved oxygen, Fe<sup>2+</sup> and Fe(OH)<sub>2</sub> can be oxidized to less soluble Fe(OH)<sub>3</sub> (Equations 1.2a,b). Fe(OH)<sub>2</sub> and Fe(OH)<sub>3</sub> are polymerized and further transformed to various oxyhydroxides (Equation 1.3) (Chaves, 2005; Sikora and Macdonald, 2000; Yang et al., 2021). Equation 1.4 summarizes the process of aqueous iron corrosion.



The generated iron (hydro) oxides at the surface of Fe<sup>0</sup> are adsorbents and are able to scavenge all classes of contaminants (Chaves, 2005; Noubactep, 2011; Ghauch, 2015; Guan et al., 2015; Gheju, 2018). Also, the aqueous iron corrosion process induces the generation of reducing

agents, i.e.  $\text{Fe}^{2+}$  and  $\text{H}_2$ , which can be involved into reduction reactions with contaminants in groundwater (Matheson and Tratnyek, 1994; Noubactep, 2015). In addition, the presence of a large reservoir with iron, favorable pH caused by iron corrosion, and hydrogen ( $\text{H}_2$ ) availability support microbial activities (Wilkin et al., 2003). Some microbial activities could transform or degrade some contaminant compounds, which are typically unaffected by the iron (Wilkin et al., 2003).

Longevity of a PRB refers to the ability of the PRB to sustain the functions (i.e. hydraulic capture, residence time of the contaminated groundwater, and reactivity to capture contaminants) over the years and decades following installation. Despite the vast collection of application sites and laboratory experiments, the longer-term performance aspects of  $\text{Fe}^0$ -PRBs are still a source of some uncertainty in planning future applications (ITRC, 2011; Yang et al., 2021; Singh et al., 2022).

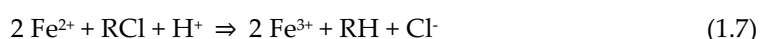
The porosity loss of the barrier is a key concern for accurate evaluation of the  $\text{Fe}^0$ -PRB longevity (Henderson and Demond, 2007; Yang et al., 2021). Reasons of the porosity loss of the  $\text{Fe}^0$ -based PRBs can be mineral precipitation (Phillips et al., 2000), gas formation (Kamolpornwijit and Liang, 2006), and/or biofilm formation (Wilkin et al., 2003).

Under the typical pH range (4.5-8.5) of PRBs operations, a constant aqueous iron corrosion occurs. Although compositions of the iron corrosion products (FeCPs) highly depend on the local chemical conditions (Pantazopoulou and Papoulia, 2001), all the possible corrosion products have much less density compared to the parent metal ( $\text{Fe}^0$ ). This means that iron aqueous corrosion is a volumetric expansive process (Caré et al., 2013; Caré et al., 2008; Yang et al., 2021). Moreover, the aqueous iron corrosion process leads to a reducing condition, and an increase of pH value, which can induce the precipitation of foreign precipitates (e.g. calcite) and mixed precipitates (e.g. calcium and iron carbonate) (Phillips et al., 2000; Phillips et al., 2003). The generated iron corrosion products, and other precipitates would precipitate on the surface of the iron particles, and gradually fill the pore space within the barrier.

Hydrogen is continuously generated during the operation of the  $\text{Fe}^0$ -based PRBs. Although most of the formed hydrogen can percolate out of the system (Kamolpornwijit and Liang, 2006), a portion of generated hydrogen gas bubbles together with other gas species (e.g.  $\text{CO}_2$ ,  $\text{N}_2$ ,  $\text{CH}_4$ ) may be trapped within the porous medium, thus hampering the water flow within the barrier and reducing the permeability of the PRB. Moreover, adequate organic availability and favorable chemical conditions within the PRBs lead to bacteria activities. The microbial activity and consequent biofilm formation in the pore space may be detrimental to the performance of the PRBs by decreasing the porosity of the barrier.

### 1.1.3.2 State-of-the-art knowledge on Fe-PRBs

The Fe<sup>0</sup>-PRB technology was born with the fortuitous observation, that aqueous trichloroethylene (RCl) was eliminated in Fe<sup>0</sup>-based water sampling vessels (Reynolds et al., 1990; Lee et al., 2004). This finding was interpreted as RCl reductive transformation by Fe<sup>0</sup> after Eq. 1.5 (as illustrated in Figure 1.2 (a)). The reductive transformation mechanism was later claimed to be experimentally proved (Matheson and Tratnyek, 1994; Roberts et al., 1996; Weber, 1996). However, two facts should be considered: (i) the reductive transformation concept has never been universally accepted (Jiao et al., 2009; Lavine et al., 2001; Noubactep, 2008; Warren et al., 1995), and (ii) O'Hannessin and Gillham (1998) acknowledged that the adoption of this concept was a "broad consensus". Unfortunately, while introducing the reductive transformation concept, previous works results, which can demonstrate the impossibility of this concept, were overlooked. Two examples will be mentioned here: (i) Whitney (1903) demonstrated that under environmental conditions, only protons (H<sup>+</sup> – Eq. 1a) have access to the Fe<sup>0</sup> surface, which is permanently shielded with an oxide scale, and (ii) Mikhail Khudenko (1991) demonstrated the feasibility of using Cu<sup>2+</sup> cementation by Fe<sup>0</sup> (Eq. 1.6) to generate Fe<sup>2+</sup> for the "destruction of organics" (Eq. 1.7).



A look at the mechanism of oxide scale formation reveals that it cannot be electronically conductive. In fact, the initial scale is very porous and cannot transfer electrons because air and water are not electronically conductive (an electrolyte containing aqueous solution can be ionic conductive). In subsequent stages, available pores are filled with nascent iron corrosion products (FeCPs), but they are never uniform and the oxide scale is a mixture of iron hydroxides and oxides (Nešić, 2007). An oxide scale made up of Fe<sub>3</sub>O<sub>4</sub> alone would have been electronically conductive. However, such an Fe<sub>3</sub>O<sub>4</sub> scale cannot exist under natural conditions of a Fe<sup>0</sup>-PRB. All other FeCPs are at best semi-conductors and cannot conduct electrons from Fe<sup>0</sup> under natural conditions.

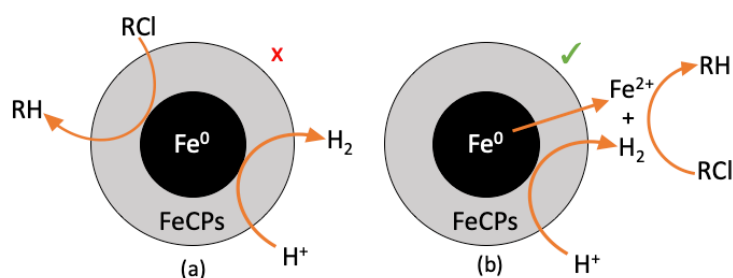


Figure 1.2 Schematic overview of the usage of Fe<sup>0</sup> to transform aqueous trichloroethylene (RCl): (a) a direct reductive transformation by Fe<sup>0</sup> is not possible; (b) only protons (H<sup>+</sup>) can be reduced by Fe<sup>0</sup> while Fe<sup>2+</sup>, H<sub>2</sub> and some FeCPs (green rusts, magnetite) can act as reducing agents

The presentation until now highlights that a reductive transformation by electrons from Fe<sup>0</sup> (Figure 1.2 (a)) is not possible (Whitney, 1903), while Fe<sup>II</sup> species can act as reducing agents (Figure 1.2 (b)). Further reducing agents within the Fe<sup>0</sup>/H<sub>2</sub>O system include green rusts, H<sub>2</sub> (Eq. 1.1a), and magnetite (Fe<sub>3</sub>O<sub>4</sub>). These reducing species have been reported to induce the transformation of several inorganic and organic contaminants under environmental conditions (Charlet et al., 1998; Liger et al., 1999; Myneni et al., 1997; Silvester et al., 2005). In particular, Jiao et al. (2009) investigated the process of CCl<sub>4</sub> reductive transformation in Fe<sup>0</sup>/H<sub>2</sub>O systems and radically ruled out the opportunity of any direct transfer of electrons from Fe<sup>0</sup>. The authors clearly established that CCl<sub>4</sub> is reduced by secondary and tertiary reducing agents. Despite these tangible results and past achievements from the broad corrosion literature (Mikhail Khudenko, 1991; Stratmann and Müller, 1994; Whitney, 1903), researchers are still supporting a consensus from O'Hannesin and Gillham (1998) while mainly arguing that their authors are experts or that the publishing journals are authoritative (Hu et al., 2021, Cao et al., 2022).

### 1.1.3.3 The core of the problem

Numerous laboratory and field scale experiments have been performed over the past three decades to provide fundamental understanding of how Fe<sup>0</sup> PRBs function, so that more sustainable designs can be achieved (Noubactep, 2016; Moraci et al., 2016; Santisukksaem and Das, 2019). As stated in 1.1.3.1, it is generally recognized that the formation of mineral precipitates within the pores of Fe<sup>0</sup> PRBs particles hampers their long-term performance (Bartzas and Komnitsas, 2010; Henderson and Demond, 2007; Li and Benson, 2010). Fe<sup>0</sup> oxidation by water (Eq. 1) generates H<sub>2</sub> gas (Reardon, 1995), which is also reported to reduce the permeability Fe<sup>0</sup> PRBs (Jeen et al., 2012; Zhang and Gillham, 2005). However, it was largely overlooked that FeCPs precipitation and H<sub>2</sub> generation are non-independent processes as both processes result from iron corrosion (Eq. 1) (Jeen et al., 2006; Li et al., 2005). In other words, FeCPs are useful as contaminant scavengers but have negative impacts on the hydraulic

performance of Fe<sup>0</sup> PRBs (Kamolpornwijit et al., 2003; Klausen et al., 2003; Kohn et al., 2005; Phillips et al., 2010). Therefore, designing a sustainable Fe<sup>0</sup> PRB is necessary to find a balance between sustained reactivity (more reactive Fe<sup>0</sup>) and sustained porosity (less expansive system) (Domga et al., 2015).

Investigations regarding the sustainability of Fe<sup>0</sup> PRBs suffers from a lack of systematic approaches (Warner and Sorel 2003, Noubactep, 2007, Noubactep, 2008). As early as 2009, Noubactep purposefully complained the lack of any holistic system's analysis within the Fe<sup>0</sup> research community (Noubactep, 2009). A proper system analysis would have considered the stoichiometry of Eq. 1.1 to realize that H<sub>2</sub> evolution and formation of FeCPs are not independent processes and should be discussed together. On the other hand, there were little efforts to consider the experimental conditions while discussing achieved results (Hu et al., 2021). The most illustrative example is perhaps the demonstration by the research group of Prof. Gillham (Gillham and O'Hannessin, 1994, O'Hannessin and Gillham, 1998) that Fe<sup>0</sup>-PRBs are sustainable remediation systems. The authors used a Fe<sup>0</sup>/sand mixture (22% Fe<sup>0</sup> and 78% sand) in a context where field Fe<sup>0</sup>-PRBs were designed using 100% Fe<sup>0</sup>, with Fe<sup>0</sup>/sand mixtures in pre-treatment zones (Mackenzie et al., 1999, Kenneke and McCutcheon, 2003, Gillham, 2008, Noubactep, 2016). In discussing their results, the authors stated that a higher Fe<sup>0</sup> ratio (> 22%) would have presented better removal efficiency (O'Hannessin and Gillham, 1998). Later on, several researchers found out that systems with less Fe<sup>0</sup> ratios were significantly more efficient than pure Fe<sup>0</sup> systems (Bi et al., 2009, Miyajima, 2012, Miyajima and Noubactep, 2012, Miyajima and Noubactep, 2013). The results of Miyajima and Noubactep (2012, 2013) revealed to the Fe<sup>0</sup> research community that mixing Fe<sup>0</sup> with an inert material is a prerequisite for sustainable Fe<sup>0</sup> filtration systems. Subsequent works by Care et al. (2013) have established the conditions of sustainable Fe<sup>0</sup> filters based on the thermodynamic of the system (Domga et al., 2015, Noubactep, 2016). The missing puzzle in this global effort is the kinetics of the system which is related (i) to the Fe<sup>0</sup> corrosion rate (intrinsic reactivity), but also (ii) to the porous nature of Fe<sup>0</sup> filters.

## 1.2 Objectives of the thesis

Although the porosity loss has been raised as a key factor affecting the longevity of a Fe-PRB (Sarr, 2001), evidences show that the porosity loss of PRBs has not been properly evaluated and studied (Moraci et al., 2016; Noubactep, 2016; Naseri et al., 2017). Many previous researches have mainly focused on the contaminant removal efficiency of the Fe<sup>0</sup> (Guan et al. 2015, Sun et al. 2016, Thakur et al. 2020), and draw less attention on the porosity variation of the barrier (Domga et al., 2015). So far, there is no exact conclusions and methods to delineate patterns of porosity loss of Fe-PRBs in long-term operations (ITRC, 2011). In this work, the primary

objective is to establish a numerical model to properly simulate the porosity loss of a Fe-PRB during long-term operation. For this purpose, a comprehensive understanding of contaminant removal mechanisms of Fe-PRBs and inherent characteristics of iron corrosion is required. The special attention will be put on the volumetric expansive nature of iron corrosion, and the effect of porosity loss caused by the iron corrosion products. The model will also be developed to simulate the change of groundwater flow pattern due to the porosity variation of the Fe-PRBs.

### 1.3 Methodology

Available data reporting porosity loss, their estimation methods, and the corresponding geochemical conditions from Fe<sup>0</sup>-PRBs literature (including field reports, laboratory column tests, and numerical model studies) are summarized and analysed. A new mathematical model based on Faraday's Law is established to describe the porosity change caused by iron corrosion products (FeCPs) in a hypothetical Fe<sup>0</sup>-based PRB through-flowed by deionized water. In addition, a three-dimensional (3-D) numerical groundwater flow and transport model of a Fe<sup>0</sup>-PRB was developed using the finite element software COMSOL to assess how porosity heterogeneity of the barrier medium may affect groundwater flow over time and influence the long-term effectiveness.

### 1.4 Structure of the thesis

The remainder of the thesis is organized as follows. **Chapter 2** reviews the field Fe<sup>0</sup>-PRBs reports, Fe<sup>0</sup>-PRBs column test studies, and numerical model studies on Fe<sup>0</sup>-PRBs, summarizes the reported porosity loss values, their estimation methods, and information on possible affecting factors. The aim of this chapter is to analyze the porosity loss values of different fields, investigate the factors which have significant influence on long-term porosity loss, and compare the simulation results of the models with those from the field.

A mathematical model is presented in **Chapter 3** to simulate the long-term porosity loss of Fe<sup>0</sup>-based PRBs as induced by deionized water. Only the volumetric expansive corrosion of iron contributes to the porosity loss of the system are regarded. Faraday's law was applied to describe the correlation of the amount of corroded iron and the iron corrosion rates. Different coefficients of passivation were taken into account to describe different growth features of corrosion products. Measured porosity results from Luo et al. (2013) were used to calibrate the parameters in that chapter.

In **Chapter 4**, the possible impacts of porosity heterogeneity of a continuous-wall Fe<sup>0</sup>-PRB on their long-term effectiveness was assessed based on case studies. A three-dimensional (3-D) groundwater transport model was developed to simulate the groundwater flow within the Fe<sup>0</sup>-PRB and its surrounding aquifer. A 3-D high resolution aquifer outcrop analogue was adopted

to set the hydraulic properties of the aquifer. Four individual scenarios were studied and the porosity and hydraulic conductivity reduction of the barrier medium, redistribution of groundwater and by-passing flows, contaminant plume evolution, as well as the residence time of groundwater were investigated.

**Chapter 5** summarizes the achieved results (Chapter 2 through Chapter 4), and emphasizes the significance of this work for the further development of the Fe<sup>0</sup> remediation technology.

**Chapter 6** concludes with recommendations for further investigation on the design of sustainable Fe<sup>0</sup> filters.

## Reference

- Agrawal, A., Tratnyek, P.G., 1995. Reduction of nitro aromatic compounds by zero-valent iron metal. *Environmental Science & Technology*, 30(1): 153-160.
- Alowitz, M.J., Scherer, M.M., 2002. Kinetics of nitrate, nitrite, and Cr (VI) reduction by iron metal. *Environmental Science & Technology*, 36(3): 299-306.
- Bartzas, G., Komnitsas, K., 2010. Solid phase studies and geochemical modelling of low-cost permeable reactive barriers. *Journal of Hazardous Materials*, 183(1-3): 301-308
- Blowes, D. et al., 1999. In Situ Permeable Reactive Barrier for the Treatment of Hexavalent Chromium and Trichloroethylene in Ground Water. Volume 2. Performance Monitoring. Report Number: EPA/600/R 99/095 B, 8 Sep 1999, 240.
- Brown, G.E., Jr. et al., 1999. Metal Oxide Surfaces and Their Interactions with Aqueous Solutions and Microbial Organisms. *Chem Rev*, 99(1): 77-174. DOI:10.1021/cr980011z
- Caré, S. et al., 2013. Modeling the permeability loss of metallic iron water filtration systems. *Clean–Soil, Air, Water*, 41(3): 275-282.
- Caré, S., Nguyen, Q.T., l'Hostis, V., Berthaud, Y., 2008. Mechanical properties of the rust layer induced by impressed current method in reinforced mortar. *Cement and Concrete Research*, 38(8-9): 1079-1091
- Carey, M.A., Fretwell, B.A., Mosley, N.G., Smith, J.W.N., 2002. Guidance on the use of permeable reactive barriers for remediating contaminated groundwater. National Groundwater and Contaminated Land Centre Report NC/01/51, UK Environment Agency, Bristol. 140pp.
- Charlet, L., Liger, E., Gerasimo, P., 1998. Decontamination of TCE-and U-rich waters by granular iron: role of sorbed Fe (II). *Journal of Environmental Engineering*, 124(1): 25-30.
- Chaves, L.H.G., 2005. The role of green rust in the environment: a review. *Revista Brasileira de Engenharia Agrícola e Ambiental*, 9(2): 284-288

- Chen, Q. et al., 2019. Past, present, and future of groundwater remediation research: A scientometric analysis. *International journal of environmental research and public health*, 16(20): 3975.
- Cundy, A.B., Hopkinson, L., Whitby, R.L.D., 2008. Use of iron-based technologies in contaminated land and groundwater remediation: A review. *Science of the total environment*, 400(1-3): 42-51.
- Domga, R., Togue-Kamga, F., Noubactep, C., Tchatchueng, J.-B., 2015. Discussing porosity loss of Fe<sup>0</sup> packed water filters at ground level. *Chemical Engineering Journal*, 263: 127-134
- Feng, P. et al., 2015. Weak magnetic field accelerates chromate removal by zero-valent iron. *Journal of Environmental Sciences*, 31: 175-183.
- Fienen, M.N., Arshad, M., 2016. The international scale of the groundwater issue. In: *Integrated Groundwater Management*. Springer, Cham. pp. 21-48.
- Ghauch A. (2015): Iron-based metallic systems: An excellent choice for sustainable water treatment. *Freiberg Online Geosci.* 32, 1–80.
- Gheju M. (2018): Progress in understanding the mechanism of Cr<sup>VI</sup> Removal in Fe<sup>0</sup>-based filtration systems. *Water* 10, 651.
- Gillham, R.W., 2009. Development of the granular iron permeable reactive barrier technology (good science or good fortune), pp. 5-15.
- Gillham, R.W., O'Hannesin, S.F., 1994. Enhanced degradation of halogenated aliphatics by zero-valent iron. *Groundwater*, 32(6): 958-967.
- Gillham, R.W., Vogan, J., Gui, L., Duchene, M., Son, J., 2010. Iron barrier walls for chlorinated solvent remediation, In situ remediation of chlorinated solvent plumes. Springer, pp. 537-571.
- Guan, X. et al., 2015. The limitations of applying zero-valent iron technology in contaminants sequestration and the corresponding countermeasures: the development in zero-valent iron technology in the last two decades (1994–2014). *Water research*, 75: 224-248
- Hammonds, P., 1989. An Introduction to Corrosion and its Prevention, *Comprehensive Chemical Kinetics*. Elsevier, pp. 233-279
- Henderson, A.D., Demond, A.H., 2007. Long-term performance of zero-valent iron permeable reactive barriers: a critical review. *Environmental Engineering Science*, 24(4): 401-423
- Huang, J. et al., 2021. Fe (II) redox chemistry in the environment. *Chemical reviews*, 121(13): 8161-8233.
- IITRC, 2005. Permeable reactive barriers: Lessons learned/new directions. IITRC Washington DC.
- IITRC, 2011. Permeable reactive barrier: Technology update. The Interstate Technology & Regulatory Council (IITRC) Washington, DC, USA.
- Jeen, S.-W., Amos, R.T., Blowes, D.W., 2012. Modeling gas formation and mineral precipitation in a granular iron column. *Environmental science & technology*, 46(12): 6742-6749.

- Jeen, S.-W., Gillham, R.W., Blowes, D.W., 2006. Effects of carbonate precipitates on long-term performance of granular iron for reductive dechlorination of TCE. *Environmental Science & Technology*, 40(20): 6432-6437.
- Jeen, S.-W., Gillham, R.W., Gui, L., 2009. Effects of initial iron corrosion rate on long-term performance of iron permeable reactive barriers: Column experiments and numerical simulation. *Journal of contaminant Hydrology*, 103(3-4): 145-156
- Jeen, S.-W., Mayer, K.U., Gillham, R.W., Blowes, D.W., 2007. Reactive transport modeling of trichloroethene treatment with declining reactivity of iron. *Environmental science & technology*, 41(4): 1432-1438.
- Jiao, Y. et al., 2009. Reductive dechlorination of carbon tetrachloride by zero-valent iron and related iron corrosion. *Applied Catalysis B: Environmental*, 91(1-2): 434-440
- Jirasko, D., 2012. Problems connected with use of permeable Reactive Barriers for groundwater treatment. Construction on brownfields. Czech Technical Univ. Prague.
- Kamolpornwijit, W., Liang, L., 2006. Investigation of gas production and entrapment in granular iron medium. *Journal of contaminant hydrology*, 82(3-4): 338-356.
- Kamolpornwijit, W., Liang, L., Moline, G.R., Hart, T., West, O.R., 2004. Identification and quantification of mineral precipitation in Fe<sup>0</sup> filings from a column study. *Environmental science & technology*, 38(21): 5757-5765
- Kamolpornwijit, W., Liang, L., West, O.R., Moline, G.R., Sullivan, A.B., 2003. Preferential flow path development and its influence on long-term PRB performance: column study. *Journal of contaminant hydrology*, 66(3-4): 161-178
- Kenneke, J.F., McCutcheon, S.C., 2003. Use of pretreatment zones and zero-valent iron for the remediation of chloroalkenes in an oxic aquifer. *Environmental science & technology*, 37(12): 2829-2835
- Keum, Y.-S., Li, Q.X., 2004. Reduction of nitroaromatic pesticides with zero-valent iron. *Chemosphere*, 54(3): 255-263
- Khan, A.H. et al., 2000. Appraisal of a simple arsenic removal method for ground water of Bangladesh. *Journal of Environmental Science & Health Part A*, 35(7): 1021-1041
- Klausen, J. et al., 2003. Longevity of granular iron in groundwater treatment processes: solution composition effects on reduction of organohalides and nitroaromatic compounds. *Environmental Science & Technology*, 37(6): 1208-1218
- Kohn, T., Livi, K.J.T., Roberts, A.L., Vikesland, P.J., 2005. Longevity of granular iron in groundwater treatment processes: corrosion product development. *Environmental Science & Technology*, 39(8): 2867-2879

- Landolt, D., 2007. Corrosion and surface chemistry of metals. CRC press.
- Lavine, B.K., Auslander, G., Ritter, J., 2001. Polarographic studies of zero valent iron as a reductant for remediation of nitroaromatics in the environment. *Microchemical Journal*, 70(2): 69-83.
- Li, L., Benson, C.H., 2010. Evaluation of five strategies to limit the impact of fouling in permeable reactive barriers. *Journal of Hazardous materials*, 181(1-3): 170-180
- Li, L., Benson, C.H., Lawson, E.M., 2005. Impact of mineral fouling on hydraulic behavior of permeable reactive barriers. *Groundwater*, 43(4): 582-596
- Li, X. et al., 2021. Bibliometric analysis of zerovalent iron particles research for environmental remediation from 2000 to 2019. *Environmental Science and Pollution Research*, 28(26): 34200-34210.
- Li, X.-q., Zhang, W.-x., 2007. Sequestration of metal cations with zerovalent iron nanoparticles a study with high resolution X-ray photoelectron spectroscopy (HR-XPS). *The Journal of Physical Chemistry C*, 111(19): 6939-6946.
- Liang, L. et al., 2013. Kinetics and mechanisms of pH-dependent selenite removal by zero valent iron. *Water research*, 47(15): 5846-5855.
- Liger, E., Charlet, L., Van Cappellen, P., 1999. Surface catalysis of uranium (VI) reduction by iron (II). *Geochimica et Cosmochimica Acta*, 63(19-20): 2939-2955
- Ludwig, R.D. et al., 2009. Treatment of arsenic, heavy metals, and acidity using a mixed ZVI-compost PRB. *Environmental Science & Technology*, 43(6): 1970-1976.
- Mackenzie, P.D., Horney, D.P., Sivavec, T.M., 1999. Mineral precipitation and porosity losses in granular iron columns. *Journal of Hazardous Materials*, 68(1-2): 1-17
- Matheson, L.J., Tratnyek, P.G., 1994. Reductive dehalogenation of chlorinated methanes by iron metal. *Environmental science & technology*, 28(12): 2045-2053
- McLean, W., Jankowski, J., Lavitt, N., 2000. Groundwater quality and sustainability in an alluvial aquifer, Australia, pp. 567-573
- Mikhail Khudenko, B., 1991. Feasibility evaluation of a novel method for destruction of organics. *Water Science and Technology*, 23(10-12): 1873-1881.
- Miyajima, K., 2012. Optimizing the Design of Metallic Iron Filters for Water Treatment. *FOG-Freiberg Online Geoscience*, 32
- Miyajima, K., Noubactep, C., 2012. Effects of mixing granular iron with sand on the efficiency of methylene blue discoloration. *Chemical Engineering Journal*, 200: 433-438.
- Miyajima, K., Noubactep, C., 2013. Impact of Fe<sub>0</sub> amendment on methylene blue discoloration by sand columns. *Chemical Engineering Journal*, 217: 314-320.
- Moraci, N., Ielo, D., Bilardi, S., Calabro, P.S., 2016. Modelling long-term hydraulic conductivity behaviour

- of zero valent iron column tests for permeable reactive barrier design. *Canadian Geotechnical Journal*, 53(6): 946-961
- Morales, J., Hutcheson, R., Cheng, I.F., 2002. Dechlorination of chlorinated phenols by catalyzed and uncatalyzed Fe (0) and Mg (0) particles. *Journal of Hazardous materials*, 90(1): 97-108
- Morris, B.L. et al., 2003. Groundwater and its susceptibility to degradation: a global assessment of the problem and options for management.
- Mwakabona, H.T., Ndé-Tchoupé, A.I., Njau, K.N., Noubactep, C., Wydra, K.D., 2017. Metallic iron for safe drinking water provision: Considering a lost knowledge. *Water research*, 117: 127-142
- Myneni, S.C.B., Tokunaga, T.K., Brown Jr, G.E., 1997. Abiotic selenium redox transformations in the presence of Fe (II, III) oxides. *Science*, 278(5340): 1106-1109
- Nam, S., Tratnyek, P.G., 2000. Reduction of azo dyes with zero-valent iron. *Water Research*, 34(6): 1837-1845.
- Naseri E., Ndé-Tchoupé A.I., Mwakabona H.T., Nanseu-Njiki C.P., Noubactep C., Njau K.N., Wydra K.D. (2017): Making Fe<sup>0</sup>-based filters a universal solution for safe drinking water provision. *Sustainability* 9, 1224.
- Nešić, S., 2007. Key issues related to modelling of internal corrosion of oil and gas pipelines—A review. *Corrosion science*, 49(12): 4308-4338
- Neumann, A. et al., 2013. Arsenic removal with composite iron matrix filters in Bangladesh: a field and laboratory study. *Environmental science & technology*, 47(9): 4544-4554
- Noubactep, C., 2008. A critical review on the process of contaminant removal in Fe<sup>0</sup>-H<sub>2</sub>O systems. *Environ Technol*, 29(8): 909-20. DOI:10.1080/09593330802131602
- Noubactep, C., 2009. An analysis of the evolution of reactive species in Fe<sup>0</sup>/H<sub>2</sub>O systems. *Journal of Hazardous materials*, 168(2-3): 1626-1631.
- Noubactep, C., 2010. The suitability of metallic iron for environmental remediation. *Environmental Progress & Sustainable Energy*, 29(3): 286-291.
- Noubactep C. (2011): Metallic iron for safe drinking water production. *Freiberg Online Geosci.* 27, 1–38.
- Noubactep, C., 2016. Predicting the hydraulic conductivity of metallic iron filters: Modeling gone astray. *Water*, 8(4): 162
- Noubactep, C., Caré, S., 2010a. Dimensioning metallic iron beds for efficient contaminant removal. *Chemical Engineering Journal*, 163(3): 454-460
- Noubactep, C., Caré, S., 2010b. Enhancing sustainability of household water filters by mixing metallic iron with porous materials. *Chemical Engineering Journal*, 162(2): 635-642
- Noubactep, C., Caré, S., Btatteu K, B.D., Nanseu-Njiki, C.P., 2012. Enhancing the sustainability of

- household Fe<sup>0</sup>/sand filters by using bimetallics and MnO<sub>2</sub>. *Clean–Soil, Air, Water*, 40(1): 100-109
- O'Hannesin, S.F., Gillham, R.W., 1998. Long-term performance of an in situ "iron wall" for remediation of VOCs. *Groundwater*, 36(1): 164-170
- Obiri-Nyarko, F., Grajales-Mesa, S.J., Malina, G., 2014. An overview of permeable reactive barriers for in situ sustainable groundwater remediation. *Chemosphere*, 111: 243-259
- Pantazopoulou, S.J., Papoulia, K.D., 2001. Modeling cover-cracking due to reinforcement corrosion in RC structures. *Journal of engineering mechanics*, 127(4): 342-351.
- Phillips, D.H. et al., 2000. Performance evaluation of a zerovalent iron reactive barrier: mineralogical characteristics. *Environmental Science & Technology*, 34(19): 4169-4176.
- Phillips, D.H. et al., 2010. Ten year performance evaluation of a field-scale zero-valent iron permeable reactive barrier installed to remediate trichloroethene contaminated groundwater. *Environmental Science & Technology*, 44(10): 3861-3869.
- Phillips, D.H., Watson, D.B., Roh, Y., Gu, B., 2003. Mineralogical characteristics and transformations during long-term operation of a zerovalent iron reactive barrier. *Journal of Environmental Quality*, 32(6): 2033-2045
- Pilling, N.B., 1923. The oxidation of metals at high temperature. *J. Inst. Met.*, 29: 529-582.
- Puls, R.W., 2006. Long-term performance of permeable reactive barriers: lessons learned on design, contaminant treatment, longevity, performance monitoring and cost-an overview. *Soil and Water Pollution Monitoring, Protection and Remediation*: 221-229.
- Reardon, E.J., 1995. Anaerobic corrosion of granular iron: Measurement and interpretation of hydrogen evolution rates. *Environmental science & technology*, 29(12): 2936-2945.
- Reynolds, G.W., Hoff, J.T., Gillham, R.W., 1990. Sampling bias caused by materials used to monitor halocarbons in groundwater. *Environmental Science & Technology*, 24(1): 135-142.
- Richardson, J.P., Nicklow, J.W., 2002. In situ permeable reactive barriers for groundwater contamination. *Soil and Sediment Contamination*, 11(2): 241-268
- Roberts, A.L., Totten, L.A., Arnold, W.A., Burris, D.R., Campbell, T.J., 1996. Reductive elimination of chlorinated ethylenes by zero-valent metals. *Environmental Science & Technology*, 30(8): 2654-2659.
- Santisukkasaem, U., Das, D.B., 2019. A non-dimensional analysis of permeability loss in zero-valent iron permeable reactive barrier (PRB). *Transport in Porous Media*, 126(1): 139-159
- Sarr, D., 2001. Zero-Valent-Iron Permeable Reactive Barriers- How Long Will They Last? *Remediation*, 11(2): 1-18

- Sayles, G.D., You, G., Wang, M., Kupferle, M.J., 1997. DDT, DDD, and DDE dechlorination by zero-valent iron. *Environmental Science & Technology*, 31(12): 3448-3454.
- Scherer, M.M., Richter, S., Valentine, R.L., Alvarez, P.J.J., 2000. Chemistry and microbiology of permeable reactive barriers for in situ groundwater clean up. *Critical reviews in microbiology*, 26(4): 221-264
- Sikora, E., Macdonald, D.D., 2000. The passivity of iron in the presence of ethylenediaminetetraacetic acid I. General electrochemical behavior. *Journal of the Electrochemical Society*, 147(11): 4087
- Silvester, E. et al., 2005. Redox potential measurements and Mössbauer spectrometry of FeII adsorbed onto FeIII (oxyhydr) oxides. *Geochimica et Cosmochimica Acta*, 69(20): 4801-4815
- Skinner, S.J.W., Schutte, C.F., 2006. The feasibility of a permeable reactive barrier to treat acidic sulphate- and nitrate-contaminated groundwater. *Water Sa*, 32(2): 129-136.
- Smith, J.W.N., Boshoff, G., Bone, B.D., 2003. Good practice guidance on permeable reactive barriers for remediating polluted groundwater, and a review of their use in the UK. *Land Contamination & Reclamation*, 11(4): 411-418.
- Stefanoni, M., Angst, U.M., Elsener, B., 2018. Electrochemistry and capillary condensation theory reveal the mechanism of corrosion in dense porous media. *Scientific reports*, 8(1): 1-10.
- Stratmann, M., Müller, J., 1994. The mechanism of the oxygen reduction on rust-covered metal substrates. *Corrosion Science*, 36(2): 327-359
- Su, C., Puls, R.W., 2001. Arsenate and arsenite removal by zerovalent iron: kinetics, redox transformation, and implications for in situ groundwater remediation. *Environmental science & technology*, 35(7): 1487-1492.
- Su, C., Puls, R.W., 2004. Significance of iron (II, III) hydroxycarbonate green rust in arsenic remediation using zerovalent iron in laboratory column tests. *Environmental science & technology*, 38(19): 5224-5231.
- Sun, H., Wang, L., Zhang, R., Sui, J., Xu, G., 2006. Treatment of groundwater polluted by arsenic compounds by zero valent iron. *Journal of Hazardous Materials*, 129(1-3): 297-303.
- Sun, Y. et al., 2014. Effect of weak magnetic field on arsenate and arsenite removal from water by zerovalent iron: an XAFS investigation. *Environmental science & technology*, 48(12): 6850-6858.
- Thakur, A.K., Vithanage, M., Das, D.B., Kumar, M., 2020. A review on design, material selection, mechanism, and modelling of permeable reactive barrier for community-scale groundwater treatment. *Environmental Technology & Innovation*, 19: 2352-1864.
- Thiruvengkatahari, R., Vigneswaran, S., Naidu, R., 2008. Permeable reactive barrier for groundwater remediation. *Journal of Industrial and Engineering Chemistry*, 14(2): 145-156.

- Totten, L.A., Assaf-Anid, N.M., 2004. Abiotic dehalogenation by metals, Dehalogenation. Springer, pp. 261-287.
- Tratnyek, P.G., Miehr, R., Bandstra, J.Z., 2002. Kinetics of reduction of TNT by iron metal. IAHS PUBLICATION: 427-434
- Usepa, U., 2002. Field applications of in situ remediation technologies: Permeable reactive barriers. Technology Innovation Office, Office of Solid Waste and Emergency Response ....
- Wang, Q. et al., 2022. In situ remediation of Cr (VI) contaminated groundwater by ZVI-PRB and the corresponding indigenous microbial community responses: a field-scale study. Science of The Total Environment, 805: 150260.
- Warner, S.D., Sorel, D., 2002. Chlorinated solvent and DNAPL remediation. American Chemical Society, Washington, DC.
- Warner, S.D., Sorel, D., 2003. Ten years of permeable reactive barriers: Lessons learned and future expectations. ACS Publications.
- Warren, K.D., Arnold, R.G., Bishop, T.L., Lindholm, L.C., Betterton, E.A., 1995. Kinetics and mechanism of reductive dehalogenation of carbon tetrachloride using zero-valence metals. Journal of hazardous materials, 41(2-3): 217-227.
- Weber, E.J., 1996. Iron-mediated reductive transformations: investigation of reaction mechanism. Environmental Science & Technology, 30(2): 716-719
- Whitney, W.R., 1903. The Corrosion of Iron. Journal of the American Chemical Society, 25(4): 394-406.
- Wilkin, R.T. et al., 2018. Geochemical and isotope study of trichloroethene degradation in a zero-valent iron permeable reactive barrier: A twenty-two-year performance evaluation. Environmental science & technology, 53(1): 296-306
- Wilkin, R.T., Puls, R.W., Sewell, G.W., 2003. Long-term performance of permeable reactive barriers using zero-valent iron: geochemical and microbiological effects. Ground Water, 41(4): 493
- Wilkin, R.T., Su, C., Ford, R.G., Paul, C.J., 2005. Chromium-removal processes during groundwater remediation by a zerovalent iron permeable reactive barrier. Environmental science & technology, 39(12): 4599-4605
- Xie, L., Shang, C., 2007. The effects of operational parameters and common anions on the reactivity of zero-valent iron in bromate reduction. Chemosphere, 66(9): 1652-1659.
- Yang, H., Hu, R., Ruppert, H., Noubactep, C., 2021. Modeling porosity loss in Fe<sup>0</sup>-based permeable reactive barriers with Faraday's law. Scientific Reports, 11(1): 1-13.
- Yang, J.E., Kim, J.S., Ok, Y.S., Yoo, K.R., 2007. Mechanistic evidence and efficiency of the Cr (VI) reduction in water by different sources of zerovalent irons. Water Science and Technology, 55(1-2): 197-202.

- Yang, S.-C. et al., 2010. Application of zerovalent iron (Fe<sup>0</sup>) to enhance degradation of HCHs and DDX in soil from a former organochlorine pesticides manufacturing plant. *Chemosphere*, 79(7): 727-732.
- Zhang, Y., Gillham, R.W., 2005. Effects of gas generation and precipitates on performance of Fe PRBs. *Groundwater*, 43(1): 113-121.

## Chapter 2

### 2. Porosity loss in iron-based permeable reactive barriers: A review

Huichen Yang<sup>1\*</sup>, Ran Tao<sup>1</sup>, Rui Hu<sup>2</sup>, Quan Liu<sup>1</sup>, Reza Taherdangkoo<sup>3</sup>, Yuxi Liu<sup>4</sup>, Hans Ruppert<sup>5</sup>, and Chicgoua Noubactep<sup>1,6,7,8</sup>

<sup>1</sup> Angewandte Geologie, Universität Göttingen, Goldschmidtstraße 3, D - 37077 Göttingen, Germany; huichen.yang@geo.uni-goettingen.de (H.Y), ran.tao@geo.uni-goettingen.de (T.R), quan.liu@geo.uni-goettingen.de (Q.L), cnoubac@gwdg.de (C.N)

<sup>2</sup> School of Earth Science and Engineering, Hohai University, Fo Cheng Xi Road 8, 211100 Nanjing, P.R. China; rhu@hhu.edu.cn (R.H)

<sup>3</sup> TU Bergakademie Freiberg, Institute of Geotechnics, Gustav-Zeuner-Str. 1, 09599, Freiberg, Germany; reza.Taherdangkoo@ifgt.tu-freiberg.de (R.T)

<sup>4</sup> Institut für Mathematische Stochastik, Universität Göttingen, Goldschmidtstraße 7, D - 37077 Göttingen, Germany; yuxi.liu@stud.uni-goettingen.de (Y.L)

<sup>5</sup> Department of Sedimentology & Environmental Geology, University of Göttingen, Goldschmidtstraße 3, Göttingen D-37077, Germany; hruppert@gwdg.de (H.R)

<sup>6</sup> Centre for Modern Indian Studies (CeMIS), Universität Göttingen, Waldweg 26, D - 37073 Göttingen, Germany; cnoubac@gwdg.de (C.N.)

<sup>7</sup> School of Materials, Energy, Water and Environmental Sciences, Nelson Mandela African Institution of Science and Technology (NM-AIST), Arusha 23311, Tanzania

<sup>8</sup> Faculty of Science and Technology, Campus of Banekane, Université des Montagnes, P.O. Box 208 Bangangté, Cameroon

#### Abstract

A more accurate assessment of the longevity of granular iron permeable reactive barriers (Fe<sup>0</sup>-PRBs) is a prerequisite to establish its acceptance as a sustainable technology for groundwater remediation. Porosity loss is inherent to Fe<sup>0</sup>-PRBs and the characterization of its interplay is fundamental for the design of PRB systems. This study presents a review of the Fe<sup>0</sup>-PRBs literature that reports the porosity loss, including field reports, laboratory column tests, and numerical model studies. Data on reported porosity loss, their estimation methods, and the corresponding geochemical conditions are summarized and analysed. The results reveal that the current estimation methods for porosity loss of Fe<sup>0</sup>-PRBs, which are based on core sample studies and stoichiometric calculations, may significantly underestimate the actual porosity loss. The results of laboratory column tests are difficult to compare with the field cases, especially for short-term tests using high Darcy fluxes. The small iron corrosion rate applied in numerical model studies may cause an underestimation of the amount of generated iron corrosion products, and an improper prediction of Fe<sup>0</sup>-PRBs longevity. The Darcy flux has the strongest correlation with the long-term porosity loss. The heterogeneity of the aquifer and of the barrier should be well studied to design and construct a long lasting Fe<sup>0</sup>-PRB.

Keywords: Groundwater remediation, Numerical model, Permeable reactive barriers, Porosity loss, Zero-valent iron.

## 2.1 Introduction

The use of metallic iron ( $\text{Fe}^0$ ) for groundwater remediation in subsurface permeable reactive barriers (PRBs) has attracted much attention during the past three decades (Blowes et al., 1999; Guan et al., 2019; Obiri-Nyarko et al., 2014).  $\text{Fe}^0$ -PRBs can remove various contaminants from groundwater (Fu et al., 2014; Sun et al., 2016) and has gained considerable acceptance as an effective and economically-feasible technology for groundwater remediation (Henderson and Demond, 2007). However, since  $\text{Fe}^0$  consumption,  $\text{Fe}^{2+}/\text{Fe}^{3+}$  release, and hydroxides/oxides precipitation inevitably occur in the PRBs during the contaminant removal processes (Hu et al., 2020), the remediation effectiveness of a  $\text{Fe}^0$ -PRB alters during the operation (Phillips et al., 2000; Phillips et al., 2003; Wilkin et al., 2018; Wilkin et al., 2002; Wilkin et al., 2003; Yang et al., 2021). Despite a large number of studies and field applications on  $\text{Fe}^0$ -PRB technology, questions still remain on the  $\text{Fe}^0$ -PRB longevity prediction (Henderson and Demond, 2007; ITRC, 2011; Li et al., 2006).

The reactivity and porosity loss of a barrier are two main concerns for accurate evaluation of the  $\text{Fe}^0$ -PRB longevity (Henderson and Demond, 2007; Yang et al., 2021). The reactivity loss of  $\text{Fe}^0$ -PRBs is well studied by previous researchers (Guan et al., 2015; Jeen, 2018; Jeen et al., 2012; Jeen et al., 2007), and is generally considered to be caused by iron corrosion products and precipitates, which can form on the surface of iron particles, compromise the electron transfer from the iron body, and decrease the contaminants removal (Jeen et al., 2007). There is a controversial discussion on whether the iron body ( $\text{Fe}^0$ ) plays any role in the process of contaminant reductive transformation in the  $\text{Fe}^0/\text{H}_2\text{O}$  systems (Hu, 2020; Konadu-Amoah et al., 2022; Noubactep, 2008). This aspect is not addressed herein since the focus of this study is on porosity loss of the  $\text{Fe}^0$ -PRBs. Nonetheless, Furukawa et al. (2002) and Wilkin et al. (2005) revealed that the development of iron corrosion products (FeCPs) within the  $\text{Fe}^0$ -PRBs may in fact enhance the removal efficiency for contaminants. This point is supported by the experiment results of Schreier and Reinhard (1994) and Hao et al. (2005), which showed a lag time between the start of experiments and reductive transformation of the contaminant species. This lag time corresponds to the quantitative generation of FeCPs. Therefore, as long as FeCPs are continuously generated by iron corrosion, reactivity loss may not be a threatening concern for the long-term performance of in-situ  $\text{Fe}^0$ -PRBs. This view is also proved by some field observations (ITRC, 2011; Johnson et al., 2005; Wang et al., 2022; Wilkin et al., 2018). Wilkin et al. (2018) reported that a  $\text{Fe}^0$ -PRB at Elizabeth City (installed in 1996) can continue to remove chlorinated hydrocarbons from groundwater after 22 years of operation.

In addition, the porosity loss of a Fe<sup>0</sup>-PRB can change the hydraulic properties of the barrier medium, and results in the reorientation of groundwater flow (Li et al., 2006; Yang et al., 2021). Johnsen et al. (2005) reported that a portion of groundwater was being diverted beneath the Fe<sup>0</sup>-PRB at the Cornhusker Army Ammunition Plant due to the reducing porosity of the barrier after 20 months of operation. Phillips et al. (2010) conducted a multi-tracer test in the Monkstown Fe<sup>0</sup>-PRB field and pointed out that some preferential flows have formed within the barrier and bypass flow have occurred around the PRB because of the decreasing hydraulic conductivity of the barrier. The preferential flows can reduce the residence time of the groundwater within the PRB, and cause incomplete contaminants removal. Also, the bypass flow caused by porosity loss around a PRB will deteriorate the effectiveness in groundwater remediation, and threatens the longevity of the PRB. Therefore, the porosity loss of the barrier plays a crucial role in evaluating the longevity of a Fe<sup>0</sup>-PRB.

Although the porosity loss has been raised as a key factor affecting the longevity of a Fe<sup>0</sup>-PRB (Sarr, 2001), the porosity loss of PRBs has not been properly evaluated and studied (Moraci et al., 2016; Santisukkasaem and Das, 2019; Yang et al., 2021). There have been more than 10 review papers on Fe<sup>0</sup>-PRBs published during the past two decades. Henderson and Demond (2007) have conducted a detailed review of the parameters contributing to field Fe<sup>0</sup>-PRBs failures, and found that the most common causes of PRB failures are design flaws (i.e. improper hydraulic characterisation of the surrounding aquifer) rather than reactivity loss or porosity loss. Fu et al. (2014) have reviewed the removal efficiencies of various contaminants by zero-valent-iron (ZVI), and discussed the reaction mechanisms of different contaminant species. Guan et al. (2015) have summarized the contaminant removal processes of ZVI, and noted that the major limitations of ZVI is the reducing contaminant removal efficiency due to its intrinsic passive layer and precipitation of metal hydroxides and metal carbonates. Sun et al. (2016) have carried out a comprehensive analysis of the influences of iron characteristics, operating conditions and solution chemistry on contaminants removal by ZVI, and demonstrated that all factors could significantly affect ZVI performance toward contaminants removal. Nonetheless, many previous researches have mainly focused on the contaminant removal efficiency of the Fe<sup>0</sup>, and draw less attention on the changes of the porosity within the barrier. So far, there are no exact conclusions and methods to delineate patterns of porosity loss of Fe<sup>0</sup>-PRBs in long-term operations (ITRC, 2011; Noubactep, 2016a; Yang et al., 2021). Therefore, in order to establish Fe<sup>0</sup>-PRBs as a sustainable technology and to achieve a more accurate assessment of Fe<sup>0</sup>-PRB longevity, it is necessary to review existing studies on porosity loss in Fe<sup>0</sup>-PRBs. This study reviews the field Fe<sup>0</sup>-PRBs reports, Fe<sup>0</sup>-PRBs column test studies, and numerical model

studies on Fe<sup>0</sup>-PRBs, summarizes the reported porosity loss values, their estimation methods, and information on possible affecting factors. The aim of this review is to analyse the porosity loss values of different fields, to investigate the factors which have great influence on long-term porosity loss, and to compare the simulation results of the models with those in the field.

## 2.2 Background

### 2.2.1 Contaminant removal mechanism

It is well established that reduction, adsorption, co-precipitation, size-exclusion and microbial activities are the fundamental mechanisms of contaminant removal in Fe<sup>0</sup>-based PRBs (Cundy et al., 2008; Guan et al., 2015; Konadu-Amoah et al., 2022). The contaminant removal mechanisms in Fe<sup>0</sup>/H<sub>2</sub>O system are illustrated in Figure 2.1.

The generation of iron (hydro)oxides is the root cause of contaminant remediation (Ghauch, 2015; Gheju, 2011; Guan et al., 2015; Hu et al., 2020). Since Fe<sup>0</sup> is not stable under environmental conditions, and the voltage of the redox couple H<sup>+</sup>/H<sub>2</sub> (E<sub>0</sub>=0.00 V) is higher than that of Fe<sup>II</sup>/Fe<sup>0</sup> (E<sub>0</sub>=-0.44 V) (Landolt, 2007), the transfer of electrons from the Fe<sup>0</sup> body (solid state) to the Fe/H<sub>2</sub>O interface occurs when Fe<sup>0</sup> is immersed in an aqueous solution (Hammonds, 1989; Nešić, 2007). The oxidative dissolution of Fe<sup>0</sup> by protons(H<sup>+</sup>) from water is shown in the red dashed box in Figure 1. In the presence of oxidants (e.g. O<sub>2</sub>), the generated Fe<sup>2+</sup> and Fe(OH)<sub>2</sub> (Fe<sup>2+</sup>+2OH<sup>-</sup>⇌Fe(OH)<sub>2</sub>) can be oxidized to lower soluble Fe(OH)<sub>3</sub>. Fe(OH)<sub>2</sub> and Fe(OH)<sub>3</sub> are polymerized and can further transform into various (hydro)oxides (Chaves, 2005; Sikora and Macdonald, 2000; Yang et al., 2021) (green dashed box in Figure 1). The generated iron (hydro)oxides at the surface of Fe<sup>0</sup> are adsorbents, and are able to scavenge contaminants (Chaves, 2005; Guan et al., 2015).

Also, the aqueous iron corrosion process induces the generation of reducing agents, i.e. Fe<sup>2+</sup> and H<sub>2</sub>, which can get being involved into reduction reactions with contaminants in groundwater. In addition, the presence of a large reservoir with iron, favorable pH caused by iron corrosion, and hydrogen availability can support the activity of iron-reducing, sulfate-reducing, and methanogenic bacteria (Tsinde, 2021; Wilkin et al., 2003). Some microbial activities could transform or degrade the contaminant compounds, which are typically unaffected by the iron (Wilkin et al., 2003).

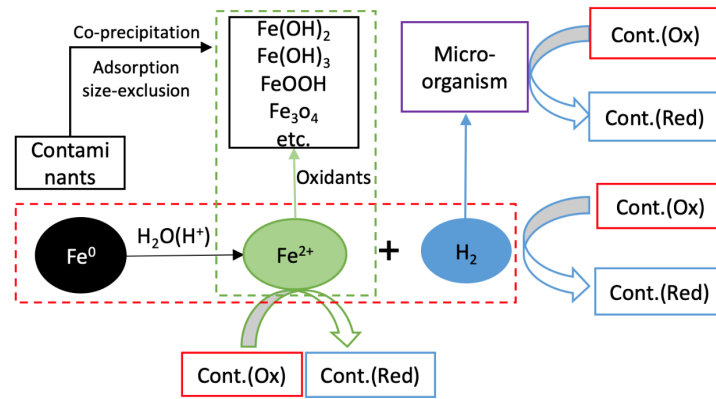


Figure 2.1 Contaminant removal mechanisms in Fe-based PRBs. Cont. (Ox) refers to the oxidized form of a contaminant, and Cont. (Red) refers to the corresponding reduced form of a contaminant.

### 2.2.2 Reasons for porosity loss in Fe-based PRBs

Laboratory column tests (Kamolpornwijit et al., 2004; Kamolpornwijit et al., 2003) and field reports (Phillips et al., 2000; Phillips et al., 2003; Wilkin et al., 2018; Wilkin et al., 2005) of  $Fe^0$ -based PRBs have shown the evidence of clogging of the pore space in the iron zone over time, which can reduce the porosity and the hydraulic conductivity of the barrier medium. The reasons of the porosity loss of the  $Fe^0$ -based PRBs could be mineral precipitation (Phillips et al., 2000), gas formation (Kamolpornwijit and Liang, 2006), and biofilm formation (Wilkin et al., 2003), as depicted in Figure 2.2.

Under typical pH range (4.5-8.5) of PRBs operation, a constant aqueous iron corrosion occurs. Although compositions of the iron corrosion products (FeCPs) highly depend on the local chemical conditions (Pantazopoulou and Papoulia, 2001), all the possible corrosion products have much less density compared to the parent metal ( $Fe^0$ ) (Caré et al., 2008; Domga et al., 2015). This means that iron aqueous corrosion is a volumetric expansive process (Caré et al., 2013; Caré et al., 2008; Yang et al., 2021). Moreover, the aqueous iron corrosion process leads to a reducing condition, and an increase of the pH value, which can induce the precipitation of other precipitates (e.g. calcite) and mixed precipitates (e.g. calcium and iron carbonate) (Phillips et al., 2000; Phillips et al., 2003). The generated iron corrosion products, and other precipitates are located on the surface of the iron particles, and gradually fill the pore space within the barrier.

Hydrogen, as another iron corrosion product, is continuously generated during the operation of the  $Fe^0$ -based PRBs. Although most of the formed hydrogen can percolate out of the system (Kamolpornwijit and Liang, 2006), a portion of generated hydrogen gas bubbles together with

other gas species (e.g. CO<sub>2</sub>, N<sub>2</sub>, CH<sub>4</sub>) may be trapped within the porous medium, and thus prevent water flow within the barrier by reducing the permeability of the PRB.

Moreover, adequate organic availability and favorable chemical conditions within the PRBs lead to bacteria activities. The microbial activity and consequent biofilm formation in the pore space may be detrimental to the performance of the PRBs by decreasing the porosity of the barrier.

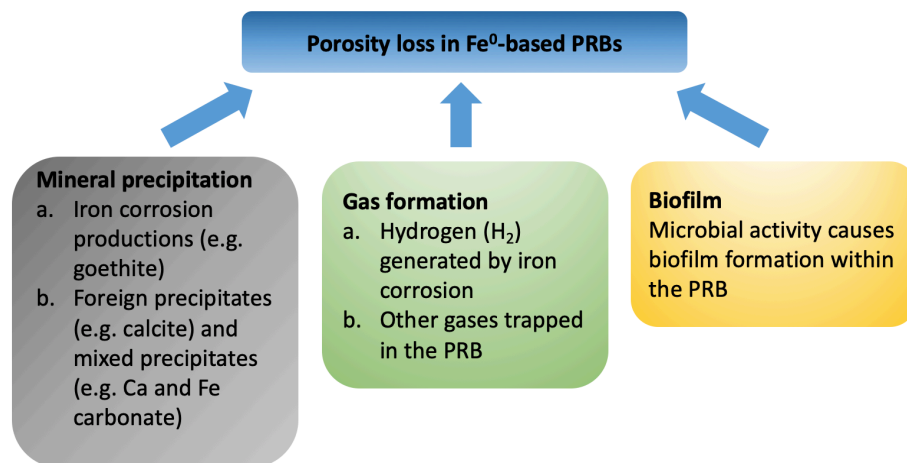


Figure 2.2 Possible reasons for porosity loss in Fe<sup>0</sup>-based PRBs

### 2.3 Field studies of Fe<sup>0</sup>-PRBs

Iron is the most efficient and popular PRB filter for groundwater remediation, and has been extensively utilized in field PRB applications (Thakur et al., 2020). The academic literature on field reports of in-situ Fe<sup>0</sup>-PRBs has become very large over the past three decades. Although the loss of porosity has long been recognized as a key factor affecting the longevity of Fe<sup>0</sup>-PRBs (Mackenzie et al., 1999; Sarr, 2001), the specific porosity loss or the reduction of hydraulic conductivity within the PRB has not been properly evaluated and reported in literature. Klein and Schad (2000) reported a full-scale funnel and gate Fe<sup>0</sup>-PRB system at the Beka site in Tübingen, Germany installed 1998 to remove chlorinated hydrocarbons (CHC), in particular trichloroethene (TCE), cis-1,2-dichloroethene (cDCE) and vinyl-chloride (VC) in the groundwater. The performance of the Fe<sup>0</sup>-PRB was evaluated by the concentrations of CHC in the monitoring wells downstream the barrier, and the results indicated that the contaminants were mainly degraded to concentrations below the regulatory limit. However, the reduction of porosity of the PRB was not evaluated. Sorel et al. (2003) provided performance data of a Fe<sup>0</sup>-PRB installed in Sunnyvale, California, which successfully removed volatile organic carbons (VOCs) from the groundwater before flowing downgradient. The low measured values of

cation concentration were stated in this paper to indicate the mineral precipitation within the PRB, while no specific porosity loss values were provided. Guan et al. (2019) reported a funnel and gate Fe<sup>0</sup>-PRB treatment system located in Qingdao, China, which was designed to remove nitrate from the groundwater. Nonetheless, the porosity loss within the PRB as well as the potential threat to the longevity of the system were not discussed. In conclusion, most of the previous field reports on Fe<sup>0</sup>-PRBs focused on the treatment efficiency of the PRB system for target contaminants. The evaluation of porosity loss within the barrier did not received much research attention. After reviewing 46 field reports from 1998 to 2022, this study summarized the measured/evaluated porosity loss values in following sections. (Guan et al., 2019; Klein and Schad, 2000; Sorel et al., 2003)

### 2.3.1 Porosity loss and estimation methods

A summary of field observations regarding PRB characteristics, reported porosity loss, and their estimation methods is presented in Table 2.1. Field evidence reveals that the most significant porosity loss occurs near the entrance face of a Fe<sup>0</sup>-PRB, especially in the first 25-50 cm of the barrier medium (Phillips et al., 2000, 2003; Wilkin et al. 2005, 2019; Li et al. 2006). In this study, the reported porosity loss within the entrance area of field Fe<sup>0</sup>-PRBs is considered, since the rapid reduction of pore space at the entrance face can result in a by-passing flow around the Fe<sup>0</sup>-PRB and considerably affect the remediation of the groundwater.

Table 2.1. Summary of field Fe<sup>0</sup>-PRB characteristics, porosity loss and estimation methods based on literature.

Site location	Reference	PRB characteristics	Porosity loss [1]	Estimation methods
Canadian Forces Base, Borden, Ontario, Canada	(Nicholson et al., 1983; O'Hannesin and Gillham, 1998; RTDF, 2001)	Continuous trench. 5.5 m wide, 10 m deep, 1.6 m thick. Remove TCE and DCE	No obvious decline in porosity in 5 years	Core samples with scanning electron microscopy (SEM) techniques. Iron oxides, calcium and iron carbonates were found.
Denver Federal Center, Denver, Colorado, USA	(Furukawa et al., 2002; McMahon et al., 1999; Wilkin et al., 2002; Wilkin et al., 2003)	Funnel and gate. Four gates, 12 m wide, 9.5 deep, 0.6 – 1.8 m thick. Remove TCE, DCE, and TCA	0.0035 – 0.005 per year.	Stoichiometric calculations. Porosity loss estimated from decreases in dissolved inorganic carbon and calcium concentration. Assuming calcite and siderite precipitation.
Former mill site, Monticello, Utah, USA	(Morrison et al., 2002; Ott, 2000)	Funnel and gate. 30 m wide, 4.5 – 6 m deep, 1.2 m thick. Remove U and V	0.007-0.015 per year.	Stoichiometric calculations. Porosity loss calculated from mass of Ca, U or V deposits.
Freight Yard, Copenhagen, Denmark	(Kiilerich et al., 2000; Sarr, 2001)	Continuous trench. 15.2 m wide, 6.0 m	0.007 per year.	Stoichiometric calculations. Porosity loss calculated from calcium and carbonate contents.

		deep, 1.0 m thick. Remove DCE		
Industrial site, New York, USA	(Sarr, 2001; Vogan et al., 1999)	Continuous trench. 394 m wide, 5.5 m deep, 0.3 m thick. Remove TCE, DCE, and VC	0.03 per year.	Core samples with electron dispersive X-ray (EDX), and SEM techniques. Calcite, aragonite, siderite, and green rust were identified.
Lowry Air Forces Base, Colorado, USA	(RTDF, 2001; Sarr, 2001)	Funnel and gate. 3 m wide, 6 m deep, 1.5 m thick. Remove TCE, PCE, DCE, and VC	0.024 per year. Ground water flows toward nearby creek after 4 years of operation.	Core samples. Carbonates, aragonite, green rusts, amorphous iron hydroxides, and magnetite were identified.
Moffett Federal Airfield, Mountain View, California, USA	(Gavaskar et al., 2005; Sass et al., 1998; Yabusaki et al., 2001)	Funnel and gate. 3 m wide, 5.5 m deep, 1.8 m thick. Remove TCE and DCE	0.015 - 0.03 per year.	Core samples with Raman spectroscopy and X-ray diffraction (XRD) techniques. Magnetite, hematite, aragonite, marcasite, and amorphous ferric hydroxide were identified.
Monkstown, Newtownabbey, Northern Ireland	(Phillips et al., 2010)	Funnel and gate. 7.3 m long, 1.2 m diameter. Remove TCE and DCE	35% of the ZVI filing have corroded in upper 25 cm	Core samples with XRD and SEM techniques. Ca and Fe carbonates, Fe sulfides, carbonate green rusts, and Fe (hydr)oxides were identified. Magnetite was the major mineral.
U.S. Coast Guard Support Center, Elizabeth City, North Carolina, USA	(Blowes et al., 1999; Furukawa et al., 2002; Wilkin et al., 2014; Wilkin et al., 2018; Wilkin et al., 2002; Wilkin et al., 2003; Wilkin et al., 2005)	Continuous trench. 46 m wide, 7.3 m deep, 0.6 m thick. Remove TCE, Cr(VI)	0.01 – 0.02 per year.	Core samples with XRD and SEM techniques. Lepidocrecite, magnetite, aragonite, siderite, carbonate-green rust, FeS and biofilm were identified.
Vapokon site, Denmark	(Lai and Lo, 2004; Lai et al., 2006)	Funnel and gate. 14.5 m wide, 9.0 m deep, 0.8 m thick. Remove PCE, TCE, and VC	0.0088 per year.	Stoichiometric calculations. Porosity loss calculated by assuming that calcite and mackinawite were the only precipitates, and iron corrosion rate to be 0.4 mmol/kg/d (Reardon 1995).
Y-12 site, Oak Ridge; Tennessee, USA	(Gu et al., 2002; Korte, 2001; Liang, 2001; Ott, 2000; Phillips et al., 2000; Phillips et al., 2003)	Continuous trench. 68.5 m wide, 6.7 to 9.7 m deep, 0.6 m thick. Remove U, Tc, nitric acid, and PCE	0.15 mm thick precipitate in first 30 months. 30%- 80% ZVI replaced by iron hydroxide rinds.	Core samples with XRD and SEM- EDX (energy dispersive X-ray analyzer). Goethite, akaganeite, FeS, aragonite and siderite were identified.

Porosity loss within the field Fe<sup>0</sup>-PRBs is generally estimated based on volumes of secondary minerals observed in core samples, or based on stoichiometric calculations using measured concentration difference of dissolved mineral-forming ions between the up-gradient and down-gradient of the barrier (Li et al., 2005; Sarr, 2001). As shown in table 1, the most overarching cause for the porosity loss within the Fe<sup>0</sup>-PRBs is considered to be mineral

precipitation. The most common minerals formed in Fe<sup>0</sup>-PRBs are magnetite, hematite, goethite, lepidocrocite, calcite, aragonite, siderite, green rust, ferrous hydroxide, ferrous sulphide, and marcasite (Li et al., 2005; Li et al., 2006). Foreign and mixed precipitates, such as calcium and iron carbonates, are generally formed near the entrance face of the barrier, whereas iron corrosion products, such as ferrous hydroxide, iron (hydr-)oxides, magnetite, and green rust, are found throughout the Fe<sup>0</sup>-PRB. Microbial community in collected core samples are enriched in the up-gradient influent portion of the Fe<sup>0</sup>-PRB (Phillips et al., 2010; Wilkin et al., 2003). However, no specific correlation between microbial activity and porosity loss has been reported (O'Hannesin and Gillham, 1998; Wang et al., 2022). The reported field Fe<sup>0</sup>-PRBs porosity loss values with different estimation methods are summarized in boxplot in Figure 2.3.

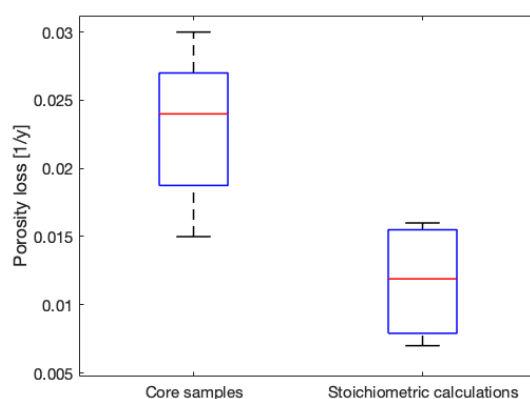


Figure 2.3 Boxplot of reported field Fe<sup>0</sup>-PRBs porosity loss values measured in core samples and estimated from stoichiometric calculations

As shown in Figure 3, the porosity loss values obtained from core samples are remarkably larger than that estimated by stoichiometric calculations. Inadequate consideration of stoichiometric calculations may account for the large difference. The porosity loss in the Copenhagen Freight Yard Fe<sup>0</sup>-PRB was calculated based on the change in calcium and carbonate concentration in the groundwater across the barrier (Kiilerich et al., 2000). Wilkin et al. (2003) calculated the porosity loss in the Denver Federal Center Fe<sup>0</sup>-PRB by assuming that inorganic carbon is present only in aragonite and siderite. For the Vapoken site Fe<sup>0</sup>-PRB, the porosity loss was calculated by assuming that calcite and mackinawite were the only precipitates formed inside the barrier (Lai et al., 2006). To sum up, the general assumption in the above studies is that only foreign precipitates and/or mixed precipitates (e.g. Ca and Fe carbonate) contribute to the porosity loss. However, the first cause of the porosity loss is the precipitation of iron corrosion products, such as iron (hydr-)oxides caused by constant aqueous

iron corrosion in Fe<sup>0</sup>-PRBs (Noubactep, 2008; Yang et al., 2021). Therefore, the stoichiometric calculation method used in previous studies can largely underestimate the porosity loss in a Fe<sup>0</sup>-PRB by ignoring the contribution of iron corrosion products.

Moreover, since some Fe-phases, such as e.g. Fe(OH)<sub>2</sub>, are not stable when taken out of the system, the disturbed core samples may not accurately represent the in-situ situation. At present, there are no routine procedures for preparing and analyzing the mineral precipitates from the Fe<sup>0</sup>-PRBs, and different preparation methods can cause different identification results of minerals (Phillips et al., 2003). In addition, the core sample studies can only estimate the porosity loss caused by mineral precipitation and biofilms. Porosity loss results from gas formation are missing. Therefore, the actual porosity loss of in-situ Fe<sup>0</sup>-PRBs may be much greater than those reported in the literature.

Some in-situ hydrogeological tests have been conducted to measure the hydraulic properties of Fe<sup>0</sup>-PRBs. For Copenhagen Freight Yard Fe<sup>0</sup>-PRB, the permeability of the barrier medium decreased 87 percent in 15 months based on slug tests results, while 0.007 per year of porosity loss was calculated from reduction of calcium and carbonate concentrations (Kiilerich et al., 2000). The decreased permeability measured by slug tests is exceedingly larger than that indicated by the estimated porosity loss. Phillips et al. (2010) conducted a multi-tracer test in the field of Monkstown Fe<sup>0</sup>-PRB to access hydraulic parameters in the system. The porosity loss rate derived from the tracer tests is 0.043/y, which is significantly larger than the other reported porosity loss values in literature. The large difference between the in-situ hydrogeological tests results and the reported porosity loss values in literature give strong evidence for the underestimation of the porosity loss in Fe<sup>0</sup>-PRBs studies.

### 2.3.2 Field Fe-PRBs porosity loss affecting factors

Table 2 summarized the reported porosity losses of field Fe<sup>0</sup>-PRBs and factors possibly affecting the porosity loss, including iron characteristics and geochemical conditions of influent groundwater. The Pearson correlation coefficients shown in Table 2 between each factor versus the porosity loss are calculated as follows (Myers, 1990):

$$R_{xy} = \frac{\sum_{i=1}^n (x_i - \bar{x})(y_i - \bar{y})}{\sqrt{\sum_{i=1}^n (x_i - \bar{x})^2} \sqrt{\sum_{i=1}^n (y_i - \bar{y})^2}} \quad (2.1)$$

where  $n$  is sample number,  $x_i$ ,  $y_i$  are sample points indexed with  $i$ ,  $\bar{x}$  is the sample mean, which is  $\bar{x} = \frac{1}{n} \sum_{i=1}^n x_i$ , and analogously for  $\bar{y}$ .

Table 2.2 Summary of iron characteristics, geochemical condition of influent groundwater, porosity loss of field Fe<sup>0</sup>-PRBs, and the correlation coefficients between each factor and porosity loss.

Site location	W <sub>iron</sub>	Grain size [mm]	Darcy flux [m/d]	pH	Ca <sup>2+</sup> [mg/L]	CO <sub>3</sub> <sup>2-</sup> [mg/L]	SO <sub>4</sub> <sup>2-</sup> [mg/L]	Porosity loss [1/y]
Lowry Air Forces Base, Colorado, USA	1	-	0.3	6.5	290	795	1000	0.024
Moffett Federal Airfield, Mountain View, California, USA	1	-	0.054	7.1	158	400	350	0.015
Industrial site, New York, USA	1	-	0.45	7.4	90.6	310	17.2	0.03
Denver Federal Center, Denver, Colorado, USA	1	2	0.25	7.5	107	560	260	0.016
U.S. Coast Guard Support Center, Elizabeth City, North Carolina, USA	1	0.5	0.15	5.8	12.5	155	49	0.02
Freight Yard, Copenhagen, Denmark	1	-	0.1	7.7	130	625	110	0.007
Former mill site, Monticello, Utah, USA	1	2	0.15	6.7	339	460	1170	0.015
Vapokon site, Denmark	1	-	0.27	7.2	179	422	120	0.0088
Correlation coefficient	0	-	0.67	-0.32	0.10	0.17	0.08	-

As shown in table 2.2, the Darcy flux value has the highest correlation coefficient with reported porosity loss among all key factors, which indicates that the porosity loss of Fe<sup>0</sup>-PRBs is most sensitive to the in-situ groundwater flow velocity. A scatter plot of Darcy flux versus reported field Fe<sup>0</sup>-PRB porosity loss is shown in Figure 2.4. Their strong positive correlation between porosity loss in Fe<sup>0</sup>-PRBs and groundwater Darcy flux can be interpreted by two possible hypothesis. The first hypothesis is the large iron corrosion rate caused by a high flow velocity of water (Liang et al., 2013). A higher corrosion rate of iron can lead to a larger amount of iron corrosion precipitates within the barrier. The second hypothesis is that a higher influent flow rate brings in more mineral-forming ions per unit time into the system, which results in the formation of the greater amount of foreign or mixed precipitates. This statement is consistent with the findings of the modelling study from Li et al. (2006), who reported that a higher Darcy flux of groundwater can induce a larger porosity loss. Since the groundwater Darcy flux is a key factor affecting porosity loss, the site hydrogeology must be well understood for optimal

design of a Fe<sup>0</sup>-PRB. The heterogeneity of the aquifer, as well as the heterogeneity of the barrier itself should be well-studied.

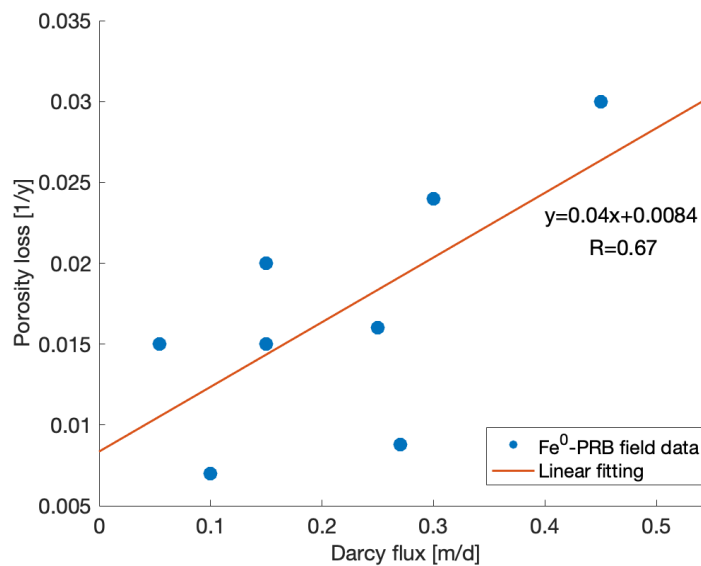


Figure 2.4 Scatter plot of Darcy flux versus reported field Fe<sup>0</sup>-PRB porosity loss

There are only weak correlations between porosity loss of barrier and other factors are revealed, such as iron characteristics, and the mineral-forming ion concentrations of influent groundwater. It is worth to notice that all field Fe<sup>0</sup>-PRBs summarized in this study utilized pure iron bed (100% Fe<sup>0</sup>) in the reactive zone, and each PRB system was reported to maintain its functionality during the long-term operations. However, as discussed above, the reported porosity loss values in the literature underestimate the actual porosity loss in the field. Preferential flows and bypass flows may occur, and the sustainability of these 100% Fe<sup>0</sup> PRBs needs to be reassessed. Tao et al. (2022) stated that only hybrid Fe<sup>0</sup>/H<sub>2</sub>O filtration systems are sustainable. The pure iron beds suffer from the high risk of clogging due to the large amount of generated iron corrosion products. Mixing iron with non-reactive aggregates such as sand in the PRB system can effectively lower the risk of clogging and extend the longevity.

The question raised in the past that a decreased iron ratio may negatively influence the extent of decontamination (Bi et al., 2009). Nonetheless, it has been proved that barriers with Fe<sup>0</sup> to sand ratios far below 100% have a quantitative contaminant removal effect (Song et al., 2005; Wang et al., 2022). For example, Wang et al. (2022) reported almost complete (close to 100%) removal rates of Cr(VI) in a Fe<sup>0</sup>-PRB containing 20% iron. Moreover, the authors detected an increase of Cr(VI) concentration at the effluent end of the PRB containing 30% iron. The increasing Cr(VI) concentration may be caused by the formed preferential flows due to the

porosity loss within the PRB, and could be even a proof of the unsustainability of high iron/sand ratio PRB systems.

#### **2.4 Fe<sup>0</sup>-PRB laboratory column tests**

Laboratory column test is an important tool to investigate contaminant removal mechanisms, pollutant transformation efficiencies, and the longevity of the Fe<sup>0</sup>-PRBs. Similar to the situation of Fe<sup>0</sup>-PRBs field reports, the column tests studies have mainly focused on the removal efficiency of target contaminants. The porosity loss over time of the barrier medium has not received much attention, and information about porosity loss values is limited. This study reviews 32 papers on column tests from 1995 to 2019, and summarizes the reported porosity loss, the column settings and porosity loss estimation methods (Table 2.3).

Table 2.3 Summary of column test settings (including iron characteristics, geochemical condition of influent flow), the reported porosity loss values, and the estimation methods.

Study	W <sub>iron</sub>	Grain size [mm]	Darcy flux [m/d]	pH	Ca <sup>2+</sup> [mg/L]	CO <sub>3</sub> <sup>2-</sup> [mg/L]	SO <sub>4</sub> <sup>2-</sup> [mg/L]	Duration [d]	Porosity loss [1/y]	Estimation methods
Bartzas and Komnitsas (2010)	0.5	1	1.524	1.8	0	0	5840	45	1.3	Sample extract and solid phase characterization studies.
Jeen et al. (2006)	1	-	2.3	7	0	0	0	730	0.03	Stoichiometric calculations.
				7	100	100	0		0.057	
				8	500	500	0		0.1	
(Kamolpornwijit et al., 2004)	1	1	9.4	7	288	252	72	680	0.14	Stoichiometric calculations. Assuming all precipitation occurred in first 50 cm and single precipitation species as goethite.
Kamolpornwijit and Liang (2006)	1	1	0.3	6.9	276	252	52	400	0.23	Tracer tests
Kamolpornwijit et al. (2003)	1	1	6.1	4.5	829	252	73.5	420	0.24	Stoichiometric calculations. Calculated from the reduction of nitrate.
Luo et al. (2013)	1	2	8.9	5.91	0.08	0	0.5	16	5.7	X-ray computed
				8.32	20.6	230	9.8		6.8	

				3.35	54	0	9.5		3	tomography image analysis
Mackenzie et al. (1999)	1	1	1.2	8	300	300	0	0.5	4.38	Stoichiometric calculations. Assuming Fe(OH) <sub>2</sub> is the dominant precipitate
Parbs et al. (2007)	1	2	0.4	7	0	0	0	800	0.096	Stoichiometric calculations. Assuming calcite and siderite were the major precipitates.
Vikesland et al. (2003)	1	1	1.8	7	0	122	0	1100	0.046	Stoichiometric calculations. Assuming the precipitated mineral was either carbonate green rust or magnetite.
Xin et al. (2018)	0.05	0.007	0.049	7	0	0	0	180	0.097	Tracer tests.
				7	40	30	48		0.097	Porosity is

				8	400	120	4800		0.14	calculated based on the hydraulic conductivity and Kozeny-Carman equation
Zhang and Gillham (2005)	1	1	0.56	7	0	0	0	500	0.044	Stoichiometric calculations. Assuming Fe <sub>3</sub> O <sub>4</sub> was the only precipitate.
				8	300	300	0		0.074	

Laboratory column tests are usually aerobic, confined systems, which utilize high contaminant concentrations and high flow velocities (Henderson and Demond, 2007). Figure 2.5 illustrates reported porosity loss in column tests, as well as the Darcy flux versus test durations. For short-term column tests, especially for test duration less than 200 days, the porosity loss values are more than an order of magnitude larger than that from Fe<sup>0</sup>-PRB field reports. Thus, the porosity loss obtained from short-term column tests may not be representative of an in-situ Fe<sup>0</sup>-PRB. The high Darcy flux utilized in short-term column tests can be a reasonable explanation for the large difference. The flow velocity in column tests is much larger than the average Darcy flux in field Fe<sup>0</sup>-PRBs (0.16 m/d as shown in Figure 5), and is intentionally higher in order to speed the aging of the reactive media and simulate long time scales. For instance, Kamolpornwijit et al. (2003) conducted a Fe<sup>0</sup>-PRB column test with a Darcy flux 20 times larger than average Darcy fluxes. To scale the aging of the column test to represent 'real-time', the surface-loading rate was used. It was assumed that the surface-loading rate of the fast-flow column test is 20 times that of average flow, as the surface-loading rate is proportional to Darcy flux. Thus, a 30-day operation of column test is equivalent to approximately 2 years in the field. Luo et al. (2013) performed the column experiments under 8.9 m/d Darcy flux, which is 56 times greater than the average flow velocity. They considered that 16 days at this flow velocity represents an equivalent reaction period of 2.2 years under typical field conditions. However, this prediction did not include the effect of kinetics on precipitation due to increased flow velocity, as well as the transformation of iron corrosion products over the long-term operation (Kamolpornwijit et al., 2003). Therefore, short-term column studies with high flow velocities may not be representative of actual conditions for long-term Fe<sup>0</sup>-PRBs. In order to investigate the porosity loss of the real Fe<sup>0</sup>-PRBs, a long-term (at least over 200 days) column test is required, and the accelerated Darcy flux should not be applied in the test.

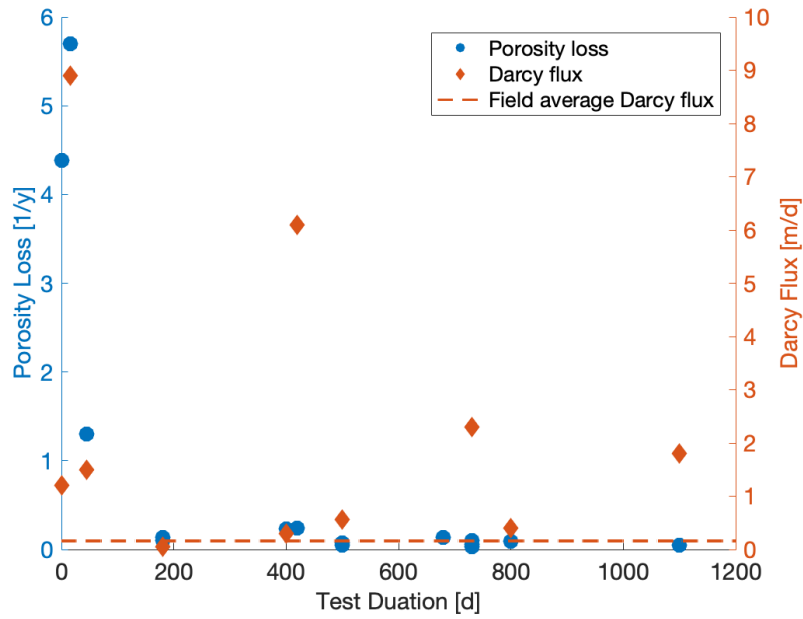


Figure 2.5 Column test porosity loss values and Darcy flux versus column test durations

Similar to the cases of field Fe<sup>0</sup>-PRBs studies, solid phase studies on core samples and stoichiometric calculations are two main methods to estimate porosity loss in column tests. The effect of gas formation is also considered in some column studies. Jeen et al. (2006) calculated the porosity on the basis of the mass-volume-balance equations, assuming the total volume of the column is occupied by iron, water, secondary minerals, and formed gas. Zhang et al. (2005) estimated the gas formation from the changes in the relative weight of the column. For the iron column which did not receive mineral-forming ions, the decline in weight over time was assumed to be a reasonable measure of the volume of entrapped gas.

Although in some column studies the stoichiometric calculation methods considered the formed gas, the actual porosity loss values are yet to be determined. Improper assumptions were applied in the calculations. For instance, Vikesland et al. (2003) assumed that the precipitated material was either carbonate green rust or magnetite. Zhang et al. (2005) assumed that oxidized iron exists only as magnetite Fe<sub>3</sub>O<sub>4</sub>. Parbs et al. (2007) calculated the porosity loss caused by mineral precipitations using a decrease in calcium concentration, assuming calcite and siderite are the precipitates. As stated before, the iron corrosion products are the first reason for porosity loss and should be seriously considered in porosity loss calculations. Neglecting of iron corrosion products may lead to overestimation of entrapped gas volume, and inaccurate evaluation of the porosity loss in Fe<sup>0</sup>-PRBs.

## 2.5 Numerical model studies on Fe<sup>0</sup>-PRBs

Apart from field studies and laboratory column tests, numerical modelling is a common tool to assess the long-term performance of a Fe<sup>0</sup>-PRB. Many numerical models have been developed to simulate the contaminant degradations and mineral precipitation within the Fe<sup>0</sup>-PRBs (Li et al., 2005; Li et al., 2006; Mayer et al., 2001; Moraci et al., 2016; Wu et al., 2017; Yabusaki et al., 2001). Nonetheless, previous modelling studies mainly focused on the contaminant remediation process. Porosity loss within the barrier, and its resulting changes in groundwater flow and impact on the long-term effectiveness of the PRB, have not been adequately studied. For instance, Prommer et al. (2008) developed a process-based numerical model to simulate the transport and reactions of chlorinated hydrocarbon in the presence of iron, which included a reaction network for the transformation of chlorinated hydrocarbons by iron. But the porosity loss in the iron zone and its influence on the system was not reported. Jeen et al. (2008) incorporated the secondary mineral precipitation and reactivity loss of the iron into a multi-component reactive transport code to evaluate the changes of the reactivity of different iron materials for cis-DCE treatment. Although it is stated that the porosity and hydraulic conductivity were updated, the porosity change was not reported in the literature. In this section, 34 numerical studies (from 1999 to 2021) regarding specific porosity loss are reviewed, and its simulation methods and results are summarized. (Jeen et al., 2008; Prommer et al., 2008)

### 2.5.1 Simulation methods for porosity loss

Iron corrosion by water in numerical studies can be simulated by a rate expression  $R_{\text{H}_2\text{O-Fe}^0}$  with a first-order dependence on the iron surface area (Li et al., 2005; Li et al., 2006; Mayer et al., 2001; Wu et al., 2017; Yabusaki et al., 2001):

$$R_{\text{H}_2\text{O-Fe}^0} = -\max \left\{ \left[ k_{\text{H}_2\text{O-Fe}^0} S_{\text{Fe}^0} \left( 1 - \frac{\text{IAP}_{\text{H}_2\text{O-Fe}^0}}{K_{\text{H}_2\text{O-Fe}^0}} \right) \right], 0 \right\}, \quad (2.2)$$

where  $k_{\text{H}_2\text{O-Fe}^0}$  [mol m<sup>-2</sup> s<sup>-1</sup>] is the iron corrosion rate normalized to the iron surface area,  $S_{\text{Fe}^0}$  [m<sup>2</sup> L<sup>-1</sup>] is the reactive surface area of iron, IAP is the ion activity product. An equilibrium constant of  $\log K_{\text{H}_2\text{O-Fe}^0} = -11.78$  was calculated on the basis of data from Reardon (1995) and Stumm et al. (1996), and  $\log k_{\text{H}_2\text{O-Fe}^0}$  is assumed to be equal -11.3 based on Reardon (1995).

The mineral precipitation is usually simulated by following transition state theory (Lasaga, 1984; Mayer et al., 2001; Yabusaki et al., 2001) and is expressed as:

$$R_i^m = -k_{eff,i} \left( 1 - \frac{\text{IAP}_i^m}{K_i^m} \right), \quad (2.3)$$

where  $R_i^m$  [mol L<sup>-1</sup> H<sub>2</sub>O s<sup>-1</sup>] is the rate of mineral precipitation (R>0) or dissolution (R<0),  $k_{eff,i}$  [mol L<sup>-1</sup> H<sub>2</sub>O s<sup>-1</sup>] is the effective rate constant for the dissolution of individual mineral phase,  $IAP_i^m$  is the ion activity product, and  $K_i^m$  [-] is the corresponding solubility constant. Table 2.4 summarizes the solubility constants, and the effective rate constants of mineral precipitation within Fe<sup>0</sup>-PRBs (Li et al., 2006; Mayer et al., 2001; Yabusaki et al., 2001).

Table 2.4 Summary of solubility constants, and effective rate constants of mineral precipitation within the Fe<sup>0</sup>-PRBs

Mineral dissolution-precipitation reactions	log K [-]	log $k_{eff}$ [mol L <sup>-1</sup> s <sup>-1</sup> ]
CaCO <sub>3</sub> ↔ Ca <sup>2+</sup> + CO <sub>3</sub> <sup>2-</sup>	8.475	-8.8
CaMg(CO <sub>3</sub> ) <sub>2</sub> ↔ Ca <sup>2+</sup> + Mg <sup>2+</sup> + 2CO <sub>3</sub> <sup>2-</sup>	17.09	-10.1
Fe(OH) <sub>3</sub> + 3H <sup>+</sup> ↔ Fe <sup>3+</sup> + 3H <sub>2</sub> O	-4.891	-8.6
FeCO <sub>3</sub> ↔ Fe <sup>2+</sup> + CO <sub>3</sub> <sup>2-</sup>	10.45	-9.6
FeS + H <sup>+</sup> ↔ Fe <sup>2+</sup> + HS <sup>-</sup>	4.648	-9.6
Fe(OH) <sub>2</sub> + 2H <sup>+</sup> ↔ Fe <sup>2+</sup> + 2H <sub>2</sub> O	-13.905	-8.6
MnCO <sub>3</sub> ↔ Mn <sup>2+</sup> + CO <sub>3</sub> <sup>2-</sup>	10.41	-8.1
Mn(OH) <sub>2</sub> + 2H <sup>+</sup> ↔ Mn <sup>2+</sup> + 2H <sub>2</sub> O	-15.088	-8.6

Another approach to calculate the porosity loss caused by iron corrosion products, which is on the basis of the volumetric expansion of iron during corrosion (Caré et al., 2013; Caré et al., 2008; Noubactep, 2016b), is introduced by Care et al. (2013). A coefficient of volumetric expansion ( $\eta$ ) is utilized in this approach as:

$$\eta = \frac{V_{FeCPS}}{V_{Fe^0}} > 1, \quad (2.4)$$

where  $V_{FeCPS}$  [m<sup>3</sup>] is the volume of iron corrosion products that precipitate within the barrier,  $V_{Fe^0}$  [m<sup>3</sup>] is the volume of Fe<sup>0</sup> before the corrosion begins. The calculated volumetric expansion coefficients of main corrosion products are listed in Table 2.5.

Table 2.5 Summary of volumetric expansion coefficients of iron and its main corrosion products (Caré et al., 2013)

Mineral	Formula	$\eta$ [-]
Iron	Fe <sup>0</sup>	1
Fe <sup>II</sup> hydroxide	Fe(OH) <sub>2</sub>	3.47
Fe <sup>III</sup> hydroxide	Fe(OH) <sub>3</sub>	4.53

Goethite	$\alpha$ -FeOOH	2.67
Maghemite	$\gamma$ -Fe <sub>2</sub> O <sub>3</sub>	1.91
Hematite	$\alpha$ -Fe <sub>2</sub> O <sub>3</sub>	1.98
Siderite	FeCO <sub>3</sub>	3.86
Magnetite	Fe <sub>3</sub> O <sub>4</sub>	1.97

Gas formation and discharge are also simulated in numerical models and are described using a formulation by Cirpka and Kitanidis (2001), which relates partial gas pressures to gas saturations with equilibrium partitioning of gas between aqueous and gaseous phases (Amos and Mayer, 2006; Jeen et al., 2012; Weber et al., 2013):

$$R_d = k_g \max \left[ \left( \frac{S_g}{S_{g,max}} - 1 \right); 0 \right], \quad (2.5)$$

where  $R_d$  [mol L<sup>-1</sup> H<sub>2</sub>O s<sup>-1</sup>] is the degassing rate,  $k_g$  [mol L<sup>-1</sup> H<sub>2</sub>O s<sup>-1</sup>] is the degassing rate constant,  $S_g$  [m<sup>3</sup> gas m<sup>-3</sup> pore volume] is the gas saturation, and  $S_{g,max}$  [m<sup>3</sup> gas m<sup>-3</sup> pore volume] is the maximum gas saturation. (Cirpka and Kitanidis, 2001)

### 2.5.2 Simulation results of porosity loss

Table 2.6 Summary of simulated porosity loss in numerical studies, model characteristics, applied geochemical conditions, and the considered factors for simulated porosity loss including Pearson correlation coefficients of some factors versus porosity losses.

Study	Used code	Model type	$W_{iron}$	Grain size [mm]	Darcy flux [m/d]	pH	Ca <sup>2+</sup> [mg/L]	CO <sub>3</sub> <sup>2-</sup> [mg/L]	Porosity loss [1/y]	Considered factors
Mayer et al. (2001)	Min3P	2-D model	1	0.4	0.15	6.94	22	144	0.007	Mineral precipitation
Yabusaki et al. (2001)	OS3D	1-D model	1	-	0.054	7.1	158	400	0.0256	Mineral precipitation
(Vikesland et al., 2003)	CXTFIT	1-D model	0.9	1	1.8	7	0	122	0.04	Formation of regions of immobile water
Li et al. (2006)	Modflow and RT3D	3-D model	1	-	0.4	7	40	60	0.0136	Mineral precipitation
Jeen et al. (2007)	Min3P	1-D model	1	-	0.1	7	100	100	0.006	Mineral precipitation
					0.2	7	100	100	0.006	
					0.1	8	200	200	0.004	
Jeen et al. (2009)	Min3P	1-D model	1	-	0.5	7.35	120	450	0.028	Mineral precipitation
Gui et al. (2009)	Min3P	1-D model	1	-	0.44	6.8	0	0	0	Mineral precipitation
					0.44	7	120	450	0.032	
Weber et al. (2013)	Min3P	1-D model	1	1	0.2	7	120	120	0.035	Mineral precipitation and gas formation
Moraci et al. (2016)	-	1-D model	1	0.5	0.07	7	40	0	0.02	Mineral precipitation
					1.9	7	40	0	0.035	
					0.38	7	50	0	0.07	
Wu et al. (2017)	Modflow and MT3DMS	1-D model	0.3	0.5	0.04	7	0	0	-0.001	Mineral precipitation
Correlation coefficient	-	-	0	-	0.38	-0.16	0.06	0.50	-	-

Table 2.6 summarizes the data from numerical studies on Fe<sup>0</sup>-PRBs which simulated the porosity loss process, including model types, geochemical conditions, considered affecting factors for porosity loss, and the simulated porosity losses.

Mayer et al. (2001) developed the first reactive transport model to simulate an in-situ Fe<sup>0</sup>-PRB. The simulations successfully reproduced the treatment of the contaminants, such as hexavalent chromium and chlorinated solvents. The porosity of the barrier was affected by the iron corrosion and mineral precipitation processes. Iron corrosion was calculated with the corrosion rate derived from Reardon (1995) (Equation 2.2). The mineral precipitation was simulated according to transition state theory (Equation 2.3), and the precipitation of nine precipitates (Fe(OH)<sub>2</sub>, Fe(OH)<sub>3</sub>, FeCO<sub>3</sub>, FeS, Cr(OH)<sub>3</sub>, CaCO<sub>3</sub>, CaMg(CO<sub>3</sub>)<sub>2</sub>, MnCO<sub>3</sub>, Mn(OH)<sub>2</sub>) were considered in the model. The porosity loss caused by the formation of gas was not considered. The simulation results showed that the porosity decreased from 0.5 to approximately 0.36 in the entry area of the barrier over the 20 year operation, which was 0.007/y porosity loss.

Yabusaki et al. (2001) established a 1-D reactive transport model to simulate the treatment for TCE for the Moffett Field Fe<sup>0</sup>-PRB. Precipitation of ferrous hydroxide (Fe(OH)<sub>2</sub>), siderite (FeCO<sub>3</sub>), iron sulphide (FeS), aragonite (CaCO<sub>3</sub>), and brucite (Mg(OH)<sub>2</sub>) was assumed to decrease the porosity of the barrier. The mineral precipitation process was calculated applying the transition state theory (Equation 2.3), and the simulation results showed that the porosity was reduced from 0.66 to 0.6344 after 1 year operation, which was 0.0256/y porosity loss.

Li et al. (2006) established a 3-D reactive transport model to investigate the porosity reductions caused by mineral precipitation. The employed geochemical algorithm followed the methods introduced by Mayer et al. (2001) and Yabusaki et al. (2001) to simulate the mineral precipitation, and a porosity loss result of 0.0136/y was simulated under the geochemical conditions of a field Fe<sup>0</sup>-PRB.

Jeen et al. (2007) applied the reactive transport code developed by Mayer et al. (2001) and modified the kinetic expression by coupling the accumulation of secondary minerals and reactivity loss. The evolving iron reactivity was simulated by updating the reactive surface area of iron as:  $S = S_0 \exp(-aX)$ , where  $S$  is the reactive surface area of iron,  $S_0$  is the initial reactive surface area,  $a$  is the proportionality constant, and  $X$  is the volume fraction of the mineral phase. A 1-D simulation was performed to reproduce the observations from column experiments. Porosity loss predictions of 0.006/y, and 0.004/y were achieved for systems receiving no, and high CaCO<sub>3</sub> concentration respectively.

Li et al. (2012) incorporated the impact of gas formation into the existing code (Jeen et al. 2007). The gas phase formation and gas discharge were simulated using the Equation 2.5. The

modelling showed a gas phase saturation of 20% in the effluent at the end of the barrier over 350 days of operation.

Vikesland et al. (2003) conducted tracer tests with water containing tritium ( $^3\text{H}_2\text{O}$ ) in  $\text{Fe}^0$  columns. A dual-region transport model was applied to fit the breakthrough curves of the tracer tests. It was assumed that only a portion of the water in the column is mobile (“flowing”). The mineral precipitation and gas formation within the porous media generated immobile (“stagnant”) zones, and mobile water only slowly exchanged with the water in the immobile zones (Toride et al. 1993, Vikesland et al. 2003). The application of the dual-region transport model revealed that the immobile water-filled region increased from initially negligible to amounts ranging between 3% and 14% of the total porosity after 1000 days of simulation, which may have a significant influence on the groundwater transport.

Affecting factors for simulated porosity loss were investigated in previous models. Li et al. (2006) performed parametric studies to identify the most important factors to include them in a model evaluating porosity loss. The concentration of  $\text{CO}_3^{2-}$  had the largest effect on porosity loss within 0.2 m from the entrance face, because  $\text{CO}_3^{2-}$  concentration controls the formation of carbonate minerals. The rate coefficient for iron corrosion had a great influence on porosity loss, particularly for distances more than 0.05m from the entrance face, since the iron corrosion controls the release of  $\text{Fe}^{2+}$  and  $\text{OH}^-$  and the formation of iron corrosion products. Jeen et al. (2018) conducted sensitivity analyses for model parameters on predicting the long-term performance of a  $\text{Fe}^0$ -PRB. The model parameters tested include iron corrosion rate, aragonite and  $\text{Fe}_2(\text{OH})_2\text{CO}_3$  precipitation rates, and proportionality constants for each mineral. The results revealed that the most important and sensitive parameters were secondary mineral precipitation rates (Jeen, 2018).

In this study, the correlation coefficients between possible factors and simulated porosity loss values from different model studies are calculated and shown in Table 6. It can be concluded that the concentration of  $\text{CO}_3^{2-}$  in the influent flow, and the Darcy flux have the strongest positive correlations with the porosity loss of  $\text{Fe}^0$ -PRBs among the reviewed numerical model studies.

## 2.6 Discussion

Figure 2.6 shows the boxplots of summarized porosity loss values in field reports, column studies, and numerical model simulations. The concept of surface-loading rate was used in column tests data to scale the fast-flow and short-duration tests to represent a ‘real’ time situation. As discussed above, this calculation does not include the effect of kinetics on

precipitation due to the increased Darcy flux, and the complex transformation of iron corrosion products in long-term operations, which may cause underestimation of the porosity loss. Results indicate that the summarized porosity loss values of column tests are significantly larger than that of actual field reports. Thus, it is difficult to compare laboratory column studies with field installations. The possible interpretations are that column studies using high contaminant concentrations may not appropriately represent low contaminant in-situ fluxes, and short-term columns with high flow rates may not be representative of true iron media aging. Therefore, to investigate the Fe<sup>0</sup>-PRBs longevity with column tests, a proper conversion method, which can reasonably scale the fast-flow column data to represent a field Fe<sup>0</sup>-PRB, should be developed. Otherwise, short-term column tests with high Darcy flux should be avoided in order to study the Fe<sup>0</sup>-PRBs longevity.

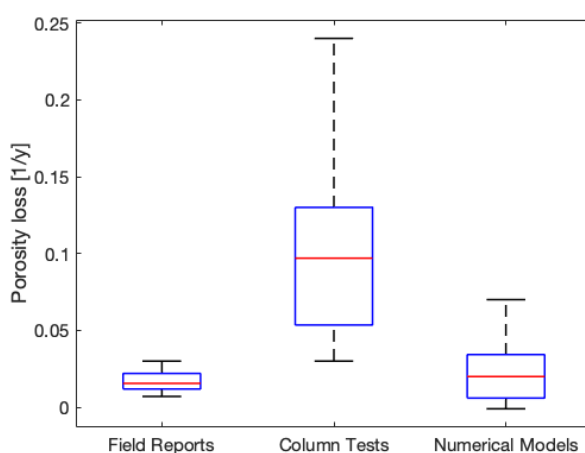


Figure 2.6 Boxplots of Fe-PRBs porosity loss values in field reports, column tests, and numerical model simulations

Porosity loss results of numerical studies mostly fall within the range of reported field Fe<sup>0</sup>-PRBs and column studies. However, as shown in Figure 6, some model simulations are smaller than reported porosity loss in field, which suggests that the effects of iron corrosion products have been underestimated in some numerical studies (Jeen et al., 2007; Mayer et al., 2001; Wu et al., 2017). For instance, the simulation results from the model developed by Wu et al. (2017) showed that the total porosity of the Fe<sup>0</sup>-PRB increases by 0.001 after 40 years of operation. These results have conflict with the fact that the iron corrosion is a volumetric expansive process when pH is higher than 4.5. Thus, under field conditions, the porosity of a Fe<sup>0</sup>-PRB can only decrease during operations. The underestimation of iron corrosion products in some numerical models could be caused by the small iron corrosion rates used in the simulations.

The iron corrosion rate is the key factor to investigate the iron corrosion process and the long-term porosity loss of the Fe<sup>0</sup>-PRBs (Yang et al., 2021). Table 2.7 lists the experimental corrosion rate values of granular iron in Fe<sup>0</sup>-PRB literature.

Table 2.7 Experimental corrosion rates of granular iron in Fe<sup>0</sup>-PRBs literature

Study	Grain size [mm]	Iron surface area	Inflow	Corrosion rate
Reardon (1995)	0.5-2	1.5 m <sup>2</sup> /g	Saline ground water	0.7±0.5 mmol/(kg·d)
Yabusaki et al. (2001)	n.s	1.88×10 <sup>-6</sup> m <sup>2</sup> /m <sup>3</sup>	Groundwater	3×10 <sup>-12</sup> -5×10 <sup>-12</sup> mol/(m <sup>2</sup> ·s)
Chen et al. (2001)	0.15	0.077 m <sup>2</sup> /g	TCE solution, anaerobic condition	0.092-0.0181 L/(h·m <sup>2</sup> )
Kamolpornwijit et al. (2004)	0.5-2	n.s	Groundwater	0.5-6.16 mmol/(kg·d)

As shown in Table 2.7, different units were used in each study, which increases the difficulty of comparison analysis of different studies (Yang et al. 2021). In order to compare the results, the corrosion rates were converted to the same unit (mm/y), shown in Table 8. The unit (mm/y) is a common unit to describe the corrosion rate for all metals. The results of Kamolpornwijit et al. (2004) cannot be converted to penetration rate because the iron surface area was not reported. The unit of mmol/(kg·d) was firstly introduced by Reardon (1995) to describe iron corrosion rates. However, as stated in Reardon (1995), 'this unit is uncorrected for the surface area'. Therefore, the corrosion rates in mmol/(kg·d) are not comparable if another material with a different surface area is used. It is inappropriate for further studies (e.g. Kamolpornwijit et al. 2004) to use the unit of mmol/(kg·d) and compare the results with Reardon (1995) since another iron material with different surface area was tested. Thus, a uniform unit of iron corrosion rate (e.g. mm/y) was proposed in Fe<sup>0</sup>-PRB studies to reduce confusion.

Table 2.8 Experimental corrosion rates in mm/y unit

Study	Corrosion rate (mm/y)
Reardon (1995)	1.2×10 <sup>-6</sup>
Yabusaki et al. (2001)	6.73×10 <sup>-7</sup> to 1.12×10 <sup>-6</sup>
Chen et al. (2001)	1.6×10 <sup>2</sup> to 8×10 <sup>2</sup>

As listed in Table 2.8, the corrosion rates obtained from Reardon (1995) and Yabusaki et al. (2001) are of the same order of magnitude, but there is a significant difference to the corrosion rates given by Chen et al. (2001), which are approximately 4 orders of magnitudes larger. The different measurement methods may account for the discrepancy. Reardon (1995) monitored the hydrogen pressure increase in sealed cells, and the increasing hydrogen partial pressure may inhibit the iron corrosion reaction. Chen et al. (2001) added di-sodium ethylene-diaminetetraacetic acid (EDTA) in the solutions to prevent the forming of precipitates and monitored the dissolved iron concentration in the outflow. The addition of a chelating agent (EDTA) may extremely accelerate the iron corrosion process by removing the corrosive layer. The iron corrosion behaviour in water or humid environment is extensively investigated in other research areas, e.g. steel reinforced concrete industry (Yang et al. 2009). Grauer et al. (1984) measured the corrosion rates of iron in anoxic water. Li et al. (2004) compiled 156 experimental tests of corrosion rates of reinforcing steel in previous literature. The experimental iron corrosion rates are summarized in Table 2.9.

Table 2.9 Experimental corrosion rates in other research areas

Study	Corrosion rate (mm/y)
Grauer (1984)	$1 \times 10^{-2}$ to $2 \times 10^{-2}$
Liu (1996)	$5.8 \times 10^{-4}$ to $3.15 \times 10^{-3}$
Li (2004)	$1.7 \times 10^{-3}$ to $8.5 \times 10^{-3}$
Yang (2009)	$1.2 \times 10^{-3}$ to $8 \times 10^{-3}$

Iron corrosion is a complex process and the corrosion rate is affected by several factors. Since the experimental conditions are distinct, the data in Table 2.9 cannot represent the corrosion rates for Fe<sup>0</sup>-PRBs. However, Table 2.9 can give an idea of the ranges of corrosion rate of iron. When we compare the iron corrosion rates in Table 8 and Table 9, it can be found that neither the corrosion rates derived from Reardon (1995), Yabusaki et al. (2001), nor Chen et al. (2001) fall within the range of reported iron corrosion rates in Table 2.9. Thus, the question still remains to determine the proper corrosion rate value for Fe<sup>0</sup>-PRBs.

Table 2.10 lists the iron corrosion rates used in different Fe<sup>0</sup>-PRBs numerical model studies.

Table 2.10 Corrosion rates used in Fe<sup>0</sup>-PRBs models

Study	Corrosion rate	Source
-------	----------------	--------

Mayer et al. (2001)	$1.2 \times 10^{-6}$ mm/y	Reardon 1995
Jeen et al. (2007)	$1.2 \times 10^{-6}$ mm/y	Reardon 1995
Jeen et al. (2009)	$1.2 \times 10^{-6}$ mm/y	Reardon 1995
Jeen et al. (2011)	$1.2 \times 10^{-6}$ mm/y	Reardon 1995
Jeen et al. (2012)	$1.2 \times 10^{-6}$ mm/y	Reardon 1995
Henderson and Demond (2011)	$1.2 \times 10^{-6}$ mm/y	Reardon 1995
Velimirovic et al. (2014)	$1.2 \times 10^{-6}$ mm/y	Reardon 1995
Bilardi et al. (2013)	$1.2 \times 10^{-6}$ mm/y	Reardon 1995
Wu et al. (2017)	$1.2 \times 10^{-6}$ mm/y	Reardon 1995
Yabusaki et al. (2001)	$6.73 \times 10^{-7}$ to $1.12 \times 10^{-6}$	Column tests
Li et al. (2006)	$1.8 \times 10^{-6}$ and $2.3 \times 10^{-7}$ mm/y	Calibration with field measurement

As shown in Table 2.10, most models applied the corrosion rate value derived from Reardon (1995). The corrosion rate used by Li et al. (2006) was calibrated with field measurements in the Moffett Federal Airfield (Yabusaki et al., 2001) by including a porosity loss of 0.015/y. The calibrated corrosion rate is of the same order of magnitude with the reported corrosion rate in Reardon (1995). However, the reported porosity loss may not represent the actual porosity loss in field, and the derived iron corrosion rate in Li et al. (2006) may be much smaller than the real iron corrosion rate.

The iron corrosion rate can vary over several orders of magnitude (Melchers and Petersen, 2018; Yang et al., 2021), and is especially dependent on the iron material, as well as the reaction conditions. It is controversial to use iron corrosion rate derived from Reardon (1995) in every Fe<sup>0</sup>-PRB model. The small corrosion rate utilized in the simulations may lead to an underestimation of the amount of iron corrosion products, and the porosity loss after long-term operation.

## 2.7 Conclusions and outlook

In order to achieve an accurate assessment of Fe<sup>0</sup>-PRBs longevity, the porosity loss of the barrier is an essential factor to be considered. This study reviewed the Fe<sup>0</sup>-PRBs literature, including field Fe<sup>0</sup>-PRBs reports, column test studies, and numerical model simulations. The data of the reported porosity loss values, its evaluation methods, and the corresponding geochemical

conditions in individual studies were critically summarized and analysed. The analysis reveals the following conclusions:

- The estimated porosity loss values in field reports differ largely from that based on hydraulic tests, such as slug tests and tracer tests. The current estimation methods for porosity loss of Fe<sup>0</sup>-PRBs, which is based on core sample studies and stoichiometric calculations, may underestimate the porosity loss of Fe<sup>0</sup>-PRBs in the field, and cause a misunderstanding of the impact of porosity loss on Fe<sup>0</sup>-PRBs longevity.
- The porosity loss values, which were estimated by solid phase studies on core samples, are significantly greater than that estimated by stoichiometric calculations. The general unsatisfying assumption of stoichiometric calculations was that only foreign precipitates or mixed precipitates were regarded neglecting the porosity loss by iron corrosion products. The inadequate consideration and improperly applied assumption of stoichiometric calculations may lead to an underestimation of the amount of iron corrosion products.
- The in-situ Darcy flux has the highest positive correlation with the long-term porosity loss. Thus, the site hydrogeology, as well as the heterogeneity of the barrier, must be well studied prior to design and construct a Fe<sup>0</sup>-PRB.
- It is difficult to compare the short-term column tests using high Darcy flux with field installations. Although the concept of surface-loading rate was utilized to scale the short-term column tests to represent the 'real' time simulation, the calculation does not include the kinetics of precipitation due to increased flow velocity and transformation of iron corrosion products, and may induce a large error. Thus, to investigate the porosity loss, long-term (at least more than 200 days) column tests are required, and the accelerated Darcy flux should be avoided.
- Small iron corrosion rate utilized in numerical model studies may cause a small simulated porosity loss compared to field Fe<sup>0</sup>-PRBs. The proper iron corrosion rate, which can be used for a realistic simulation of the long-term porosity loss of Fe<sup>0</sup>-PRBs, is yet to be determined.

In addition, after reviewing the reported porosity loss values in Fe<sup>0</sup>-PRB literature, we suggest some potential topics for future research to properly predict the long-term porosity loss of a Fe<sup>0</sup>-PRB. The first challenge is developing a method to evaluate the actual porosity loss of a field Fe<sup>0</sup>-PRB. As analysed above, the current evaluation methods consider inappropriate assumptions and underestimate the porosity loss in the field. Application of hydraulic tests, e.g. multi-level tracer tests, may provide a more accurate result of porosity variation in the field.

The second challenge is to determine right iron corrosion rates for Fe<sup>0</sup> applied in the PRBs. The iron corrosion rate has a vital influence on the porosity loss prediction. The minor value of iron corrosion rate applied in current model studies can cause great underestimation of long-term porosity loss. The third challenge is to determine the amount of iron corrosion products. The composition of the iron corrosion products can be very complex, and is constantly changing over time. A method quantitatively describing the amount of iron corrosion products under various conditions is yet to be investigated.

## References

- Amos, R.T., Mayer, K.U., 2006. Investigating the role of gas bubble formation and entrapment in contaminated aquifers: Reactive transport modelling. *Journal of contaminant hydrology*, 87(1-2): 123-154.
- Bartzas, G., Komnitsas, K., 2010. Solid phase studies and geochemical modelling of low-cost permeable reactive barriers. *Journal of Hazardous Materials*, 183(1-3): 301-308
- Bi, E., Devlin, J.F., Huang, B., 2009. Effects of mixing granular iron with sand on the kinetics of trichloroethylene reduction. *Groundwater Monitoring & Remediation*, 29(2): 56-62.
- Bilardi, S., Amos, R.T., Blowes, D.W., Calabrò, P.S., Moraci, N., 2013. Reactive transport modeling of ZVI column experiments for nickel remediation. *Groundwater Monitoring & Remediation*, 33(1): 97-104
- Blowes, D. et al., 1999. In Situ Permeable Reactive Barrier for the Treatment of Hexavalent Chromium and Trichloroethylene in Ground Water. Volume 2. Performance Monitoring. Report Number: EPA/600/R 99/095 B, 8 Sep 1999, 240.
- Caré, S. et al., 2013. Modeling the permeability loss of metallic iron water filtration systems. *Clean–Soil, Air, Water*, 41(3): 275-282.
- Caré, S., Nguyen, Q.T., l'Hostis, V., Berthaud, Y., 2008. Mechanical properties of the rust layer induced by impressed current method in reinforced mortar. *Cement and Concrete Research*, 38(8-9): 1079-1091
- Chaves, L.H.G., 2005. The role of green rust in the environment: a review. *Revista Brasileira de Engenharia Agrícola e Ambiental*, 9(2): 284-288
- Chen, J.-L., Al-Abed, S.R., Ryan, J.A., Li, Z., 2001. Effects of pH on dechlorination of trichloroethylene by zero-valent iron. *Journal of hazardous materials*, 83(3): 243-254
- Cirpka, O.A., Kitanidis, P.K., 2001. Transport of volatile compounds in porous media in the presence of a

- trapped gas phase. *Journal of contaminant hydrology*, 49(3-4): 263-285.
- Cundy, A.B., Hopkinson, L., Whitby, R.L.D., 2008. Use of iron-based technologies in contaminated land and groundwater remediation: A review. *Science of the total environment*, 400(1-3): 42-51.
- Domga, R., Togue-Kamga, F., Noubactep, C., Tchatchueng, J.-B., 2015. Discussing porosity loss of Fe0 packed water filters at ground level. *Chemical Engineering Journal*, 263: 127-134
- Fu, F., Dionysiou, D.D., Liu, H., 2014. The use of zero-valent iron for groundwater remediation and wastewater treatment: a review. *Journal of hazardous materials*, 267: 194-205
- Furukawa, Y., Kim, J.-w., Watkins, J., Wilkin, R.T., 2002. Formation of ferrihydrite and associated iron corrosion products in permeable reactive barriers of zero-valent iron. *Environmental Science & Technology*, 36(24): 5469-5475
- Gavaskar, A. et al., 2005. Long Term Performance Assessment of a Permeable Reactive Barrier at Former Naval AITR Station Moffett Field. NAVAL FACILITIES ENGINEERING SERVICE CENTER PORT HUENEME CA.
- Ghauch, A., 2015. Iron-based metallic systems: an excellent choice for sustainable water treatment. *FOG-Freiberg Online Geoscience*, 38
- Gheju, M., 2011. Hexavalent chromium reduction with zero-valent iron (ZVI) in aquatic systems. *Water, Air, & Soil Pollution*, 222(1-4): 103-148
- Grauer, R., 1984. Behältermaterialien für die Endlagerung hoch-radioaktiver Abfälle. Korrosionschemische Aspekte. *Nagra NTB 84-19*.
- Gu, B. et al., 2002. Microbiological characteristics in a zero-valent iron reactive barrier. *Environmental monitoring and assessment*, 77(3): 293-309
- Guan, Q. et al., 2019. Assessment of the use of a zero-valent iron permeable reactive barrier for nitrate removal from groundwater in the alluvial plain of the Dagu River, China. *Environmental Earth Sciences*, 78(7): 244
- Guan, X. et al., 2015. The limitations of applying zero-valent iron technology in contaminants sequestration and the corresponding countermeasures: the development in zero-valent iron technology in the last two decades (1994–2014). *Water research*, 75: 224-248
- Gui, L., Yang, Y., Jeon, S.-W., Gillham, R.W., Blowes, D.W., 2009. Reduction of chromate by granular iron in the presence of dissolved CaCO<sub>3</sub>. *Applied geochemistry*, 24(4): 677-686.
- Hammonds, P., 1989. *An Introduction to Corrosion and its Prevention*, Comprehensive Chemical Kinetics. Elsevier, pp. 233-279
- Hao, Z.-W., Xu, X.-H., Wang, D.-H., 2005. Reductive denitrification of nitrate by scrap iron filings. *Journal of Zhejiang University. Science. B*, 6(3): 182.

- Henderson, A.D., Demond, A.H., 2007. Long-term performance of zero-valent iron permeable reactive barriers: a critical review. *Environmental Engineering Science*, 24(4): 401-423
- Henderson, A.D., Demond, A.H., 2011. Impact of solids formation and gas production on the permeability of ZVI PRBs. *Journal of Environmental Engineering*, 137(8): 689-696
- Hu, R. et al., 2020. Metallic iron for environmental remediation: Starting an overdue progress in knowledge. *Water*, 12(3): 641.
- Hu, R.Y., H.; Tao, R.; Cui, X.; Xiao, M.; Amoah, B.K.; Cao, V.; Lufingo, M.; Soppa-Sangue, N.P.; Ndé-Tchoupé, A.I.; Gatcha-Bandjun, N.; Sipowo-Tala, V.R.; Gwenzi, W.; Noubactep, C, 2020. Metallic Iron for Environmental Remediation: Starting an Overdue Progress in Knowledge. *water*, 12(641).
- ITRC, 2011. Permeable reactive barrier: Technology update. The Interstate Technology & Regulatory Council (ITRC) Washington, DC, USA.
- Jeen, S.-W., 2018. Sensitivity Analyses for Modeling Evolving Reactivity of Granular Iron for the Treatment of Trichloroethylene. *Water*, 10(12): 1878.
- Jeen, S.-W., Amos, R.T., Blowes, D.W., 2012. Modeling gas formation and mineral precipitation in a granular iron column. *Environmental science & technology*, 46(12): 6742-6749.
- Jeen, S.-W., Gillham, R.W., Blowes, D.W., 2006. Effects of carbonate precipitates on long-term performance of granular iron for reductive dechlorination of TCE. *Environmental Science & Technology*, 40(20): 6432-6437.
- Jeen, S.-W., Gillham, R.W., Gui, L., 2009. Effects of initial iron corrosion rate on long-term performance of iron permeable reactive barriers: Column experiments and numerical simulation. *Journal of contaminant Hydrology*, 103(3-4): 145-156
- Jeen, S.-W., Gillham, R.W., Przepiora, A., 2011. Predictions of long-term performance of granular iron permeable reactive barriers: Field-scale evaluation. *Journal of Contaminant Hydrology*, 123(1-2): 50-64.
- Jeen, S.-W., Mayer, K.U., Gillham, R.W., Blowes, D.W., 2007. Reactive transport modeling of trichloroethene treatment with declining reactivity of iron. *Environmental science & technology*, 41(4): 1432-1438.
- Jeen, S.-W., O, J.S., Gillham, R.W., 2008. Modeling Geochemical and Reactivity Changes of Different Iron Materials, *GeoCongress 2008: Geotechnics of Waste Management and Remediation*, pp. 595-602.
- Johnson, R.L., Tratnyek, P.G., Miehr, R., Thoms, R.B., Bandstra, J.Z., 2005. Reduction of hydraulic conductivity and reactivity in zero-valent iron columns by oxygen and TNT. *Groundwater Monitoring & Remediation*, 25(1): 129-136.
- Kamolpornwijit, W., Liang, L., 2006. Investigation of gas production and entrapment in granular iron

- medium. *Journal of contaminant hydrology*, 82(3-4): 338-356.
- Kamolpornwijit, W., Liang, L., Moline, G.R., Hart, T., West, O.R., 2004. Identification and quantification of mineral precipitation in Fe<sup>0</sup> filings from a column study. *Environmental science & technology*, 38(21): 5757-5765
- Kamolpornwijit, W., Liang, L., West, O.R., Moline, G.R., Sullivan, A.B., 2003. Preferential flow path development and its influence on long-term PRB performance: column study. *Journal of contaminant hydrology*, 66(3-4): 161-178
- Kiilerich, O., Larsen, J.W., Nielsen, C., Deigaard, L., 2000. Field results from the use of a permeable reactive wall, pp. 377-384.
- Klein, R., Schad, H., 2000. Results from a full scale funnel-and-gate system at the Beka site in Tübingen (Germany) using zero-valent iron. Thomas Telford Ltd, pp. 2: 917-923.
- Konadu-Amoah, B. et al., 2022. Realizing the potential of metallic iron for environmental remediation: Flee or adapt? *Applied Water Science*.
- Korte, N.E., 2001. Zero-valent iron permeable reactive barriers: A review of performance.
- Lai, C.K., Lo, I., 2004. Evaluation of the Hydraulic Performance of a Full Scale Permeable Reactive Barrier by a Tracer Test.
- Lai, K.C., Lo, I.M., Birkelund, V., Kjeldsen, P., 2006. Field monitoring of a permeable reactive barrier for removal of chlorinated organics. *Journal of Environmental Engineering*, 132(2): 199-210.
- Landolt, D., 2007. *Corrosion and surface chemistry of metals*. CRC press.
- Lasaga, A.C., 1984. Chemical kinetics of water-rock interactions. *Journal of geophysical research: solid earth*, 89(B6): 4009-4025.
- Li, G., 2004. Durability behaviour and basic models of reinforced concrete deterioration under climate environments, PhD Thesis, China University of Mining and Technology, Xuzhou, China (In ....
- Li, L., Benson, C.H., Lawson, E.M., 2005. Impact of mineral fouling on hydraulic behavior of permeable reactive barriers. *Groundwater*, 43(4): 582-596
- Li, L., Benson, C.H., Lawson, E.M., 2006. Modeling porosity reductions caused by mineral fouling in continuous-wall permeable reactive barriers. *Journal of Contaminant Hydrology*, 83(1-2): 89-121
- Liang, J. et al., 2013. Impact of flow rate on corrosion of cast iron and quality of re-mineralized seawater reverse osmosis (SWRO) membrane product water. *Desalination*, 322: 76-83
- Liang, L., 2001. Long-term monitoring of permeable reactive barriers-progress report. Oak Ridge National Lab.(ORNL), Oak Ridge, TN (United States).
- Liu, Y., 1996. Modeling the time-to corrosion cracking of the cover concrete in chloride contaminated reinforced concrete structures, Virginia Tech.

- Luo, P., Bailey, E.H., Mooney, S.J., 2013. Quantification of changes in zero valent iron morphology using X-ray computed tomography. *Journal of Environmental Sciences*, 25(11): 2344-2351
- Mackenzie, P.D., Horney, D.P., Sivavec, T.M., 1999. Mineral precipitation and porosity losses in granular iron columns. *Journal of Hazardous Materials*, 68(1-2): 1-17
- Mayer, K.U., Blowes, D.W., Frind, E.O., 2001. Reactive transport modeling of an in situ reactive barrier for the treatment of hexavalent chromium and trichloroethylene in groundwater. *Water Resources Research*, 37(12): 3091-3103
- McMahon, P.B., Dennehy, K.F., Sandstrom, M.W., 1999. Hydraulic and geochemical performance of a permeable reactive barrier containing zero-valent iron, Denver Federal Center. *Groundwater*, 37(3): 396-404.
- Melchers, R.E., Petersen, R.B., 2018. A reinterpretation of the Romanoff NBS data for corrosion of steels in soils. *Corrosion Engineering, Science and Technology*, 53(2): 131-140
- Moraci, N., Ielo, D., Bilardi, S., Calabro, P.S., 2016. Modelling long-term hydraulic conductivity behaviour of zero valent iron column tests for permeable reactive barrier design. *Canadian Geotechnical Journal*, 53(6): 946-961
- Morrison, S.J., Metzler, D.R., Dwyer, B.P., 2002. Removal of As, Mn, Mo, Se, U, V and Zn from groundwater by zero-valent iron in a passive treatment cell: reaction progress modeling. *Journal of Contaminant Hydrology*, 56(1-2): 99-116
- Myers, R.H., 1990. *Classical and modern regression with applications*, 2. Duxbury press Belmont, CA.
- Nešić, S., 2007. Key issues related to modelling of internal corrosion of oil and gas pipelines—A review. *Corrosion science*, 49(12): 4308-4338
- Nicholson, R.V., Cherry, J.A., Reardon, E.J., 1983. Migration of contaminants in groundwater at a landfill: A case study 6. Hydrogeochemistry. *Journal of Hydrology*, 63(1-2): 131-176
- Noubactep, C., 2008. A critical review on the process of contaminant removal in Fe<sup>0</sup>-H<sub>2</sub>O systems. *Environ Technol*, 29(8): 909-20. DOI:10.1080/09593330802131602
- Noubactep, C., 2016a. Predicting the hydraulic conductivity of metallic iron filters: Modeling gone astray. *Water*, 8(4): 162
- Noubactep, C., 2016b. Research on metallic iron for environmental remediation: Stopping growing sloppy science. *Chemosphere*, 153: 528-530.
- O'Hannesin, S.F., Gillham, R.W., 1998. Long-term performance of an in situ "iron wall" for remediation of VOCs. *Groundwater*, 36(1): 164-170
- Obiri-Nyarko, F., Grajales-Mesa, S.J., Malina, G., 2014. An overview of permeable reactive barriers for in situ sustainable groundwater remediation. *Chemosphere*, 111: 243-259

- Ott, N., 2000. Permeable reactive barriers for inorganics. USEPA, Washington DC.
- Pantazopoulou, S.J., Papoulia, K.D., 2001. Modeling cover-cracking due to reinforcement corrosion in RC structures. *Journal of engineering mechanics*, 127(4): 342-351.
- Parbs, A., Ebert, M., Dahmke, A., 2007. Long-term effects of dissolved carbonate species on the degradation of trichloroethylene by zerovalent iron. *Environmental science & technology*, 41(1): 291-296.
- Phillips, D.H. et al., 2000. Performance evaluation of a zerovalent iron reactive barrier: mineralogical characteristics. *Environmental Science & Technology*, 34(19): 4169-4176.
- Phillips, D.H. et al., 2010. Ten year performance evaluation of a field-scale zero-valent iron permeable reactive barrier installed to remediate trichloroethene contaminated groundwater. *Environmental Science & Technology*, 44(10): 3861-3869.
- Phillips, D.H., Watson, D.B., Roh, Y., Gu, B., 2003. Mineralogical characteristics and transformations during long-term operation of a zerovalent iron reactive barrier. *Journal of Environmental Quality*, 32(6): 2033-2045
- Prommer, H., Aziz, L.H., Bolaño, N., Taubald, H., Schüth, C., 2008. Modelling of geochemical and isotopic changes in a column experiment for degradation of TCE by zero-valent iron. *Journal of Contaminant Hydrology*, 97(1-2): 13-26.
- Reardon, E.J., 1995. Anaerobic corrosion of granular iron: Measurement and interpretation of hydrogen evolution rates. *Environmental science & technology*, 29(12): 2936-2945.
- RTDF, 2001. Permeable reactive barrier installation profiles.
- Santisukkasaem, U., Das, D.B., 2019. A non-dimensional analysis of permeability loss in zero-valent iron permeable reactive barrier (PRB). *Transport in Porous Media*, 126(1): 139-159
- Sarr, D., 2001. Zero-Valent-Iron Permeable Reactive Barriers- How Long Will They Last? *Remediation*, 11(2): 1-18
- Sass, B.M. et al., 1998. Evaluating the Moffett Field permeable barrier using groundwater monitoring and geochemical modeling. *Designing and Applying Treatment Technologies: Remediation of Chlorinated and Recalcitrant Compounds*: 169-175.
- Schreier, C.G., Reinhard, M., 1994. Transformation of chlorinated organic compounds by iron and manganese powders in buffered water and in landfill leachate. *Chemosphere*, 29(8): 1743-1753.
- Sikora, E., Macdonald, D.D., 2000. The passivity of iron in the presence of ethylenediaminetetraacetic acid I. General electrochemical behavior. *Journal of the Electrochemical Society*, 147(11): 4087
- Song, D.-I., Kim, Y.H., Shin, W.S., 2005. A simple mathematical analysis on the effect of sand in Cr (VI) reduction using zero valent iron. *Korean Journal of Chemical Engineering*, 22(1): 67-69.

- Sorel, D., Warner, S.D., Longino, B.L., Honniball, J.H., Hamilton, L.A., 2003. Performance monitoring and dissolved hydrogen measurements at a permeable zero valent iron reactive barrier. ACS Publications.
- Stumm, W., Morgan, J.J., Drever, J.I., 1996. Aquatic chemistry. *Journal of environmental quality*, 25(5): 1162.
- Sun, Y., Li, J., Huang, T., Guan, X., 2016. The influences of iron characteristics, operating conditions and solution chemistry on contaminants removal by zero-valent iron: A review. *Water Research*, 100: 277-295.
- Thakur, A.K., Vithanage, M., Das, D.B., Kumar, M., 2020. A review on design, material selection, mechanism, and modelling of permeable reactive barrier for community-scale groundwater treatment. *Environmental Technology & Innovation*, 19: 2352-1864.
- Tsinde, R.T., 2021. Designing and Piloting a household filter for the peri-urban population of Douala (Cameroon), Georg-August-Universität Göttingen.
- Velimirovic, M. et al., 2014. Corrosion rate estimations of microscale zerovalent iron particles via direct hydrogen production measurements. *Journal of hazardous materials*, 270: 18-26
- Vikesland, P.J., Klausen, J., Zimmermann, H., Roberts, A.L., Ball, W.P., 2003. Longevity of granular iron in groundwater treatment processes: changes in solute transport properties over time. *Journal of Contaminant Hydrology*, 64(1-2): 3-33
- Vogan, J.L., Focht, R.M., Clark, D.K., Graham, S.L., 1999. Performance evaluation of a permeable reactive barrier for remediation of dissolved chlorinated solvents in groundwater. *Journal of Hazardous Materials*, 68(1-2): 97-108.
- Wang, Q. et al., 2022. In situ remediation of Cr (VI) contaminated groundwater by ZVI-PRB and the corresponding indigenous microbial community responses: a field-scale study. *Science of The Total Environment*, 805: 150260.
- Weber, A., Ruhl, A.S., Amos, R.T., 2013. Investigating dominant processes in ZVI permeable reactive barriers using reactive transport modeling. *Journal of contaminant hydrology*, 151: 68-82.
- Wilkin, R.T. et al., 2014. Fifteen-year assessment of a permeable reactive barrier for treatment of chromate and trichloroethylene in groundwater. *Science of the total environment*, 468: 186-194.
- Wilkin, R.T. et al., 2018. Geochemical and isotope study of trichloroethene degradation in a zero-valent iron permeable reactive barrier: A twenty-two-year performance evaluation. *Environmental science & technology*, 53(1): 296-306
- Wilkin, R.T., Puls, R.W., Sewell, G.W., 2002. Long-term performance of permeable reactive barriers using zero-valent iron: An evaluation at two sites. NATIONAL RISK MANAGEMENT RESEARCH LAB ADA OK.

- Wilkin, R.T., Puls, R.W., Sewell, G.W., 2003. Long-term performance of permeable reactive barriers using zero-valent iron: geochemical and microbiological effects. *Ground Water*, 41(4): 493
- Wilkin, R.T., Su, C., Ford, R.G., Paul, C.J., 2005. Chromium-removal processes during groundwater remediation by a zerovalent iron permeable reactive barrier. *Environmental science & technology*, 39(12): 4599-4605
- Wu, Q., Zheng, C., Zhang, J., Zhang, F., 2017. Nitrate removal by a permeable reactive barrier of Fe 0: A model-based evaluation. *Journal of Earth Science*, 28(3): 447-456
- Xin, J. et al., 2018. Investigating the efficiency of microscale zero valent iron-based in situ reactive zone (mZVI-IRZ) for TCE removal in fresh and saline groundwater. *Science of the Total Environment*, 626: 638-649.
- Yabusaki, S., Cantrell, K., Sass, B., Steefel, C., 2001. Multicomponent reactive transport in an in situ zero-valent iron cell. *Environmental Science & Technology*, 35(7): 1493-1503
- Yang, H., Hu, R., Ruppert, H., Noubactep, C., 2021. Modeling porosity loss in Fe<sub>0</sub>-based permeable reactive barriers with Faraday's law. *Scientific Reports*, 11(1): 1-13.
- Yang, Y.T., 2009. Research on Concrete Resistivity and Reinforced Concrete Steel Corrosion Rate. Dalian, China: Dalian University of Technology (In Chinese).
- Zhang, Y., Gillham, R.W., 2005. Effects of gas generation and precipitates on performance of Fe PRBs. *Groundwater*, 43(1): 113-121.



## Chapter 3

### 3. Modeling porosity loss in Fe<sup>0</sup>-based permeable reactive barriers with Faraday's law

Huichen Yang<sup>1\*</sup>, Rui Hu<sup>2</sup>, Hans Ruppert<sup>3</sup>, Chicgoua Noubactep<sup>1,4</sup>

<sup>1</sup> Angewandte Geologie, University of Göttingen, Goldschmidtstraße 3, D - 37077 Göttingen, Germany;  
[huichen.yang@geo.uni-goettingen.de](mailto:huichen.yang@geo.uni-goettingen.de)

<sup>2</sup> School of Earth Science and Engineering, Hohai University, Fo Cheng Xi Road 8, 211100 Nanjing, P.R. China;  
[rhu@hhu.edu.cn](mailto:rhu@hhu.edu.cn)

<sup>3</sup> Department of Sedimentology & Environmental Geology, University of Göttingen, Goldschmidtstraße 3, Göttingen D-37077, Germany; [hripper@gwdg.de](mailto:hripper@gwdg.de)

<sup>4</sup> Centre for Modern Indian Studies (CeMIS), University of Göttingen, Waldweg 26, D - 37073 Göttingen, Germany;  
[cnoubac@gwdg.de](mailto:cnoubac@gwdg.de)

\* Correspondence: [huichen.yang@geo.uni-goettingen.de](mailto:huichen.yang@geo.uni-goettingen.de)

#### Citation:

Yang H, Hu R, Ruppert H, Noubactep, C. Modeling porosity loss in Fe<sup>0</sup>-based permeable reactive barriers with Faraday's law[J]. Scientific Reports, 2021, 11(1): 1-13.

#### Abstract

Solid iron corrosion products (FeCPs), continuously generated from iron corrosion in Fe<sup>0</sup>-based permeable reactive barriers (PRB) at pH>4.5, can lead to significant porosity loss and possibility of system's failure. To avoid such failure and to estimate the long-term performance of PRBs, reliable models are required. In this study, a mathematical model is presented to describe the porosity change of a hypothetical Fe<sup>0</sup>-based PRB through-flowed by deionized water. The porosity loss is solely caused by iron corrosion process. The new model is based on Faraday's Law and considers the iron surface passivation. Experimental results from literature were used to calibrate the parameters of the model. The derived iron corrosion rates (2.60 mmol/(kg·d), 2.07 mmol/(kg·d) and 1.77 mmol/(kg·d)) are significantly larger than the corrosion rate used in previous modeling studies (0.4 mmol/(kg·d)). This suggests that the previous models have underestimated the impact of in-situ generated FeCPs on the porosity loss. The model results show that the assumptions for the iron corrosion rates on basis of a first-order dependency on iron surface area are only valid when no iron surface passivation is considered. The simulations demonstrate that volume-expansion by Fe<sup>0</sup> corrosion products alone can cause a great extent of porosity loss and suggests careful evaluation of the iron corrosion process in individual Fe<sup>0</sup>-based PRB.

#### Keywords:

Faraday's Law, Iron corrosion, Iron passivation, Permeable reactive barriers, Porosity loss, Zero-valent iron

### 3.1 Introduction

Permeable reactive barriers (PRBs) are an in-situ technology for remediation of contaminated groundwater (McMurtry and Elton, 1985; O'Hannesin and Gillham, 1998; Starr and Cherry, 1994; Tratnyek et al., 2002). It consists of subsurface filters filled with reactive materials to clean through-flowing polluted groundwater. PRB containing granular metallic iron ( $\text{Fe}^0$ ) has been demonstrated to be a promising, economically-feasible and environmentally-friendly technology for groundwater remediation (Ghauch, 2015; Gheju, 2011; Guan et al., 2015; Henderson and Demond, 2007; Lee et al., 2004). Polluted water with a broad range of chemical species such as halogenated organics (Arnold and Roberts, 2000), nitroaromatics (Agrawal and Tratnyek, 1995; Keum and Li, 2004), dyes (Nam and Tratnyek, 2000), phenolic compounds (Morales et al., 2002), heavy metals (Rangsivek and Jekel, 2005) and various oxyanions (Neumann et al., 2013; Sun et al., 2014) can be efficiently treated by applying metallic iron-based permeable reactive barrier.

Although the performance of  $\text{Fe}^0$ -based PRBs are generally satisfactory, questions remain on the long-term effectiveness of PRBs, which are expected to operate for decades (Gillham, 1999; Li et al., 2006; Warner and Sorel, 2003). Permeability loss is one key of concern. Researchers have reported that the main cause of permeability loss is the reduction in pore space caused by mineral precipitation on the surface of  $\text{Fe}^0$  (Johnson et al., 2005; Mackenzie et al., 1999; Phillips et al., 2000; Phillips et al., 2003; Roh et al., 2000; Vikesland et al., 2003; Wilkin et al., 2003; Wilkin et al., 2005; Zhang and Gillham, 2005). Clogging of the pore space in the reactive zone reduces the porosity and hydraulic conductivity of the reactive medium, which can result in preferential flow patterns, bypassing and changes in residence time (Li et al., 2005; Li et al., 2006).

At pH 4.5 to 8.5, which is the typical range of PRBs operation, there is continuing aqueous iron corrosion at the surface of  $\text{Fe}^0$ . The chemical composition of the FeCPs depends upon the local pH-Eh conditions under which the reaction takes place (Pantazopoulou and Papoulia, 2001). All the possible corrosion products have much less density compared to the parent metal, which makes the iron corrosion a highly volumetric expansive process (Caré et al., 2013; Pilling, 1923). Depending on the level of oxidation, iron may expand by as much as six times its original volume (Liu and Weyers, 1998). Therefore, the very first cause of permeability loss in  $\text{Fe}^0$ -based PRBs is pore filling with iron corrosion products (Domga et al., 2015).

The expansive nature of iron corrosion has been properly considered in reinforced concrete (RC) industry. In that context, the volumetric expansion of the iron induces internal pressure on the surrounding concrete, causing the cracking of cover concrete and affecting the service

life of the structures (Andrade et al., 1993). A number of investigations have been conducted for the study of the cracking of cover concrete induced by corrosion (Bhargava et al., 2005; Du et al., 2014; Lu et al., 2011). On the contrary, in the Fe<sup>0</sup>-PRB literature, iron volumetric expansion process has not been properly considered (Domga et al., 2015). A phenomenological model was established by Kouznetsova et al. (Kouznetsova et al., 2007) to estimate the long-term performance of Fe<sup>0</sup>. The model described the decline of iron reactivity as a function of space and time by observing the degradation of chlorinated ethanes, but didn't consider iron corrosion processes. Numerous detailed geochemical models were proposed to simulate the chemical reactions and flow transport inside Fe<sup>0</sup>-PRB and the effect of mineral precipitation on hydraulic properties of PRBs (Li et al., 2005; Li et al., 2006; Mayer et al., 2001; Moraci et al., 2016; Yabusaki et al., 2001). The iron corrosion rate in these models is expressed with a first-order dependence on iron surface area, and the rate coefficient was derived from the report of Reardon (Reardon, 1995). According to the modeling results, it is perceived that the permeability loss is mainly caused by foreign precipitates (e.g. CaCO<sub>3</sub>) or mixed precipitates (e.g. with FeCO<sub>3</sub>) (Li et al., 2006). Moreover, iron surface passivation is not considered in previous studies. However, above pH-4.8 and in an oxygen containing aqueous environment the generated porous oxide layers contains three-valent iron causing strong inhibition effect on the iron corrosion (Lorbeer and Lorenz, 1980). In this study, Iron surface passivation is described as linear or parabolic growth of corrosion products (Liu, 1996; Sheir et al., 1994).

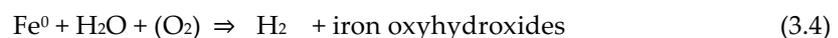
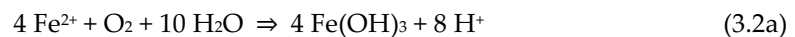
The aging behavior due to corrosion of iron particles was investigated most of the time using column tests or by measuring the hydrogen pressure build-up in long-term batch studies (Jeen et al., 2008; Kamolpornwijit et al., 2004; Kamolpornwijit et al., 2003; Reardon, 1995). According to previous studies, the estimated life-time of iron granular particles ranged from several years to several decades (Farrell et al., 2000; Klausen et al., 2003). Some studies assumed that iron particles will be completely consumed in the reaction of groundwater and estimated the life-time of Fe<sup>0</sup>-based PRB by the iron mass and iron corrosion rate (Liu et al., 2007; Odziemkowski et al., 2000; Scherer et al., 2000; Velimirovic et al., 2014). This approach to estimate the PRB service life is only valid, if the initial PRB pore volume and the used Fe<sup>0</sup>/aggregate ratio enable complete Fe<sup>0</sup> depletion (Domga et al., 2015; Noubactep, 2016). In this study, the residual amount of Fe<sup>0</sup> and the residual pore space of the PRB are calculated on a time-line to evaluate this life-time estimation method.

Therefore, in this study, a mathematical model is formulated to study the porosity loss of Fe<sup>0</sup>-based PRB solely caused by the volumetric expansive corrosion of iron based on Faraday's Law including iron surface passivation. For simplification, iron corrosion in the deionized (DI)

water is considered. Based on the results of Luo et al. (Luo et al., 2013), which show the porosity change of iron exposed to deionized water, our model is calibrated in order to simulate the porosity loss for long-term operation.

### 3.2 Fundamental of Fe/H<sub>2</sub>O system

Since Fe<sup>0</sup> is not stable under environmental conditions, and the redox couple H<sup>+</sup>/H<sub>2</sub>(E<sub>0</sub>=0.00 V) is higher than that of Fe<sup>II</sup>/Fe<sup>0</sup>(E<sub>0</sub>=-0.44 V) at a<sub>H<sup>+</sup></sub> = 1 (Hu et al., 2019; Landolt, 2007), a transfer of electrons from the Fe<sup>0</sup> body (solid state) to the Fe/H<sub>2</sub>O interface occurs whenever a Fe<sup>0</sup> specimen is immersed in an aqueous solution (Hammonds, 1989; Landolt, 2007; Nešić, 2007). Equations 3.1a,b show that the oxidative dissolution of Fe<sup>0</sup> by protons (H<sup>+</sup>) from water (H<sub>2</sub>O ⇌ H<sup>+</sup> + OH<sup>-</sup>) forms Fe<sup>2+</sup> and Fe(OH)<sub>2</sub> by increasing the pH. In the presence of dissolved oxygen, Fe<sup>2+</sup> and Fe(OH)<sub>2</sub> can be oxidized to less soluble Fe(OH)<sub>3</sub> (Equations 3.2a,b). Fe(OH)<sub>2</sub> and Fe(OH)<sub>3</sub> are polymerized and further transformed to various oxyhydroxides (Equation 3.3) (Chaves, 2005; Hu, 2020; Landolt, 2007; Sikora and Macdonald, 2000). Equation 3.4 summarizes the process of aqueous iron corrosion.



Comprehensive research on Fe<sup>0</sup> for water treatment revealed that the generation of iron oxyhydroxides (iron corrosion products or FeCPs) is the basis of contaminant removal in Fe<sup>0</sup>/H<sub>2</sub>O systems (Ghauch, 2015; Gheju, 2011; Hu et al., 2019; Noubactep, 2008). Figure 3.1 depicts the principle of contaminant removal process in Fe<sup>0</sup>/H<sub>2</sub>O system. The electrochemical corrosion of immersed Fe<sup>0</sup> induces the generation of reducing agents, i.e. Fe<sup>2+</sup>, Fe(OH)<sub>2</sub> and H<sub>2</sub> (Equation 3, 1a,b). The generated iron oxyhydroxides on Fe<sup>0</sup> (red layer) is an adsorbent for contaminants, as well as a contaminant scavenger (Equation 3, 2a,b).

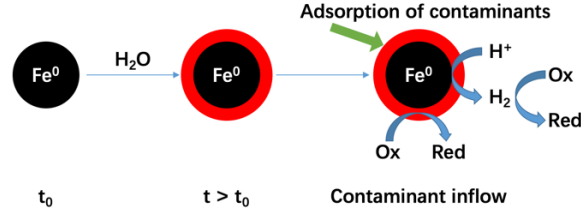


Figure 3.1 Principle of contaminant removal process in Fe<sup>0</sup>/H<sub>2</sub>O system

However, the generation of FeCPs has the side effect of being expansive. Thus, modeling the volume-expansion process is essential to design an efficient and sustainable Fe<sup>0</sup>/H<sub>2</sub>O filter system.

### 3.3 Modeling porosity loss in Fe<sup>0</sup>-based PRB

#### 3.3.1 Description of the model based on Faraday's Law

Faraday's Law describes the fundamental quantitative relationship of redox partners in electrochemistry. It depicts the relationship between the amount of material reacting during electrochemical reactions according to the average current and the total reaction time (Faraday, 1834). Equation 3.5 summarizes Faraday's Law:

$$m = \frac{QM}{Fz'} \quad (3.5)$$

where  $m$  is the mass of the substance liberated or deposited at the electrode (gram);  $Q$  is the total electric charge (Coulombs or Amperes·seconds);  $M$  is the molar mass of the substance (g/mol),  $F$  is the Faraday constant; and  $z$  is the valency of an ion formed from the reacting substance.

For Fe<sup>0</sup> oxidative dissolution electrochemical reaction (Eq. 3.1), Equation 3.5 can be transformed by using Equations 3.6 and 3.7 into Equation 3.8:

$$Q = It, \quad (3.6)$$

$$I = iA, \quad (3.7)$$

$$\partial V_{iron} = \frac{M}{zF\rho} A \cdot i \cdot \partial t, \quad (3.8)$$

where  $I$  is the current (Ampere),  $t$  the reaction time (s),  $i$  the current density (Ampere/m<sup>2</sup>) and  $A$  the surface area of iron (m<sup>2</sup>).  $\partial V_{iron}$  is the volume depletion of iron,  $\rho$  the density of iron = 7.85×10<sup>3</sup> kg/m<sup>3</sup>,  $M$  = 55.85 g/mol,  $F$  = 96500 C/mol;  $z$  is taken equal to 2 (Equation 3.1a).

Assuming the iron particle is a sphere, we obtain for one iron particle

$$\partial V_{iron} \approx A \cdot \partial r_{iron}, \quad (3.9)$$

where  $\partial r_{iron}$  is the radius depletion of the iron particle. Combining Equation 3.8 and Equation 3.9, we get:

$$\frac{\partial r_{iron}}{\partial t} = \frac{M}{zF\rho} \cdot i, \quad (3.10)$$

where  $\frac{\partial r_{iron}}{\partial t}$  is the corrosion rate (in mm/y) and  $\frac{M}{zF\rho}$  is a constant. So the corrosion rate (in mm/y) and the current density are linearly related.

### 3.3.2 Calculation of the coefficient of volumetric expansion

As discussed above, the generation of FeCPs is a volumetric-expansion process. A coefficient of volumetric expansion ( $\eta$ ) is introduced to describe this behavior. Equation 3.11 states the definition of  $\eta$ :

$$V_{oxide} = \eta V_{iron}, \quad (3.11)$$

where  $V_{oxide}$  is the volume of the generated FeCPs. The change of volume and radius can be described as follows:

$$\partial V_{expansion} = \partial V_{oxide} - \partial V_{iron} = (\eta - 1)\partial V_{iron}, \quad (3.12)$$

$$\partial r_{expansion} = \partial r_{oxide} - \partial r_{iron} = (\eta - 1)\partial r_{iron}, \quad (3.13)$$

where  $V_{expansion}$  is the expansion volume,  $r_{oxide}$  is the increased radius with the generation of FeCPs and  $r_{expansion}$  is the expansion radius of the iron particle.

If we combine Equation 3.8 and Equation 3.12, we have the expression of the total volume change ( $\Delta V$ ) over time as:

$$\Delta V = V_{expansion} = \int_0^t (\eta - 1) \frac{M}{zF\rho} \cdot A \cdot i \cdot \partial t. \quad (3.14)$$

Due to the complexity of the iron corrosion product,  $\eta$  varies with different corrosion environment and Fe<sup>0</sup> intrinsic reactivity (Hu, 2020). Table 3.1 depicts the volumetric expansion coefficients of different possible corrosion products based on the study of Caré et al. (Caré et al., 2013).

Table 3.1 Volumetric expansion coefficients of possible corrosion products

Phase	Name	volumetric expansion coefficient ( $\eta$ )
Fe(OH) <sub>3</sub>	Fe <sup>III</sup> hydroxide	4.53
FeCO <sub>3</sub>	Siderite	3.86
Fe(OH) <sub>2</sub>	Fe <sup>II</sup> hydroxide	3.47
$\alpha$ -FeOOH	Goethite	2.67
$\alpha$ -Fe <sub>2</sub> O <sub>3</sub>	Hematite	1.98
$\gamma$ -Fe <sub>2</sub> O <sub>3</sub>	Maghemite	1.91
Fe <sub>3</sub> O <sub>4</sub>	Magnetite	1.97

### 3.3.3 Estimate of growth of corrosion products and passivation

The growth of corrosion products may follow a linear or parabolic law depending on the metal properties and geochemical conditions (Liu, 1996; Sheir et al., 1994). Due the complexity of iron corrosion, both linear and parabolic law are considered in this study.

For a metal that the generated oxide film is not protective, which means that no passivation occurs, the rate of growth of oxide film remains constant:

$$y = kt, \quad (3.15)$$

where  $k$  is a constant,  $y$  is the film thickness (m) and  $t$  is the corrosion time.

For a metal that forms a protective oxide film,

$$y^2 = kt. \quad (3.16)$$

However, the relationship between corrosion rate and time is not so simple. The following equation is usually used (Tomashov, 1965):

$$y^n = kt, \quad (3.17)$$

where  $n$  is the coefficient of passivation. The value of  $n$  is usually larger than 1. In case of iron corrosion in air or corrosion in soil,  $n$  ranges from 1 to 3 depending on the suppression of diffusion of oxygen through the formed oxide film (Tomashov, 1965).

The coefficients of passivation  $n$  are taken equal to 1, 1.5 and 2 respectively in this study. For  $n = 1$ , the rate of growth of oxide film on the iron surface remains constant and the passivation of Fe<sup>0</sup> is not considered. For  $n = 2$ , it means that iron passivation occurs during the corrosion process and the generated corrosion products form a protective oxide film. For the case  $n = 1.5$ , iron passivation occurs with time but the oxide film on the surface of iron is not completely protective.

Combining Equation 3.10 and Equation 3.13, we have:

$$y = \int r_{\text{oxide}} = \int \frac{M\eta}{zF\rho} \cdot i \cdot \partial t. \quad (3.18)$$

For  $n = 1$ , with Equation 3.15 and 3.18, we obtain:

$$y = \int \frac{M\eta}{zF\rho} \cdot i \cdot \partial t = kt \quad (3.19)$$

From the right part of Equation 3.19 we can conclude, that when no passivation is considered, the current density ( $i$ ) and corrosion rate (in mm/y) (Equation 3.10) are constants.

If we consider iron passivation occurs in the system, Equation 3.17 and 3.18 transform into:

$$y^n = \left( \int \frac{M\eta}{zF\rho} \cdot i \cdot \partial t \right)^n = kt. \quad (3.20)$$

For  $n = 2$ , from Equation 3.20, we get:

$$i = \frac{k^{0.5}}{\frac{M\eta}{zF\rho}} \cdot t^{-0.5} = \alpha \cdot t^{-0.5}, \quad (3.21)$$

where  $\alpha$  is a constant. For  $n = 1.5$ , Equation 3.20 simplifies into:

$$i = \beta \cdot t^{-\frac{1}{3}}, \quad (3.22)$$

where  $\beta$  is a constant.

### 3.3.4 Estimate of surface area and porosity change

The iron surface area is constantly changing during the operation. The area changes can be calculated by the following equations:

$$A = N \cdot 4\pi r^2 = N \cdot 4\pi (r_0 - r_{depletion})^2, \quad (3.23)$$

$$r_{depletion} = \int_0^t \frac{M}{zF\rho} \cdot i \cdot \partial t, \quad (3.24)$$

where  $N$  is the total iron particle number,  $r_0$  is the initial radius of iron particles.

The total iron particle number can be calculated by equation 3.25:

$$N = \frac{V_{solid}^0 \cdot \tau_{iron}}{\frac{4}{3} \cdot \pi r_0^3}, \quad (3.25)$$

where  $V_{solid}^0$  is the initial volume occupied by the solid particles (i.e. iron and sand particles), and  $\tau_{iron}$  is the initial iron volume ratio.

The porosity of the system ( $\Phi$ ) can be described as follow:

$$\Phi = \frac{1 - V_{solid}}{V_{reactive\ zone}} = 1 - \frac{V_{solid}^0 + \Delta V}{V_{reactive\ zone}}, \quad (3.26)$$

where  $V_{reactive\ zone}$  is the volume of the reactive zone, and  $\Delta V$  is the total volume change (equation 3.14).

### 3.3.5 Model assumptions

A simplified illustration of the model is shown in Figure 3.2. As iron constantly transforms in the water, the radius of the iron particle decreases with time. In the meanwhile, the generated FeCPs, which have larger volumes than the  $Fe^0$ , fill the pore space and cause the porosity loss in the system. The following assumptions are made in this model:

- All iron particles are spheres and have identical radius, which is taken equal to 1 mm;
- Uniform  $Fe^0$  corrosion: the radius reduction of spherical  $Fe^0$  particles is the same for all particles;
- The volume of the reactive zone remains constant;
- $Fe^0$  corrosion products progressively fill the available pore space.

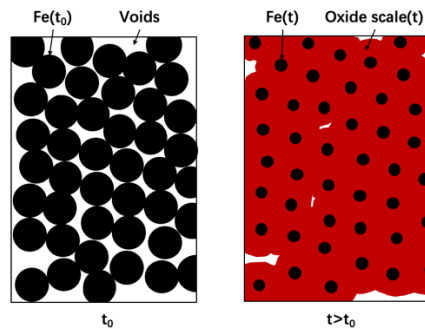


Figure 3.2 Illustration of the reactive zone before (left) and after corrosion of a layer of metallic iron (right)

### 3.3.6 Model calibration

The results of Luo et al. (Luo et al., 2013) are used to calibrate the current density in this model. The corrosion rate (in mm/y) can be obtained with the calibrated current density value (Equation 3.10).

In Luo et al.'s study, iron/sand mixtures were packed between two layers of sand in the column experiments. Three iron mixing ratios (100%, 50%, 10%, w/w) of the barrier material were tested for different water type (a synthetic groundwater, acidic drainage and deionized (DI) water). The porosity data for only 100%  $Fe^0$  columns which tested with DI water were reported. Since

this study considers the condition that iron corrodes in DI water, the porosity change data for 100% Fe<sup>0</sup> column reacted with DI water were used to calibrate the parameters of the model. These parameters were then used to simulate the porosity loss in the systems with different iron mixing ratios.

The authors reported a porosity loss from 57% to 32% when 100% Fe<sup>0</sup> column are exposed to deionized water within 16 days under 2 mL/min flow velocity. The flow condition is 56 times greater than the average flow rate at a typical PRB installation (Interstate and Regulatory, 2005). In order to estimate the real operation of PRBs, the aging of the fast flow experiment have to be scaled to real time conditions. The surface-loading rate was used in the calculation. At this fast-flow rate, 16 days represents an equivalent reaction period of 2.2 years (800 days) under typical field conditions, as the surface-loading rate is proportional to flow velocity (Kamolpornwijit et al., 2003). This prediction does not include the effect of kinetics on precipitation due to increased velocity and reduced residence time, and the operating life of PRBs will be overestimated using results from fast flow rate experiment (Kamolpornwijit et al., 2004; Kamolpornwijit et al., 2003).

The grain size was reported as between 2.38 and 0.30 mm. Since a uniform particle radius is assumed in this study, the grain size taken was equal to 2 mm.

### *3.3.7 Model results*

#### *3.3.7.1 Corrosion rates for different coefficients of passivation*

The current density (*i*) is the calibrated parameter in this study. The corrosion rate value can be then calculated (Equation 10). The corrosion rate (in mm/y) is either a constant value or a function of the corrosion time when different coefficients of passivation (*n*) are taken. The derived corrosion rate values are shown in Figure 3.3. It is assumed that goethite (FeOOH) is the only corrosion product, which is reported by Luo et al. (Luo et al., 2013) on the basis of SEM images and EDX spectra results.

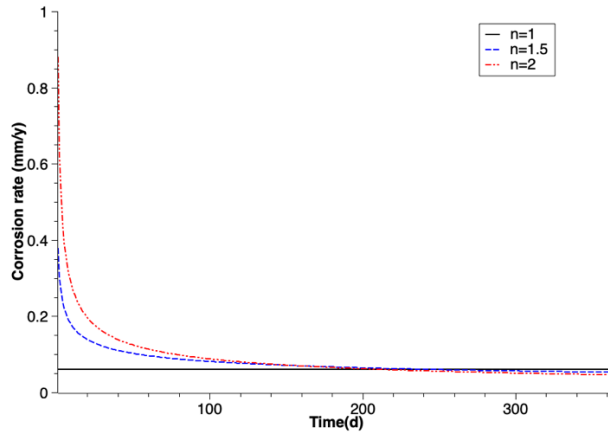


Figure 3.3 Corrosion rates versus time ( $n$  is the coefficient of passivation) assuming goethite is the corrosion product

The corrosion rate (in mm/y) is a constant ( $=0.06\text{mm/y}$ ) if the passivation of iron corrosion is neglected. When the passivation of iron is considered ( $n > 1$ ), dramatic variations of the calibrated corrosion rate values are detected in the beginning phase of corrosion. The initial corrosion rate values are significantly large, which are  $0.88\text{ mm/y}$  for the coefficient of passivation  $n = 2$  and  $0.38\text{ mm/y}$  for  $n = 1.5$ . The rates decrease rapidly and reach a relatively stable value after 200 days of corrosion. The average stable corrosion rate value is  $0.055\text{ mm/y}$ .

### 3.3.7.2 Relative porosity loss for different coefficients of passivation

Figure 3.4 depicts the simulations of long-term porosity changes for different corrosion patterns. It is assumed that goethite is the only corrosion product. The Y-axis in the figure represents the relative porosity of the system, which can be described as

$$\text{Relative porosity} = \frac{\Phi}{\Phi_0} \quad (3.27)$$

where  $\Phi$  is the porosity at time  $t$  and  $\Phi_0$  is the initial porosity of the system.

Significant porosity losses can be detected in all three simulations (Fig.3.4). The simulation with constant corrosion rate (in mm/y) shows the most remarkable porosity reduction, which decreases to 0 on day 2464. Zero relative porosity means there is no pore space left in the barrier, i.e. no underground water can flow through the PRB. Thus, the PRB has no water remediation effect after day 2464.

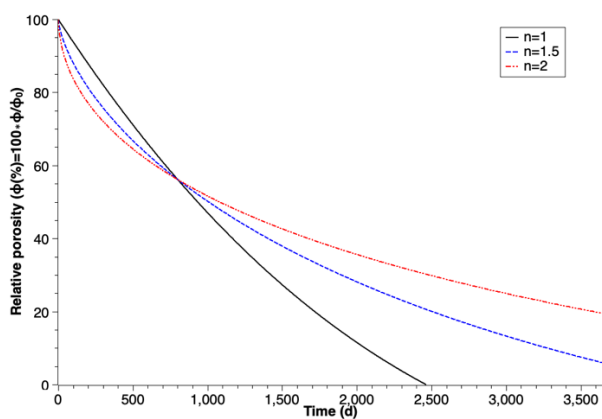


Figure 3.4 Percentage decrease of relative porosity through the formation of goethite over time for different coefficients of passivation (n)

The relative porosity values of three simulations show dissimilar features along corrosion pathway and also divergent results after long-term simulation. After 10 years of simulation, the relative porosity values decrease to 5.94% for coefficient of passivation of  $n = 1.5$  and 19.50% for  $n = 2$ . The simulation with higher coefficient of passivation (n) shows a more rapid porosity loss in the beginning phase but only slight porosity change after long-term corrosion. This indicates that the rate of diffusion process decreases with the increase of the thickness of the generated corrosion products. The differences among the three simulation results indicate that the iron passivation is an important factor determining porosity for  $\text{Fe}^0$ -based PRBs' long-term performance estimation.

### 3.3.7.3 Relative porosity loss for different iron mixing ratios

The calculated corrosion rates were utilized to simulate the porosity loss in the systems with different iron mixing ratios. Figure 3.5 depicts the relative porosity change along time with iron mixing ratios of 10%, 50% and 100% (W/W). It can be seen that a lower percentage of  $\text{Fe}^0$  within the barrier shows less porosity reduction during long-term operation.

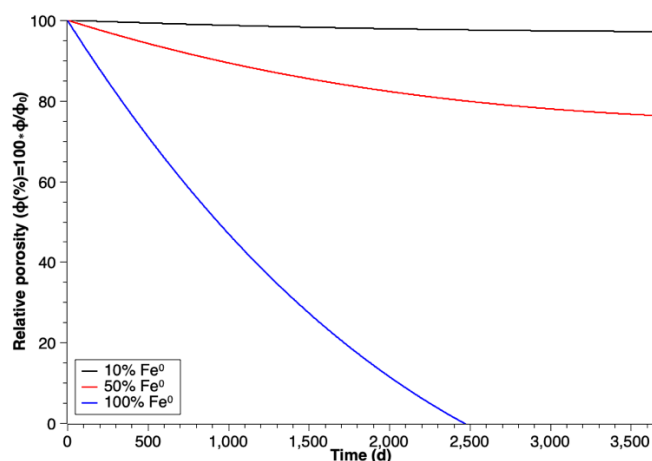


Figure 3.5 Percentage decrease of relative porosity through the formation of goethite over time for different iron mixing ratios and  $n = 1$

### 3.3.7.4 Relative porosity loss for different corrosion products

The previous simulations in this study all assume that goethite is the only corrosion product of iron corrosion. However, in the real corrosion process, other FeCPs may form. Figure 3.6 illustrates the porosity loss simulations for different possible corrosion products with no iron passivation considered. All possible iron corrosion products have a larger volume than the corroded iron. In general, the simulations with higher coefficients of volumetric expansion ( $\eta$ ) show stronger porosity reduction. The results of the simulations imply that iron corrosion products have an important effect on the porosity reduction of the PRB system.

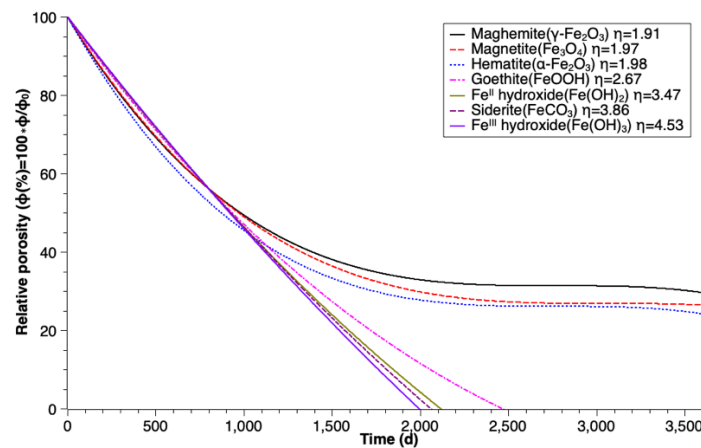


Figure 3.6 Percentage decrease of relative porosity over time for different corrosion products ( $\eta$  is the coefficient of volumetric expansion) for  $n = 1$ .

## 3.4 Implications for the estimation of the durability of Fe-based PRB

Figure 3.7 shows the calculated porosity and  $\text{Fe}^0$  volume decrease with time by the formation of goethite. According to simulation results, when the porosity value of the simulation with constant corrosion rate (in mm/y) reaches 0, there is still  $0.09 \text{ m}^3/\text{m}^3$   $\text{Fe}^0$  volume fraction left in the system. It means the PRB system loses its capability to remove contaminants before the iron is completely consumed. Therefore, the previous method to estimate the lifetime of  $\text{Fe}^0$  on basis of the corrosion rate (Velimirovic et al., 2014), which assumes the iron will be totally oxidized, cannot be used to estimate the service lifetime of iron-based PRB systems. Moreover, this study simulates only the contact of  $\text{Fe}^0$  and deionized water and considers merely the effect of expansive volume of iron corrosion. If the geochemical condition changes, e.g. the solution has

high calcium concentration, which will cause additional mineral precipitation in the iron zone and trigger even larger porosity loss, an earlier failure of PRB technique can be expected.

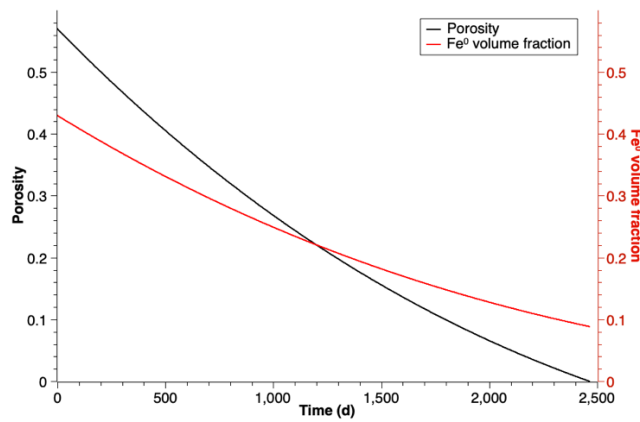
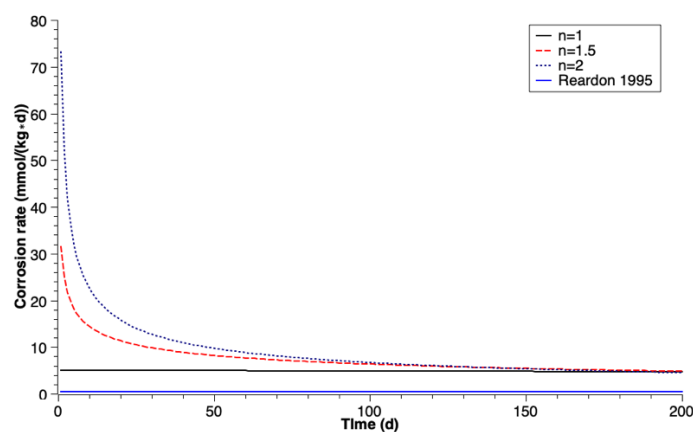


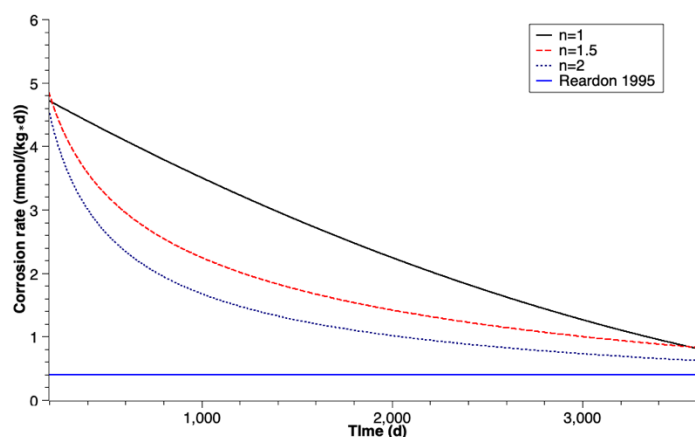
Figure 3.7 Porosity and Fe<sup>0</sup> volume fraction versus time assuming goethite as reaction product

### 3.5 Comparison of corrosion rates in different studies

It is difficult to compare the corrosion rate results of this study with those of previous studies, since different units of corrosion rate were used (e.g. mmol/(kg·d), mol/(m<sup>2</sup>·d), etc.) in former studies. The most frequently used corrosion rate value in Fe<sup>0</sup>-based PRB modeling studies is derived from the report of Reardon et al. (1995). Reardon measured the iron corrosion rates by monitoring the hydrogen pressure increase in sealed cells containing iron granules and water. The corrosion rate was given in mmol/(kg·d). The units of corrosion rates in this study are converted to mmol/(kg·d) and the results are shown in Figure 3.8a and b.



(a)



(b)

Figure 3.8 Comparison of corrosion rates with results from Reardon (1995) ( $n$  is the coefficient of passivation) assuming goethite as reaction product (a) 0 to 200 days, (b) 200 to 3650 days

Differences of more than an order of magnitude are shown between the calibrated corrosion rates in this study and the data reported by Reardon (1995) at the beginning of corrosion. The initial corrosion rates with different coefficients of passivation ( $n$ ) in this study are 5.0 mmol/(kg·d) ( $n=1$ ), 31.4 mmol/(kg·d) ( $n=1.5$ ) and 73.2 mmol/(kg·d) ( $n=2$ ) respectively. The corrosion rates strongly decrease over time and the average corrosion rates of a 10 years simulation are 2.60 mmol/(kg·d) ( $n=1$ ), 2.07 mmol/(kg·d) ( $n=1.5$ ), and 1.77 mmol/(kg·d) ( $n=2$ ) respectively. These rates are higher than the rate of 0.4 mmol/(kg·d) for deionized water published by Reardon (Reardon, 1995) but fall within the range of reported corrosion rates of 0.2-50 mmol/(kg·d) (Kamolpornwijit et al., 2004).

The relatively low corrosion rates reported by Reardon 1995 contradicts to the porosity reduction (57% to 32%) observed by Luo et al. (2013). In both cases, deionized water was in contact with granular iron. The possible reasons for this remarkable difference are (i). Reardon measured the corrosion rates with a batch experiment with no water flow (rate = 0). But in typical PRB systems, the underground water flows through the barrier under the natural hydraulic gradient, which increases the iron corrosion rate (Liang et al., 2013). (ii). Reardon monitored the hydrogen pressure increase in sealed cells. The increasing hydrogen partial pressure may inhibit the iron corrosion reaction. For a real site PRB, the generated hydrogen can escape immediately from the system. (iii). The intrinsic reactivity of iron materials varies significantly which may cause an order magnitude difference in corrosion rate (Hu et al., 2020). Model approaches on the basis of data from Reardon (1995) underestimate the iron corrosion process as well as the influence of the iron corrosion products on the porosity of the PRB system during the long-term operation. With higher corrosion rates of iron, more iron will react in the

water, and larger amount of iron corrosion products are generated. The increasing generated corrosion products can fill the pore in the barrier quickly and cause the early failure of the PRB technique.

Moreover, the reaction process is very complicated in the real PRB systems. The iron corrosion rate is easily influenced by many factors (Li et al., 2006) and can vary dramatically in different parts of the PRB. For example, dissolved oxygen (DO) is consumed once it enter the iron zone, and it can accelerate the iron corrosion process, which induces more corrosion products, and thus higher porosity reduction in the entrance zone of PRBs (Wilkin et al., 2003).

### 3.6 Considerations on reactive surface area change versus time

The reactive surface area of  $\text{Fe}^0$  in this study can be calculated by the depletion of the radius of the iron particles (equation 3.10) and the assumption of uniform corrosion. Plots of calculated reactive surface area of different coefficients of passivation ( $n$ ) over time are shown in Figure 3.9.

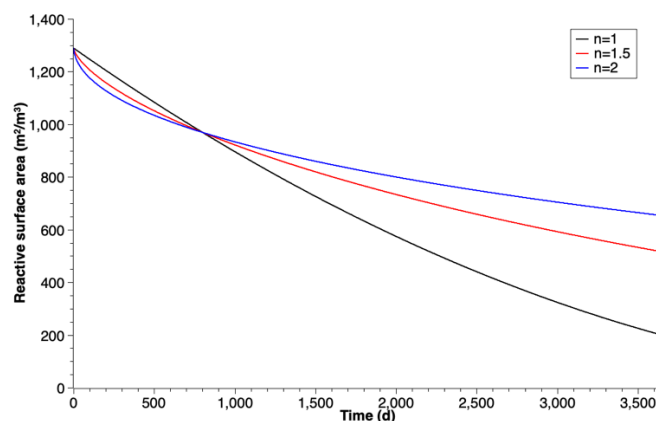


Figure 3.9 Reactive surface area of  $\text{Fe}^0$  particles versus time ( $n$  is the coefficient of passivation)

For most of previous modeling studies on simulating the operation of  $\text{Fe}^0$ -based PRBs, the reaction rate for iron corrosion by water was assumed to have a first-order dependency on the iron surface area (Alowitz and Scherer, 2002; Gandhi et al., 2002; Gu et al., 2002; Jeen et al., 2008; Li et al., 2005; Li et al., 2006; Mayer et al., 2001; Morrison et al., 2002; Westerhoff, 2003; Yabusaki et al., 2001). A plot of calibrated corrosion rates versus the calculated reactive surface area values under different coefficients of passivation is shown in Figure 3.10.

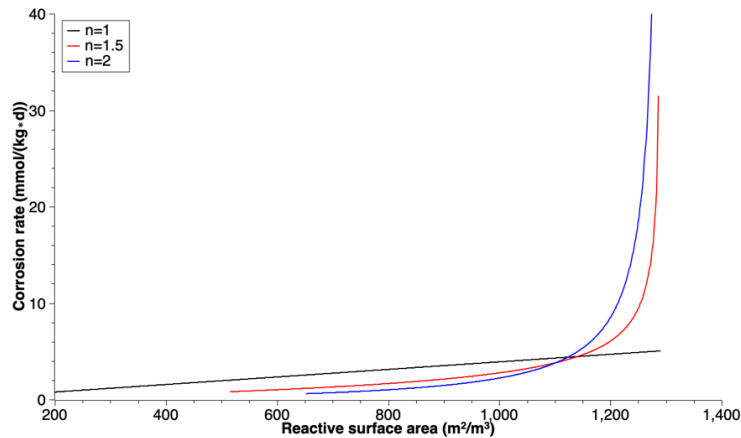


Figure 3.10 Corrosion rate versus reactive surface area with different coefficients of passivation (n)

When no iron passivation considered, which means that the current density ( $i$ ) or the corrosion rate (in mm/y) are constant, the corrosion rate in mmol/(kg·d) has a complete first-order dependency on the iron surface area (Fig.3.10). However, when the growth of corrosion products follows a parabolic law, the first-order dependence assumption is no longer applicable. The first order model underestimates the iron corrosion rate at large reactive surface area in the system. As shown in Figure 3.10, the corrosion rate results for coefficient of passivation (n) is 1.5 or 2 are significantly larger than that of first-order dependency (n=1) when the system has a large reactive surface area. This is valid especially during the beginning phase with strong increase of iron corrosion products, which causes the porosity reduction in the barrier. Thus, a more accurate expression of corrosion rate should be applied in modeling simulations in order to have a better estimation of PRB endurance.

### 3.7 Comparison of porosity loss in different studies

Table 3.2 summarized the porosity loss simulations of previous studies with the simulations in this study with assumptions that the corrosion rate (in mm/y) is a constant and goethite is the only corrosion product.

Table 3.2 Porosity loss simulations in different studies

Study	Solution	Simulated porosity loss after 1 year (%)
This study	Deionized water	12.3
Mayer et al. (2001)	Underground water	0.7
Yabusaki et al. (2001)	Underground water	2.56
Li et al. (2006)	Underground water	0.65
Li and Benson (2010)	Underground water	1.2

The porosity loss after 1 year simulation in this study is over one order of magnitude larger than the simulation results from former studies. The simulated porosity loss from these studies contradict to the measured porosity loss reported by Luo et al. (Luo et al., 2013). Possible reasons for the divergence are the different iron corrosion rates utilized in the model as discussed in section 5. In addition, this study simulated the condition that the granular iron is in contact with deionized water and only the iron corrosion process is considered. If the deionized water is replaced by underground water with multiple dissolved ions, the porosity loss, i.e. by precipitation of carbonates, can be even more significant.

### 3.8. Effect of Fe<sup>0</sup> mixing ratio

Figure 3.5 shows the simulated long-term porosity loss for systems with different Fe<sup>0</sup> mixing ratios. Table 3.3 summarized the reported porosity values after the column experiments in Luo et al.'s study (2013) and the simulated porosity values after an equivalent reaction period.

Table 3.3 Porosity values for different Fe<sup>0</sup> mixing ratios

Fe <sup>0</sup> mixing ratio (w/w, %)	Porosity (%) from Luo et al. (2013)	Simulated porosity (%)
10	56	56
50	40	50
100	32	32

The results from column experiments in Luo et al. (Luo et al., 2013) confirm that the system with lower Fe<sup>0</sup> mixing ratio in the barrier can remain higher porosity after exposure to water. The higher porosity can be explained that a lower percentage of Fe<sup>0</sup> generates less corrosion products, which reduce the likelihood of pore clogging in the system. Therefore, mixing Fe<sup>0</sup> and less reactive materials (e.g. sand) is a solution for long-term porosity loss in Fe<sup>0</sup>-based PRBs (Li and Benson, 2010). However, a low Fe<sup>0</sup> mixing ratio might reduce the ability of a PRB system to remove contaminants (Luo et al., 2013). Thus an appropriate ratio between Fe<sup>0</sup> and less reactive materials is important.

### 3.9. Conclusion

A mathematical model is presented to simulate the long-term porosity loss of Fe<sup>0</sup>-based PRBs as induced by deionized water. It is assumed that only the volumetric expansive corrosion of iron contributes to the porosity loss of the system. Faraday's law was applied to describe the correlation of the amount of corroded iron and the iron corrosion rates. Different coefficients of passivation were taken into account to describe different growth features of corrosion products. Measured porosity results from Luo et al. (Luo et al., 2013) were used to calibrate the parameters in the model. Based on experimental findings from literature and the simulations here, the following major conclusions can be drawn:

- (a) There are iron residues in the system ( $0.09 \text{ m}^3 \text{ Fe}^0 / \text{m}^3$ ) when the porosity reduces to 0, which means the groundwater can no longer flow through the Fe<sup>0</sup>-based PRB before the Fe<sup>0</sup> is completely consumed. Thus, it is not correct to assume that the iron in Fe<sup>0</sup>-based PRB is totally consumed and that the endurance of PRB can be estimated from the amount of iron and iron corrosion rate.
- (b) The derived iron corrosion rates in presented model (2.60 mmol/(kg·d), 2.07 mmol/(kg·d) and 1.77 mmol/(kg·d)) are significantly larger than the corrosion rate used in previous studies (0.4 mmol/(kg·d)). Higher iron corrosion rate means more iron can dissolve in the water, which leads to more significant porosity loss caused by larger amount of generated iron corrosion products. Thus, the previous simulations with low iron corrosion rate may underestimate the porosity loss in PRB. Moreover, we propose, a uniform unit of iron corrosion rate (e.g. mm/y) for Fe<sup>0</sup>-based PRB systems in order to improve the comparability of the different studies.
- (c) The assumption in previous modeling studies, which describes the iron corrosion rate (in mmol/(kg·d)) as a first-order dependency on iron surface area, is accurate only when iron passivation is neglected. When iron passivation is considered, such an assumption underestimates the corrosion rates especially at the beginning phase of operation.
- (d) The modelled porosity loss in this study (0.12/y with assumptions that the corrosion rate is a constant and goethite is the only corrosion product) is larger than the simulation results from previous studies (average 0.02/y). Our study demonstrates that iron corrosion products can cause large porosity loss in the filter. Iron passivation features and possible corrosion products are responsible for large differences between the simulation results. Therefore, iron corrosion processes need to be properly considered in order to accurately estimate the long-term operation of Fe<sup>0</sup>-based PRB systems.

## Reference:

- Agrawal, A., Tratnyek, P.G., 1995. Reduction of nitro aromatic compounds by zero-valent iron metal. *Environmental Science & Technology*, 30(1): 153-160.
- Alowitz, M.J., Scherer, M.M., 2002. Kinetics of nitrate, nitrite, and Cr (VI) reduction by iron metal. *Environmental Science & Technology*, 36(3): 299-306.
- Andrade, C., Alonso, C., Molina, F.J., 1993. Cover cracking as a function of bar corrosion: Part I- Experimental test. *Materials and structures*, 26(8): 453-464
- Arnold, W.A., Roberts, A.L., 2000. Pathways and kinetics of chlorinated ethylene and chlorinated acetylene reaction with Fe (0) particles. *Environmental Science & Technology*, 34(9): 1794-1805
- Bhargava, K., Ghosh, A.K., Mori, Y., Ramanujam, S., 2005. Modeling of time to corrosion-induced cover cracking in reinforced concrete structures. *Cement and Concrete Research*, 35(11): 2203-2218
- Caré, S. et al., 2013. Modeling the permeability loss of metallic iron water filtration systems. *Clean–Soil, Air, Water*, 41(3): 275-282 %@ 1863-0650.
- Chaves, L.H.G., 2005. The role of green rust in the environment: a review. *Revista Brasileira de Engenharia Agrícola e Ambiental*, 9(2): 284-288
- Domga, R., Togue-Kamga, F., Noubactep, C., Tchatchueng, J.-B., 2015. Discussing porosity loss of Fe0 packed water filters at ground level. *Chemical Engineering Journal*, 263: 127-134
- Du, X., Jin, L., Zhang, R., 2014. Modeling the cracking of cover concrete due to non-uniform corrosion of reinforcement. *Corrosion Science*, 89: 189-202
- Faraday, M., 1834. On electro-chemical decomposition, continued. Royal Society.
- Farrell, J., Kason, M., Melitas, N., Li, T., 2000. Investigation of the long-term performance of zero-valent iron for reductive dechlorination of trichloroethylene. *Environmental Science & Technology*, 34(3): 514-521
- Gandhi, S., Oh, B.-T., Schnoor, J.L., Alvarez, P.J.J., 2002. Degradation of TCE, Cr (VI), sulfate, and nitrate mixtures by granular iron in flow-through columns under different microbial conditions. *Water Research*, 36(8): 1973-1982
- Ghauch, A., 2015. Iron-based metallic systems: an excellent choice for sustainable water treatment. *FOG-Freiberg Online Geoscience*, 38
- Gheju, M., 2011. Hexavalent chromium reduction with zero-valent iron (ZVI) in aquatic systems. *Water, Air, & Soil Pollution*, 222(1-4): 103-148
- Gillham, R.W., 1999. In situ remediation of VOC-contaminated groundwater using zero-valent iron: Long-

- term performance, pp. 21-25.
- Gu, B. et al., 2002. Microbiological characteristics in a zero-valent iron reactive barrier. *Environmental monitoring and assessment*, 77(3): 293-309
- Guan, X. et al., 2015. The limitations of applying zero-valent iron technology in contaminants sequestration and the corresponding countermeasures: the development in zero-valent iron technology in the last two decades (1994–2014). *Water research*, 75: 224-248
- Hammonds, P., 1989. *An Introduction to Corrosion and its Prevention*, Comprehensive Chemical Kinetics. Elsevier, pp. 233-279
- Henderson, A.D., Demond, A.H., 2007. Long-term performance of zero-valent iron permeable reactive barriers: a critical review. *Environmental Engineering Science*, 24(4): 401-423
- Hu, R. et al., 2019. Characterizing the suitability of granular Fe<sup>0</sup> for the water treatment industry. *Processes*, 7(10): 652.
- Hu, R. et al., 2020. Metallic iron for environmental remediation: Starting an overdue progress in knowledge. *Water*, 12(3): 641.
- Hu, R.Y., H.; Tao, R.; Cui, X.; Xiao, M.; Amoah, B.K.; Cao, V.; Lufingo, M.; Soppa-Sangue, N.P.; Ndé-Tchoupé, A.I.; Gatcha-Bandjun, N.; Sipowo-Tala, V.R.; Gwenzi, W.; Noubactep, C., 2020. *Metallic Iron for Environmental Remediation: Starting an Overdue Progress in Knowledge*. *water*, 12(641).
- Interstate, T., Regulatory, C., 2005. *Permeable reactive barriers: Lessons learned/new directions*. ITRC Washington DC.
- Jeen, S.-W., O, J.S., Gillham, R.W., 2008. Modeling Geochemical and Reactivity Changes of Different Iron Materials, *GeoCongress 2008: Geotechnics of Waste Management and Remediation*, pp. 595-602.
- Johnson, R.L., Tratnyek, P.G., Miehr, R., Thoms, R.B., Bandstra, J.Z., 2005. Reduction of hydraulic conductivity and reactivity in zero-valent iron columns by oxygen and TNT. *Groundwater Monitoring & Remediation*, 25(1): 129-136.
- Kamolpornwijit, W., Liang, L., Moline, G.R., Hart, T., West, O.R., 2004. Identification and quantification of mineral precipitation in Fe<sup>0</sup> filings from a column study. *Environmental science & technology*, 38(21): 5757-5765
- Kamolpornwijit, W., Liang, L., West, O.R., Moline, G.R., Sullivan, A.B., 2003. Preferential flow path development and its influence on long-term PRB performance: column study. *Journal of contaminant hydrology*, 66(3-4): 161-178
- Keum, Y.-S., Li, Q.X., 2004. Reduction of nitroaromatic pesticides with zero-valent iron. *Chemosphere*, 54(3): 255-263
- Klausen, J. et al., 2003. Longevity of granular iron in groundwater treatment processes: solution

- composition effects on reduction of organohalides and nitroaromatic compounds. *Environmental Science & Technology*, 37(6): 1208-1218
- Kouznetsova, I., Bayer, P., Ebert, M., Finkel, M., 2007. Modelling the long-term performance of zero-valent iron using a spatio-temporal approach for iron aging. *Journal of contaminant hydrology*, 90(1-2): 58-80
- Landolt, D., 2007. *Corrosion and surface chemistry of metals*. CRC press.
- Lee, G., Rho, S., Jahng, D., 2004. Design considerations for groundwater remediation using reduced metals. *Korean Journal of Chemical Engineering*, 21(3): 621-628
- Li, L., Benson, C.H., 2010. Evaluation of five strategies to limit the impact of fouling in permeable reactive barriers. *Journal of Hazardous materials*, 181(1-3): 170-180
- Li, L., Benson, C.H., Lawson, E.M., 2005. Impact of mineral fouling on hydraulic behavior of permeable reactive barriers. *Groundwater*, 43(4): 582-596
- Li, L., Benson, C.H., Lawson, E.M., 2006. Modeling porosity reductions caused by mineral fouling in continuous-wall permeable reactive barriers. *Journal of Contaminant Hydrology*, 83(1-2): 89-121
- Liang, J. et al., 2013. Impact of flow rate on corrosion of cast iron and quality of re-mineralized seawater reverse osmosis (SWRO) membrane product water. *Desalination*, 322: 76-83
- Liu, T., Weyers, R.W., 1998. Modeling the dynamic corrosion process in chloride contaminated concrete structures. *Cement and Concrete research*, 28(3): 365-379
- Liu, Y., 1996. *Modeling the time-to corrosion cracking of the cover concrete in chloride contaminated reinforced concrete structures*, Virginia Tech.
- Liu, Y., Phenrat, T., Lowry, G.V., 2007. Effect of TCE concentration and dissolved groundwater solutes on NZVI-promoted TCE dechlorination and H<sub>2</sub> evolution. *Environmental science & technology*, 41(22): 7881-7887
- Lorbeer, P., Lorenz, W.J., 1980. The kinetics of iron dissolution and passivation in solutions containing oxygen. *Electrochimica Acta*, 25(4): 375-381
- Lu, C., Jin, W., Liu, R., 2011. Reinforcement corrosion-induced cover cracking and its time prediction for reinforced concrete structures. *Corrosion Science*, 53(4): 1337-1347
- Luo, P., Bailey, E.H., Mooney, S.J., 2013. Quantification of changes in zero valent iron morphology using X-ray computed tomography. *Journal of Environmental Sciences*, 25(11): 2344-2351
- Mackenzie, P.D., Horney, D.P., Sivavec, T.M., 1999. Mineral precipitation and porosity losses in granular iron columns. *Journal of Hazardous Materials*, 68(1-2): 1-17
- Mayer, K.U., Blowes, D.W., Frind, E.O., 2001. Reactive transport modeling of an in situ reactive barrier for the treatment of hexavalent chromium and trichloroethylene in groundwater. *Water Resources*

Research, 37(12): 3091-3103

- McMurtry, D.C., Elton, R.O., 1985. New approach to in-situ treatment of contaminated groundwaters. *Environmental Progress*, 4(3): 168-170
- Moraci, N., Ielo, D., Bilardi, S., Calabro, P.S., 2016. Modelling long-term hydraulic conductivity behaviour of zero valent iron column tests for permeable reactive barrier design. *Canadian Geotechnical Journal*, 53(6): 946-961
- Morales, J., Hutcheson, R., Cheng, I.F., 2002. Dechlorination of chlorinated phenols by catalyzed and uncatalyzed Fe (0) and Mg (0) particles. *Journal of Hazardous materials*, 90(1): 97-108
- Morrison, S.J., Metzler, D.R., Dwyer, B.P., 2002. Removal of As, Mn, Mo, Se, U, V and Zn from groundwater by zero-valent iron in a passive treatment cell: reaction progress modeling. *Journal of Contaminant Hydrology*, 56(1-2): 99-116
- Nam, S., Tratnyek, P.G., 2000. Reduction of azo dyes with zero-valent iron. *Water Research*, 34(6): 1837-1845.
- Nešić, S., 2007. Key issues related to modelling of internal corrosion of oil and gas pipelines—A review. *Corrosion science*, 49(12): 4308-4338
- Neumann, A. et al., 2013. Arsenic removal with composite iron matrix filters in Bangladesh: a field and laboratory study. *Environmental science & technology*, 47(9): 4544-4554
- Noubactep, C., 2008. A critical review on the process of contaminant removal in Fe<sup>0</sup>-H<sub>2</sub>O systems. *Environ Technol*, 29(8): 909-20. DOI:10.1080/09593330802131602
- Noubactep, C., 2016. Research on metallic iron for environmental remediation: Stopping growing sloppy science. *Chemosphere*, 153: 528-530.
- O'Hannesin, S.F., Gillham, R.W., 1998. Long-term performance of an in situ "iron wall" for remediation of VOCs. *Groundwater*, 36(1): 164-170
- Odziemkowski, M.S., Gui, L., Gillham, R.W., Irish, D.E., 2000. The role of oxide films in the reduction of n-nitrosodimethylamine with reference to the iron groundwater remediation technology. The Electrochemical Society.
- Pantazopoulou, S.J., Papoulia, K.D., 2001. Modeling cover-cracking due to reinforcement corrosion in RC structures. *Journal of engineering mechanics*, 127(4): 342-351.
- Phillips, D.H. et al., 2000. Performance evaluation of a zerovalent iron reactive barrier: mineralogical characteristics. *Environmental Science & Technology*, 34(19): 4169-4176.
- Phillips, D.H., Watson, D.B., Roh, Y., Gu, B., 2003. Mineralogical characteristics and transformations during long-term operation of a zerovalent iron reactive barrier. *Journal of Environmental Quality*, 32(6): 2033-2045

- Pilling, N.B., 1923. The oxidation of metals at high temperature. *J. Inst. Met.*, 29: 529-582.
- Rangsvivek, R., Jekel, M.R., 2005. Removal of dissolved metals by zero-valent iron (ZVI): Kinetics, equilibria, processes and implications for stormwater runoff treatment. *Water Research*, 39(17): 4153-4163.
- Reardon, E.J., 1995. Anaerobic corrosion of granular iron: Measurement and interpretation of hydrogen evolution rates. *Environmental science & technology*, 29(12): 2936-2945.
- Roh, Y., Lee, S.Y., Elless, M.P., 2000. Characterization of corrosion products in the permeable reactive barriers. *Environmental Geology*, 40(1-2): 184-194
- Scherer, M.M., Richter, S., Valentine, R.L., Alvarez, P.J.J., 2000. Chemistry and microbiology of permeable reactive barriers for in situ groundwater clean up. *Critical reviews in microbiology*, 26(4): 221-264
- Sheir, L.L., Jarman, R.A., Burstein, G.T., 1994. *Corrosion: Metal/Environment Reactions*. Newnes-Butterworths, London, 8: 3-8.
- Sikora, E., Macdonald, D.D., 2000. The passivity of iron in the presence of ethylenediaminetetraacetic acid I. General electrochemical behavior. *Journal of the Electrochemical Society*, 147(11): 4087
- Starr, R.C., Cherry, J.A., 1994. In situ remediation of contaminated ground water: The funnel-and-gate system. *Ground water*, 32(3): 465
- Sun, Y. et al., 2014. Effect of weak magnetic field on arsenate and arsenite removal from water by zerovalent iron: an XAFS investigation. *Environmental science & technology*, 48(12): 6850-6858.
- Tomashov, N.D., 1965. *Theory of corrosion and protection of metals*. 1966, 672 P. The Macmillan Company, 60 Fifth Avenue, New York 10011.
- Tratnyek, P.G., Miehr, R., Bandstra, J.Z., 2002. Kinetics of reduction of TNT by iron metal. *IAHS Publication*: 427-434
- Velimirovic, M. et al., 2014. Corrosion rate estimations of microscale zerovalent iron particles via direct hydrogen production measurements. *Journal of hazardous materials*, 270: 18-26
- Vikesland, P.J., Klausen, J., Zimmermann, H., Roberts, A.L., Ball, W.P., 2003. Longevity of granular iron in groundwater treatment processes: changes in solute transport properties over time. *Journal of Contaminant Hydrology*, 64(1-2): 3-33
- Warner, S.D., Sorel, D., 2003. *Ten years of permeable reactive barriers: Lessons learned and future expectations*. ACS Publications.
- Westerhoff, P., 2003. Reduction of nitrate, bromate, and chlorate by zero valent iron (Fe<sup>0</sup>). *Journal of Environmental Engineering*, 129(1): 10-16.
- Wilkin, R.T., Puls, R.W., Sewell, G.W., 2003. Long-term performance of permeable reactive barriers using

zero-valent iron: geochemical and microbiological effects. *Ground Water*, 41(4): 493

Wilkin, R.T., Su, C., Ford, R.G., Paul, C.J., 2005. Chromium-removal processes during groundwater remediation by a zerovalent iron permeable reactive barrier. *Environmental science & technology*, 39(12): 4599-4605

Yabusaki, S., Cantrell, K., Sass, B., Steefel, C., 2001. Multicomponent reactive transport in an in situ zero-valent iron cell. *Environmental Science & Technology*, 35(7): 1493-1503

Zhang, Y., Gillham, R.W., 2005. Effects of gas generation and precipitates on performance of Fe PRBs. *Groundwater*, 43(1): 113-121.



## Chapter 4

### 4. Numerical case studies on long-term effectiveness of metallic iron based permeable reactive barriers: importance of porosity heterogeneity of the barrier

Huichen Yang<sup>1\*</sup>, Quan Liu<sup>1</sup>, Rui Hu<sup>2</sup>, Thomas Ptak<sup>1</sup>, Reza Taherdangkoo<sup>3</sup>, Yuxi Liu<sup>4</sup>, and Chicgoua Noubactep<sup>1,5</sup>

<sup>1</sup> Angewandte Geologie, Universität Göttingen, Goldschmidtstraße 3, D - 37077 Göttingen, Germany; huichen.yang@geo.uni-goettingen.de (H.Y), quan.liu@geo.uni-goettingen.de (Q.L), tptak@gwdg.de (T.P), cnoubac@gwdg.de (C.N)

<sup>2</sup> School of Earth Science and Engineering, Hohai University, Fo Cheng Xi Road 8, 211100 Nanjing, P.R. China; rhu@hhu.edu.cn (R.H)

<sup>3</sup> TU Bergakademie Freiberg, Institute of Geotechnics, Gustav-Zeuner-Str. 1, 09599, Freiberg, Germany; reza.Taherdangkoo@ifgt.tu-freiberg.de (R.T)

<sup>4</sup> Institut für Mathematische Stochastik, Universität Göttingen, Goldschmidtstraße 7, D - 37077 Göttingen, Germany; yuxi.liu@stud.uni-goettingen.de (Y.L)

<sup>5</sup> Centre for Modern Indian Studies (CeMIS), Universität Göttingen, Waldweg 26, D - 37073 Göttingen, Germany; cnoubac@gwdg.de (C.N.)

\*Corresponding author: huichen.yang@geo.uni-goettingen.de

#### Citation:

Yang H, Liu Q, Hu R, Ptak T, Taherdangkoo R, Liu Y, Noubactep C. Numerical case studies on long-term effectiveness of metallic iron based permeable reactive barriers: importance of porosity heterogeneity of the barrier[J]. *Journal of Hydrology*, 2022: 128148.

#### **Abstract**

This paper presents a three-dimensional (3-D) numerical groundwater flow and transport model of a metallic iron based permeable reactive barrier (Fe<sup>0</sup>-PRB) to assess how porosity heterogeneity of the barrier medium may affect groundwater flow over time and influence the long-term effectiveness of a Fe<sup>0</sup>-PRB. A 3-D high resolution aquifer outcrop analogue was utilized to implement aquifer heterogeneity. To evaluate the treatment performance of the PRB, the contaminant plume migration and groundwater residence time were investigated. The findings demonstrate that heterogeneity of porosity reduction of the barrier medium is an important factor in estimating the long-term performance of a continuous-wall Fe<sup>0</sup>-PRB. Ignoring the porosity heterogeneity of the barrier medium leads to an underestimation of the by-passing flow by 30%-41% in ten-years simulation, and of contaminant plume spread over time. Groundwater residence time simulations shows no evident residence time reduction during the operation of the Fe<sup>0</sup>-PRB. Installation of a pea gravel equalization zone can effectively reduce the heterogeneity of the barrier medium, and minimize the by-passing flow.

**Keywords:** groundwater flow and transport model; groundwater remediation; long-term effectiveness; permeable reactive barrier; zero-valent iron;

## 4.1 Introduction

Metallic iron based permeable reactive barriers (Fe<sup>0</sup>-PRBs) can be considered an effective and economically-feasible in-situ technology for remediation of polluted groundwater (Gillham, 1999; Tratnyek et al., 2002; Wu et al., 2017). Polluted water with varieties of contaminants such as halogenated organics (Arnold and Roberts, 2000), nitroaromatics (Keum and Li, 2004), dyes (Nam and Tratnyek, 2000), phenolic compounds (Morales et al., 2002), heavy metals (Rangsivek and Jekel, 2005) and various oxyanions (Neumann et al., 2013) can be treated by Fe<sup>0</sup>/H<sub>2</sub>O systems. Fe<sup>0</sup>-PRBs can activate different physical and chemical mechanisms for contaminant removal including adsorption, co-precipitation, and adsorptive size-exclusion (Noubactep, 2011). Although the performance of applied Fe<sup>0</sup>-PRBs has been generally satisfactory (Agrawal and Tratnyek, 1995; Keum and Li, 2004; Phillips et al., 2000; Phillips et al., 2003; Wilkin et al., 2018; Wilkin et al., 2005), the question still remains on estimating the long-term effectiveness of Fe<sup>0</sup>-PRBs (Moraci et al., 2016).

Two main concerns for Fe<sup>0</sup>-PRBs longevity evaluation are reactivity loss and porosity loss (Caré et al., 2013; Henderson and Demond, 2007; Yang et al., 2021). The reactivity loss of Fe<sup>0</sup>-PRBs has been well studied, and is caused by the generated oxide scale in the vicinity of iron particles, which is reported compromise the electron transfer from the iron body, and decrease the reaction rates of the contaminants removal during long-term operation (Hu, 2020; Jeon et al., 2007; Jeon et al., 2008; Weber et al., 2013). The porosity loss of Fe<sup>0</sup>-PRBs is caused by clogging of the pore space due to mineral precipitation (Li et al., 2005; Phillips et al., 2000; Phillips et al., 2003) and gas formation (Kamolpornwijit and Liang, 2006; Reardon, 1995; Williams et al., 2007). Since iron is not stable under environmental conditions, iron corrosion occurs whenever a reactive iron specimen is immersed in an aqueous solution (Hu et al., 2019). Iron is corroded by protons from water, and in the presence of oxidizing agents (e.g. contaminants), corrosion products (Fe<sup>2+</sup> and Fe(OH)<sub>2</sub>) can be oxidized to less soluble Fe(OH)<sub>3</sub>. Fe(OH)<sub>2</sub> and Fe(OH)<sub>3</sub> are polymerized and further transformed to various oxyhydroxides (Hu, 2020; Landolt, 2007). All the possible corrosion products have much less density compared to the parent metal (Fe<sup>0</sup>), which means that iron corrosion is a volumetric expansive process, and can constantly reduce the pore space within the system (Caré et al., 2013). In addition, iron corrosion leads to redox conditions and an increase in pH, which induces the precipitation of secondary minerals (Phillips et al., 2000; Phillips et al., 2003; Wilkin et al., 2005). The iron corrosion products and secondary minerals may precipitate within the Fe<sup>0</sup>-PRB pore space, resulting in the reduction of porosity of the barrier medium. Moreover, as another iron corrosion product, hydrogen can be continuously generated during the operation of a Fe<sup>0</sup>-PRB. The gas bubbles may be trapped

within the porous medium, and reduce the effective porosity of the barrier for groundwater flow (Vikesland et al., 2003; Zhang and Gillham, 2005). Although the relationship between porosity loss and hydraulic conductivity loss may not necessarily be straightforward (Johnson et al., 2005), previous studies generally applied Kozeny-Carman formula to correlate porosity and hydraulic conductivity within the barrier (Li et al., 2005; Li et al., 2006; Mayer et al., 2001; Wu et al., 2017; Yabusaki et al., 2001). The reduced hydraulic conductivity of a Fe<sup>0</sup>-PRB can result in the reorientation of groundwater flow, changes in residence time and by-passing (Li et al., 2005; Li et al., 2006). For instance, Johnson et al. (Johnson et al., 2005) reported that, although the Fe<sup>0</sup>-PRB continued to completely remove contaminants from the passing groundwater, a portion of groundwater was being diverted beneath the Fe<sup>0</sup>-PRB at the Cornhusker Army Ammunition Plant after 20 months of operation.

Field observations and column experiments reveal that pore space reduction within the barrier medium is spatially heterogeneously distributed (Johnson et al., 2005; Wilkin et al., 2003; Wilkin et al., 2005). Intensive secondary mineral precipitation, which mainly consists of calcium carbonates (CaCO<sub>3</sub>) and siderite (FeCO<sub>3</sub>), occurs around the entrance face of the Fe<sup>0</sup>-PRB (Kamolpornwijit et al., 2004). And iron corrosion products, such as Magnetite (Fe<sub>3</sub>O<sub>4</sub>), ferrous hydroxide (Fe(OH)<sub>2</sub>), green rust ( $[\text{Fe}^{\text{II}}_{(1-x)}\text{Fe}^{\text{III}}_x(\text{OH})_2]^{x+}[(x/n)\text{A}^{n-}\cdot(m/n)\text{H}_2\text{O}]^{x-}$ ) and iron oxyhydroxides (FeOOH), form throughout the Fe<sup>0</sup>-PRB (Wilkin et al., 2003). Moreover, mineral precipitation can be affected by localized geochemical conditions and the groundwater flux. For instance, Li et al. (Li et al., 2006) reported that a barrier section with a high groundwater flux shows a high degree of secondary mineral precipitation. It is known that natural aquifers are heterogeneous, and that aquifer heterogeneity causes preferential groundwater flow pathways, which can result in heterogeneously distributed groundwater fluxes within the Fe<sup>0</sup>-PRB. Therefore, although the barrier medium is homogeneous when installed, spatially heterogeneous secondary mineral precipitation can cause a heterogeneous reduction of porosity, and increasing heterogeneity in porosity of the barrier medium over time can influence the groundwater flow patterns, which in turn will cause by-passing flow around the PRB and threaten the long-term effectiveness of the PRB. Considerable interest exists regarding strategies to improve the long-term performance of a Fe<sup>0</sup>-PRB (Li and Benson, 2010). One strategy is to install pea gravel equalization zones along the up gradient and down gradient faces of the PRB. The pea gravel zones have been used in several field PRBs (McMahon et al., 1999; Sorel et al., 2003), but the effectiveness is largely undocumented (Li and Benson, 2010). The effect of a pea gravel equalization zone is investigated in this study.

Developing an assessment of the long-term performance of Fe<sup>0</sup>-PRBs using field and laboratory data is limited by the long period over which mineral precipitation occurs (Vikesland et al., 2003), and by the relatively short duration of laboratory experiments. An alternative approach is conducting analyses with numerical model simulations. In past decades, numerous numerical reactive transport models have been established to simulate contaminant degradations and mineral precipitation within Fe<sup>0</sup>-PRBs (Johnson et al., 2005; Li et al., 2005; Li et al., 2006; Mayer et al., 2001; Moraci et al., 2016; Wu et al., 2017; Yabusaki et al., 2001). Mayer et al. (Mayer et al., 2001) developed a kinetic geochemical algorithm and used the code MIN3P for modeling groundwater flow and mineral precipitation in the PRB at the U.S. Coast Guard Support Center. In their study, the two-dimensional simulations showed that the removal of contaminant and secondary mineral precipitation were unevenly distributed because of aquifer heterogeneities. Li et al. (Li et al., 2005) combined the codes MODFLOW and RT3D to simulate geochemical reactions within PRBs. They concluded that the porosity reduction is sensitive to influent ion concentrations, and that it is spatially variable. In addition, although different contaminant removal processes may require different reaction time, the residence time of the groundwater within the barrier has been generally utilized to assess the effectiveness of Fe<sup>0</sup>-PRBs (Li et al., 2005; Li et al., 2006). Li et al. (Li et al., 2005) reported that the simulated groundwater residence time is decreasing over time, which may result in an insufficient reaction time to completely remove the contaminant. Nonetheless, the emphasis of previous models was mostly on the contaminant mass removal over time within the PRBs, and the long-term effectiveness of PRBs was estimated with one-dimensional or two-dimensional simulations (Mayer et al., 2001; Yabusaki et al., 2001). To date, few studies have been conducted to comprehensively investigate how heterogeneity variation of a PRB may affect the groundwater flow and influence long-term performance.

As explained above, implementing a heterogeneous aquifer, which can accurately represent a real geological situation, is crucial for the simulations. A practical approach is to make use of aquifer analogues, which have been extensively employed for reservoir characterization in the petroleum industry (Bryant and Flint, 2009). Such analogues are mainly derived by mapping outcrops and can provide a detailed representation of the natural heterogeneity of hydraulic properties (Hu et al., 2011; Huggenberger and Aigner, 1999). In this study, a 3-D high resolution aquifer outcrop analogue developed by Bayer (Bayer, 2000) was utilized to represent aquifer heterogeneity.

The objective of this paper is to assess the possible impacts of porosity heterogeneity of a continuous-wall Fe<sup>0</sup>-PRB on their long-term effectiveness based on case studies. A three-

dimensional (3-D) groundwater transport model was developed to simulate the groundwater flow within the Fe<sup>0</sup>-PRB and its surrounding aquifer. A 3-D high resolution aquifer outcrop analogue was adopted to set the hydraulic properties of the aquifer. Four individual scenarios were studied and the porosity and hydraulic conductivity reduction of the barrier medium, redistribution of groundwater and by-passing flows, contaminant plume evolution, as well as the residence time of groundwater were investigated.

## 4.2 Numerical modeling and case studies

### 4.2.1 Conceptual model

The conceptual model consists of a continuous-wall PRB and its surrounding aquifer. The size of the simulation domain is 16×10×7m. The Fe<sup>0</sup>-PRB is set to be perpendicular to the main direction of groundwater flow (x axis), and is 7m wide (y axis 2 to 9 m), 6m deep (z axis 1 to 7 m) and 1m thick (x axis 7 to 8 m). The whole PRB is divided into two parts: (1) the entrance domain and (2) the exit domain. Each portion is 50 cm in thickness. The contaminant source is located at the upstream boundary as shown in Figure 1. The PRB is composed of ZVI particles, and its initial porosity and hydraulic conductivity are homogeneously distributed. As groundwater flows through the PRB, the iron particles are corroded by the water, causing secondary mineral precipitation which results in porosity reduction within the Fe<sup>0</sup>-PRB. Table 4.1 summarized the possible chemical reactions which may occur in the Fe<sup>0</sup>-PRB (Li et al., 2005; Li et al., 2006; Yang et al., 2021).

Table 4.1 Chemical reactions in a Fe<sup>0</sup>-PRB

Aqueous iron corrosion	Secondary mineral precipitation/dissolution
$\text{Fe}^0 + 2\text{H}^+ \rightarrow \text{Fe}^{2+} + \text{H}_2$	$\text{CaCO}_3 (\text{s}) \leftrightarrow \text{Ca}^{2+} + \text{CO}_3^{2-}$
$\text{Fe}^0 + 2\text{H}_2\text{O} \rightarrow \text{Fe}(\text{OH})_2 + \text{H}_2$	$\text{MgCO}_3 (\text{s}) \leftrightarrow \text{Mg}^{2+} + \text{CO}_3^{2-}$
$4\text{Fe}^{2+} + \text{O}_2 + 10\text{H}_2\text{O} \rightarrow 4 \text{Fe}(\text{OH})_3 + 8\text{H}^+$	$\text{Mg}(\text{OH})_2 (\text{s}) \leftrightarrow \text{Mg}^{2+} + 2\text{OH}^-$
$4\text{Fe}(\text{OH})_2 + \text{O}_2 + 2\text{H}_2\text{O} \rightarrow 4\text{Fe}(\text{OH})_3$	$\text{FeCO}_3 (\text{s}) \leftrightarrow \text{Fe}^{2+} + 2\text{OH}^-$
$\text{Fe}(\text{OH})_2, \text{Fe}(\text{OH})_3 \rightarrow \text{FeO}, \text{Fe}_3\text{O}_4, \text{Fe}_2\text{O}_3,$	$\text{FeS} (\text{am}) + \text{H}_2\text{O} \leftrightarrow \text{Fe}^{2+} + \text{HS}^- + \text{OH}^-$
$\text{FeOOH} \dots$	

The effects of generated gas are not incorporated in this model. Since some previous studies have stated that gas accumulation can have a considerable influence on the hydraulic behavior of a Fe<sup>0</sup>-PRB (Parbs et al., 2007; Zhang and Gillham, 2005), the generated gas within the PRB may exacerbate the effects predicted by the model studied herein.

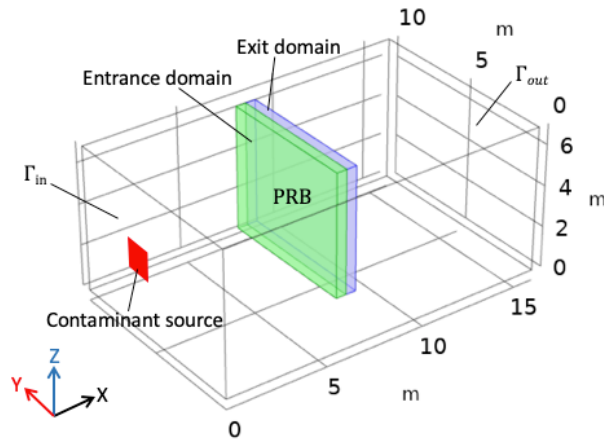


Figure 4.1 Conceptual model setup. The Fe-PRB is located in the middle of the surrounding aquifer and is oriented perpendicular to the main direction of groundwater flow (x axis). The PRB consists of an entrance domain (green area) and an exit domain (blue area). The red block represents the contaminant source.

Important assumptions employed in this study are listed as follows:

- A. The porosity reduction within the entrance domain is caused by 1) iron corrosion products, and 2) secondary mineral precipitation, whereas the porosity reduction within the exit domain is only caused by iron corrosion products (Li et al., 2006).
- B. The porosity heterogeneity of the barrier medium results from 1) preferential flow in the aquifer and 2) the heterogeneously distributed secondary mineral precipitation within the barrier.
- C. If heterogeneous precipitation is considered, the precipitation rate is proportional to the Darcy flux (Li et al., 2006).
- D. The Fe<sup>0</sup>-PRB can totally remove the contaminant from the groundwater flowing through the barrier. This assumption is based on the study of Johnsen et al. (Johnson et al., 2005), which states that the PRB can completely remove explosives when the water flows through the barrier after 20 months of operation, and on a 22-year record of a Fe<sup>0</sup>-PRB site (Wilkin et al., 2018), which reports the continuous degradation of chlorinated organic compounds.

The Fe<sup>0</sup>-PRB in this conceptual model follows the continuous-wall design, which contains a treatment barrier across the contaminant plume path (Thakur et al., 2020). The continuous-wall is the most favourable and common PRB design because of its lower installation cost and less effect on the groundwater flow than other designs (Li et al., 2005; Obiri-Nyarko et al., 2014). To focus on studying the impact of the porosity heterogeneity in PRB, other engineering designs, such as cut-off walls, are not considered.

This study does not consider the specific geochemical processes of contaminant remediation. The model presented here is the first attempt to simulate the redistribution of groundwater

flow and contaminant transport caused by the porosity heterogeneity variation of the barrier with a three-dimensional numerical model.

#### 4.2.2 Numerical modeling approach

The numerical simulations are conducted using the finite element software COMSOL (Multiphysics, 2012), which is applicable for coupling variables of different physical fields. Specifically, “Darcy’s Law” and “Transport of diluted species in porous media” modes were implemented to simulate groundwater flow and contaminant transport within the aquifer and the PRB. The “Ordinary differential equations” mode was employed to simulate the porosity reduction within the PRB over time.

The groundwater movement is governed by the Darcy’s Law using the following equation (Nield and Bejan, 2006):

$$S_s \frac{\partial h}{\partial t} + \nabla \cdot (-K \nabla h) = Q_m, \quad (4.1)$$

where  $S_s$  [1/m] and  $K$  [m/s] are the specific storage and hydraulic conductivity of the medium, respectively.  $h$  [m] is the hydraulic head, which is defined as  $h = z + p/\rho g$ , where  $z$  [m] is the elevation,  $p$  [Pa] is the pressure,  $\rho$  [kg/m<sup>3</sup>] is the density of the fluid, and  $g$  [m/s<sup>2</sup>] is the gravitational acceleration.  $Q_m$  is a source/sink term, which equals to 0 in this study.

The transport of the contaminant within the Fe<sup>0</sup>-PRB is calculated as below (Bird et al., 2006):

$$\frac{\partial}{\partial t}(\varphi C) + \nabla \cdot (-(D_e + D_D) \nabla C) + \mathbf{u} \cdot \nabla C = 0, \quad (4.2)$$

$$D_e = \frac{\varphi}{T_F} D_f, \quad (4.3)$$

where  $\varphi$  [-] is the porosity of the medium,  $C$  [mol/L] is the contaminant concentration,  $D_e$  [m<sup>2</sup>/s], and  $D_f$  [m<sup>2</sup>/s] are the effective diffusion coefficient and molecular diffusion coefficient, respectively.  $D_D$  [m<sup>2</sup>/s] is the dispersion coefficient.  $T_F$  [-] is the tortuosity of the contaminant specie, which is defined as  $T_F = \varphi^{-1/3}$ .  $\mathbf{u}$  [m/s] represents the Darcy velocity field.

Under assumption A in section 2.1, the porosity loss within PRB over time can be described as:

$$\frac{\partial \varphi}{\partial t} = -\frac{\partial n_{FeCPS}}{\partial t} - \frac{\partial n_{precipitate}}{\partial t}, \quad \text{for the entrance domain}, \quad (4.4)$$

$$\frac{\partial \varphi}{\partial t} = -\frac{\partial n_{FeCPS}}{\partial t}, \quad \text{for the exit domain}, \quad (4.5)$$

where  $\varphi$  [-] is the porosity of the PRB,  $n_{FeCPS}$  [-] is the volume fraction of the iron corrosion products,  $n_{precipitate}$  [-] is the volume fraction of the secondary mineral precipitates.

The iron corrosion is assumed to occur uniformly within the whole Fe<sup>0</sup>-PRB. Equations 4.6-4.8 were utilized to simulate the porosity reduction caused by iron corrosion products. Equation 7 describes the variation of the iron surface area with the method introduced by Mayer et al. (Mayer et al., 2001).

$$\frac{\partial n_{Fe}}{\partial t} = -rS_{Fe}, \quad (4.6)$$

$$S_{Fe} = S_{Fe}^0 \left( \frac{n_{Fe}}{n_{Fe}^0} \right)^{2/3}, \quad (4.7)$$

$$\frac{\partial n_{FeCPS}}{\partial t} = (\eta - 1) \frac{\partial n_{Fe}}{\partial t}, \quad (4.8)$$

where  $n_{Fe}$  [-] is the iron volume fraction,  $r$  [mm/y] the anaerobic iron corrosion rate,  $S_{Fe}$  [m<sup>2</sup>/m<sup>3</sup>] the iron specific surface area,  $S_{Fe}^0$  [m<sup>2</sup>/m<sup>3</sup>] the initial iron surface area,  $n_{Fe}^0$  [-] the initial iron volume fraction, and  $\eta$  [-] is the iron volumetric expansion coefficient (Caré et al., 2008).

There is an intensive porosity loss in the entrance domain resulting from secondary mineral precipitates. A precipitation rate ( $\tau$ ) [1/y] is utilized to calculate the porosity loss caused by the precipitation and is defined as:

$$\tau = \frac{\partial n_{precipitate}}{\partial t} \quad (4.9)$$

If homogeneous precipitation is considered, the precipitation rate ( $\tau$ ) is a constant. In the case of heterogeneous precipitation, since the precipitation rate is assumed to be proportional to the Darcy flux (section 2.1), it can be described as:

$$\tau = a + b \cdot V \quad (4.10)$$

where  $V$  [m/d] is the Darcy flux,  $a$  and  $b$  are two constants, and the values of  $a$  and  $b$  are calibrated with the field measurements from the work by Sarr (Sarr, 2001), which reports 0.02 per year porosity reduction.

The hydraulic conductivity of the Fe<sup>0</sup>-PRB was calculated following the Kozeny-Carman formula as follows (Carman, 1997):

$$K = C \frac{g}{v} \frac{\varphi^3}{(1 - \varphi)^2} D^2 \quad (4.11)$$

where  $K$  [m/s] is hydraulic conductivity,  $C$  [-] an empirical coefficient equal to 1/180,  $g$  [m/s<sup>2</sup>] the gravitational acceleration,  $\nu$  [m<sup>2</sup>/s] the viscosity of water and  $D$  [m] is the iron particle diameter.

Particle tracking was applied, and the advective travel times of groundwater particles within the barrier were estimated. 100 water particles were released on the entrance boundary of the PRB. The particle density was set to be proportional to the Darcy velocity. The times when water particles leave the PRB were recorded, and the average residence time of water particles was calculated.

#### 4.2.2.1 Boundary conditions

For groundwater flow simulations, the entrance and exit boundaries ( $\Gamma_{in}$  and  $\Gamma_{out}$  in Figure 1) were set to constant-head boundaries. The top boundary was set to a no-flow boundary. Infinite element domains were established in all other directions outside the simulation domain in order to eliminate boundary effects.

For contaminant transport, the source was set as a constant concentration ( $C = 0.01 \text{ mol/L}$ ). Other outer boundaries of the domain were set to open boundaries.

For contaminant remediation by the Fe<sup>0</sup>-PRB, it is assumed that the contaminant can be completely removed when groundwater flows through the Fe<sup>0</sup>-PRB (section 4.2.1). The assumption was realized by defining Fe<sup>0</sup>-PRB boundaries as:

$$-\mathbf{n} \cdot (-D_e \nabla C) = 0. \quad (4.12)$$

Where  $\mathbf{n}$  denotes a unit normal vector towards outside.

#### 4.2.3 Case studies

The effect of the barrier porosity heterogeneity variation is investigated by simulating 3 individual scenarios (case 1, case 2, and case 3). The effectiveness of a pea gravel equalization zone is assessed by case 4. Table 2 represents the simulation strategy.

In case 1, the high resolution 3D aquifer outcrop analogue developed by Bayer (Bayer, 2000) is utilized as the heterogeneous aquifer around the PRB. Heterogeneous secondary mineral precipitation is considered in case 1. For case 2 simulations, the aquifer is set to be homogeneous, and the hydraulic conductivity value of the aquifer is  $2.11 \times 10^{-3} \text{ m/s}$ , the arithmetic mean value of the heterogeneous aquifer from case 1. Heterogeneous mineral precipitation is taken into consideration and the precipitation rate is the same as in case 1. Case 3 simulations utilized the identical heterogeneous aquifer as in case 1, and the porosity

reduction of the barrier medium is assumed to be homogeneous over time, which means the precipitation rate ( $\tau$ ) is a constant. The value of the precipitation rate in case 3 is also calibrated using the field measurements by Sarr (Sarr, 2001). For case 4 simulations, the heterogeneous aquifer and the heterogeneous mineral precipitation are the same as case 1. A 1-m-thick pea gravel equalization zone is added directly up gradient of the Fe<sup>0</sup>-PRB. The gravel equalization zone had the same lateral and vertical dimensions as the Fe<sup>0</sup>-PRB (7 m wide and 6 m deep), and had a constant porosity of 0.5 and hydraulic conductivity of 0.09 m/s, which is identical to the initial setting of the PRB.

The constant hydraulic head values of the entrance and exit boundaries, and the precipitation rates ( $\tau$ ) for four cases are calibrated parameters in this model. To set meaningful values for hydraulic head of the boundaries, a steady-state simulation was conducted with the initial PRB condition, and the constant hydraulic head values were calibrated to ensure that the average Darcy flux within the PRB is 0.16 m/d (ITRC 2005). The precipitation rate ( $\tau$ ) values for the case 1, case 2, and case 3 were calibrated to fit the simulated average porosity loss within the PRB to the measured porosity loss in Sarr, 2001, who reported a porosity reduction of 0.02 per year. For case 3, since a homogeneous mineral precipitation was considered, the precipitation rate within the PRB is a constant and was calibrated to 0.02 [1/y]. For case 1 and case 2, since a heterogeneous mineral precipitation was considered, the precipitation rate ( $\tau$ ) was described by Equation 4.9, and the constants  $a$  and  $b$  were calibrated as 0.006 and 0.14, respectively. Case 4 utilized the same precipitation rate as in case 1.

Table 4.2 Simulation strategy

	Surrounding Aquifer	Barrier medium	Pea gravel zone
Case 1	Heterogeneous	Heterogeneous mineral precipitation	Without
Case 2	Homogeneous	Heterogeneous mineral precipitation	Without
Case 3	Heterogeneous	Homogeneous mineral precipitation	Without
Case 4	Heterogeneous	Heterogeneous mineral precipitation	With

As mentioned, the porosity heterogeneity of the barrier strongly depends on the groundwater flow pattern, and therefore on aquifer heterogeneity. Using the high resolution 3D aquifer outcrop analogue by Bayer (Bayer, 2000), an accurate representation of real, natural aquifer conditions is obtained. The hydraulic conductivity distribution of this analogue is illustrated in Figure 4.2. It represents unconsolidated fluvial sediments in a gravel pit near the town of Herten in southwest Germany. To obtain the analogue, sequentially taken outcrop photographs were interpreted to yield lithology maps, using sediment size, texture information and GPR surveys. Based on the lithology description, 10 cm-scale resolution of hydraulic

conductivity and porosity was obtained based on laboratory measurements. The resulting 3D hydraulic parameter distribution model was further developed by Maji and Sudicky (Maji and Sudicky, 2008) using a transition probability/Markov chain-based simulation method. The size of the outcrop analogue is  $16 \times 10 \times 7$  m with a resolution of  $5 \times 5 \times 5$  cm. The hydraulic conductivity varies from  $6 \times 10^{-7}$  to 1 m/s. The arithmetic mean value and standard deviation of hydraulic conductivity are  $2.11 \times 10^{-3}$  m/s and 0.0274 m/s, respectively. The specific storage is defined as a spatially uniform value of  $1 \times 10^{-4}$  1/m. More details can be found in Hu et al. (Hu et al., 2011) and Liu et al. (Liu et al., 2020). The spatial variability of the geochemical parameters of the groundwater derived from the high heterogeneity of the aquifer analogue was not included in this study. Nonetheless, it is worth noting that the aquifer heterogeneity can lead to a significant variation of water chemistry. For instance, the groundwater coming from the high hydraulic conductivity zones in the aquifer would contain higher amounts of dissolved oxygen and mineral-forming ions than the water from low hydraulic conductivity zones. The higher concentrations of dissolved oxygen and mineral-forming ions may cause a more rapid porosity loss in the Fe<sup>0</sup>-PRB (Li et al., 2005). Thus, the geochemical variation of the groundwater might aggravate the predicted effect based on this model.

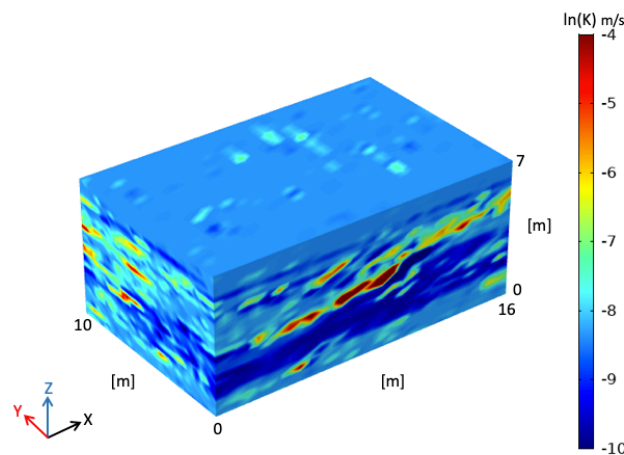


Figure 4.2 The 3-D view of the aquifer analogue  $\ln(K)$  field.

The general input parameters for the numerical simulations are summarized in Table 3. For all simulated scenarios, the initial porosity and hydraulic conductivity of the Fe<sup>0</sup>-PRB are homogeneous. The initial porosity is set to 0.5 and hydraulic conductivity is 0.09 m/s.

Table 4.3 General model input parameters

Parameter	Value	Reference
Density of water $\rho$ [kg/m <sup>3</sup> ]	1000	

Viscosity of water $\nu$ [m <sup>2</sup> /s]	$1.2 \times 10^{-6}$	(Korson et al., 1969)
Molecular diffusion coefficient $D_F$ [m <sup>2</sup> /s]	$1 \times 10^{-9}$	(Li et al., 2006)
Dispersion coefficient $D_D$ [m <sup>2</sup> /s]	$1 \times 10^{-9}$	(Li et al., 2006)
Anaerobic iron corrosion rate $r$ [mm/y]	$3 \times 10^{-6}$	(Mayer et al., 2001)
Initial iron surface area $S_{Fe}^0$ [m <sup>2</sup> /m <sup>3</sup> ]	$1.3 \times 10^3$	
Initial iron volume fraction $n_{Fe}^0$ [1]	0.5	
Iron volumetric expansion coefficient $\eta$ [1]	1.97	(Luo et al., 2013)
Gravitational acceleration $g$ [m/s <sup>2</sup> ]	9.8	
Particle diameter $D$ [mm]	2	

### 4.3 Results

#### 4.3.1 Porosity and hydraulic conductivity reduction

As stated in the description of the conceptual model, the simulated Fe<sup>0</sup>-PRB is divided into two sections: (1) the entrance domain and (2) the exit domain. The porosity reduction within the entrance domain is caused by secondary mineral precipitation plus iron corrosion, while the porosity of the exit domain is reduced merely because of the iron corrosion products.

##### 4.3.1.1 The entrance domain

Within the entrance zone, both secondary mineral precipitation and iron corrosion are simulated numerically. The relative average porosity and hydraulic conductivity reductions for the four cases are shown in Figure 4.3. As stated above, the precipitation rates for case 1 and case 3 are calibrated to make the simulated average porosity reduction within the PRB entrance domain fit the field measurements reported by Sarr (Sarr, 2001). Therefore, the average porosity reduction as well as the average hydraulic conductivity reduction of two cases are identical over time.

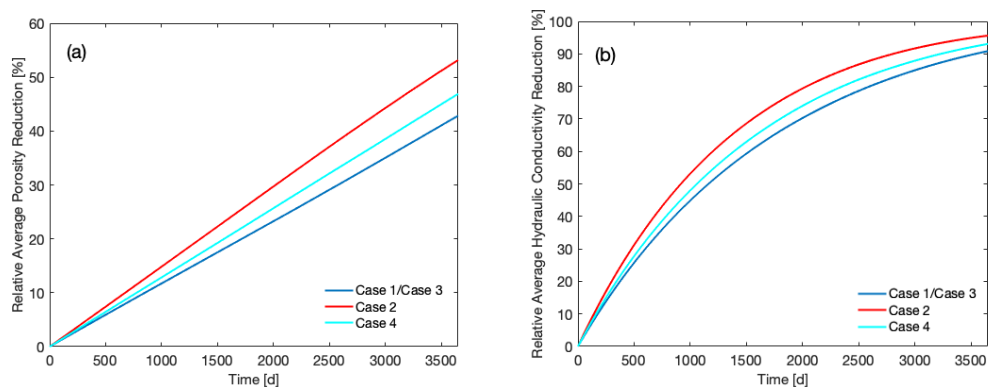


Figure 4.3 (a) Relative average porosity reduction and (b) hydraulic conductivity reduction within the PRB entrance domain. The blue line represents the simulation results for case 1 and case 3. The red line represents the simulation results for case 2. The cyan line represents the simulation result for case 4. The average porosity and hydraulic conductivity reductions are identical for case 1 and case 3.

The average porosity loss after ten years equals to 0.21 for case 1 and case 3, and 0.26 for case 2. This difference can be considered not significant. The identical initial average Darcy flux within the PRB may account for the minor difference. For case 1 and case 2, the mineral precipitation within the PRB is heterogeneous and the precipitation rate is assumed to be proportional to the Darcy flux. The same initial average flux results in the same amount of mineral precipitation at the beginning, and similar porosity reduction during the operation. For case 4, the average porosity loss after ten years equals to 0.23, which is larger than that for case 1. Nonetheless, as shown in Figure 3, although porosity reduction is around 50%, the entrance domain of the Fe<sup>0</sup>-PRB loses over 90% of hydraulic conductivity after 10 years.

Figure 4.4 shows the initial porosity distribution in the PRB entrance domain and surrounding aquifer on a portion of a 2D section of the model domain (y-z section, x=7.25 m) and the porosity distribution after 5 and 10 years of operation for all four cases.

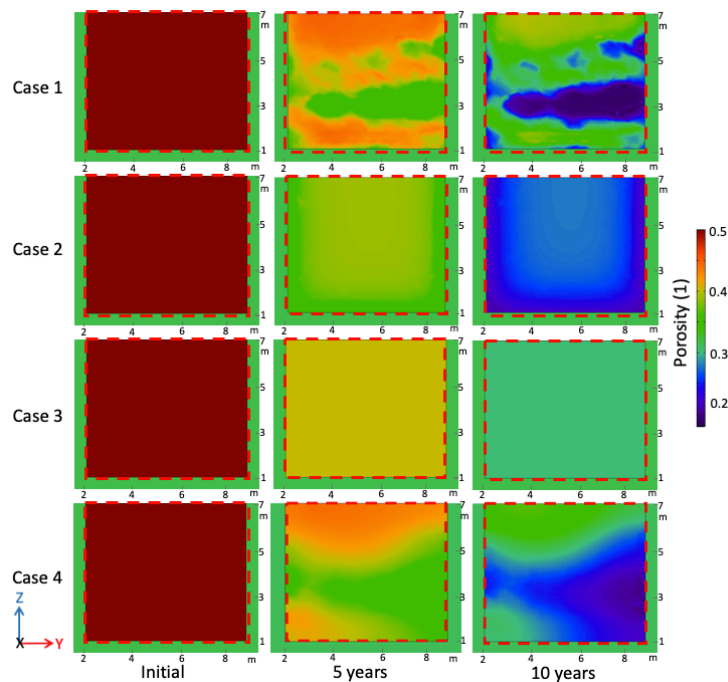


Figure 4.4 Porosity distribution within the PRB entrance domain and the surrounding aquifer on a portion of a 2D section of the model domain (y-z section, x=7.25 m) for all four cases, initial porosity condition and porosity distribution after 5 and 10 years of operation. The red dashed lines represent the border of the PRB.

For case 1, the porosity of the entrance domain is highly heterogeneous because of the preferential flow in the heterogeneous aquifer and heterogeneously distributed mineral

precipitation. The heterogeneity in porosity increases with the operation time. For case 2, the porosity of the medium within the entrance domain remains almost uniform through time, except on the edges of the PRB where larger porosity reduction occurs. This larger porosity reduction is caused by the increased flux on the edges of the barrier as the initial hydraulic conductivity of the PRB is higher than that of the aquifer. For case 3, although the surrounding aquifer is heterogeneous, the porosity distribution is homogeneous over time as the secondary mineral precipitation is homogeneously distributed within the barrier. The simulation results of all cases differ substantially. The maximum porosity reduction of case 1 (0.37 after 10 years) is larger than that of case 2 (0.25 after 10 years). The largest difference occurs in the zones with the highest initial Darcy flux, which are preferential flow paths. Nonetheless, the porosity reduction for case 1 and case 3 are generally less than for case 2, except within preferential flow paths, which is consistent with the average porosity reduction results shown in Figure 3. For case 4, the simulated porosity distribution shows less heterogeneity compared to that of case 1, which indicates that the pea gravel zone can successfully equalize the groundwater flow, and minimize the effect of preferential flow in the aquifer. Although the maximum porosity loss in case 4 (0.32 after 10 years) is smaller than that in case 1, the average porosity loss of the barrier in case 4 is greater than that in case 1 as shown in Figure 3.

#### 4.3.1.2 The exit domain

Since the only consideration in the exit domain is the iron corrosion, and it is assumed that the iron corrosion rate (in mm/y) is not a function of the Darcy flux, the porosity and hydraulic conductivity reduction within the exit domain (shown in Figure 4.5) are the same for all studied cases. As shown in the figure, the porosity loss is  $6.4 \times 10^{-4}$  in a ten-year period. This result is consistent with the field measurement reported by Wilkin et al. 2003, which is less than  $2 \times 10^{-5}$  porosity reduction per year. Although the precipitation of iron corrosion products is the basic reason for porosity reduction in Fe<sup>0</sup>-PRBs (Hu, 2020), the simulated porosity and hydraulic conductivity reductions caused by iron corrosion are relatively low. The possible reason is the small iron corrosion rate used in this study, which is derived from previous work on Fe<sup>0</sup>-PRBs (Jeen et al., 2011; Jeen et al., 2007; Mayer et al., 2001). Nonetheless, the iron corrosion rate can vary over several orders of magnitude (Melchers and Petersen, 2018), and is especially dependent on the flow and chemical conditions. If a larger iron corrosion rate is employed in a specific case, the porosity reduction caused by iron corrosion can be enormous and have a significant influence on the long-term performance of the PRB.

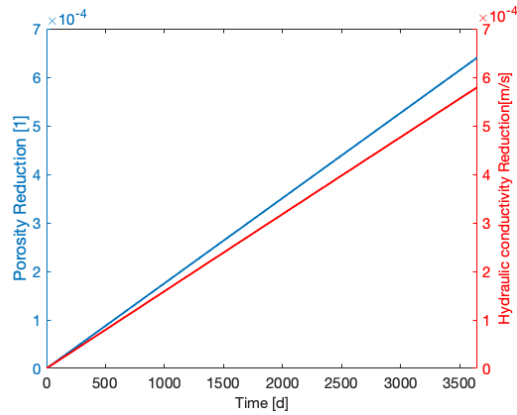


Figure 4.5 Porosity and hydraulic conductivity reduction over time within the exit domain.

#### 4.3.2 Redistribution of groundwater flow and by-passing

Figure 4.6 illustrates the initial horizontal Darcy flux distribution in the PRB and aquifer on a portion of the 2D section of the model domain (y-z section,  $x=7.25$  m) and the Darcy flux variations after 5 years and 10 years of operation for all cases.

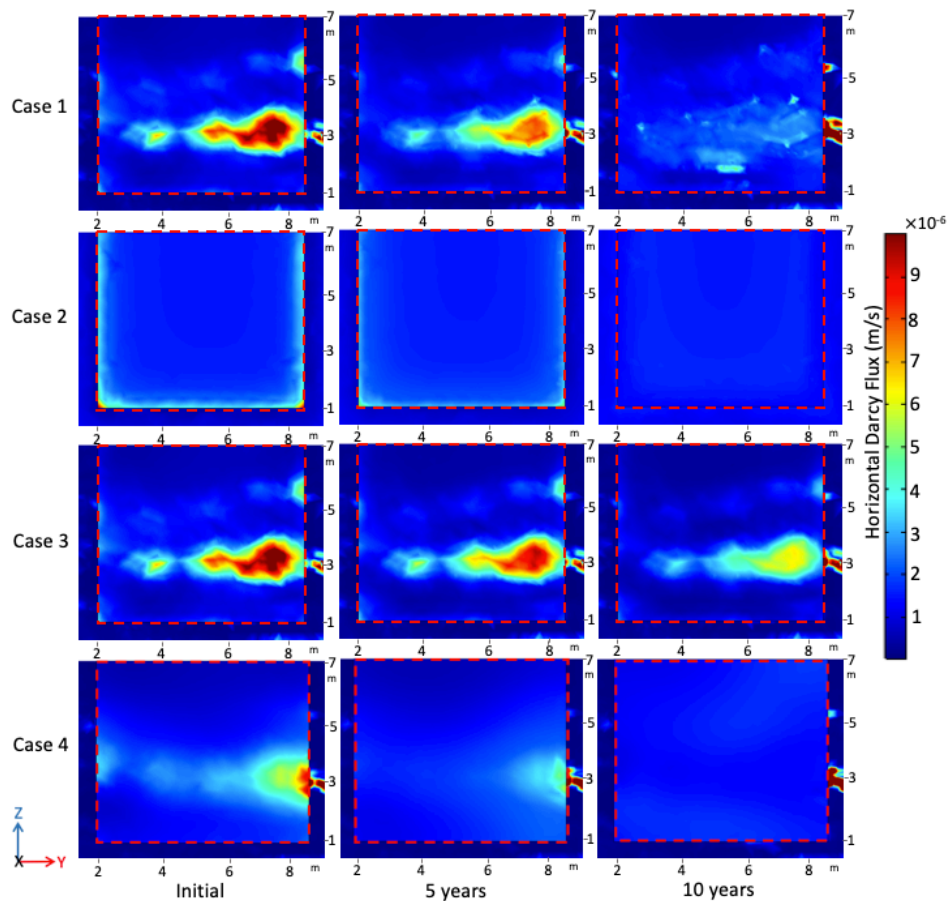


Figure 4.6 Horizontal Darcy flux distribution within the PRB and its surrounding aquifer on a portion of the 2D section of the model domain (y-z section,  $x=7.25$  m) for all four cases, initial condition and Darcy flux distribution after 5 and 10 years of operation. The red dotted frame represents the border of the PRB.

The areas with higher flux caused by aquifer heterogeneity can be detected at the early stage of operation for case 1 and case 3. As the precipitation rate enhances with increasing the groundwater flux, porosity reduction as well as hydraulic conductivity reduction of initially high flux zones are more significant, which leads to the disappearance of these zones in case 1 and case 3. The decrease of fluid flux within initially high flux zones is more significant for case 1 than for case 3. In case 1, the initial high flux zone almost disappears after 10 years of operation. For case 3, the flux within the initially high flux zones remains higher than within the surrounding area. Additionally, for areas with initially low fluxes, the simulated fluxes also decrease with time for case 3. However, in case 1 simulations, fluxes gradually increase in these areas. Moreover, the generation of high fluxes right outside the PRB is illustrated in Figure 6 for case 1 and case 3, which indicates the by-passing of groundwater flow around the PRB. Case 1 shows a higher degree of by-passing compared to case 3. For case 2, the preferential flow does not exist as the aquifer is homogeneous. At the early stage, high fluxes appear on the edges of the PRB. During the operation, because of the precipitation caused by the high fluxes, the porosity and hydraulic conductivity of the edges of the PRB decrease rapidly, which leads to the elimination of the relatively high flux zones. For case 4, the initial high flux zones caused by aquifer heterogeneity cannot be clearly detected in the simulation results, although a heterogeneous aquifer is considered. The horizontal Darcy flux becomes more evenly distributed over time.

Figure 4.7 shows the temporal variation of average Darcy flux within the  $\text{Fe}^0$ -PRB for all cases. As shown in Figure 4.7, when the surrounding aquifer is homogeneous (case 2), or the mineral precipitation is homogeneous (case 3), the average flux within the PRB continuously decreases. In case 2, a more significant average flux reduction than in case 3 is observed after 10 years of operation. On the contrary, for the case with a pea gravel equalization zone in front of the PRB (case 4), the simulated average Darcy flux within the  $\text{Fe}^0$ -PRB keep increasing over time. For case 1, in which the aquifer as well as the mineral precipitation are heterogeneous, the average flux remains relatively stable over time, except for the fluctuation between 1500 and 2000 days. The different flux changes within the areas with low initial fluxes rates may explain the difference of average fluxes with time for case 1 and case 3. For case 3, the fluxes in all areas decrease over time, which results in the continuously decreasing average flux. For case 1, although the fluxes within the initially high flux zones decrease with time, the fluxes increase in areas with initially low fluxes, which yields a stable average flux for case 1 over time.

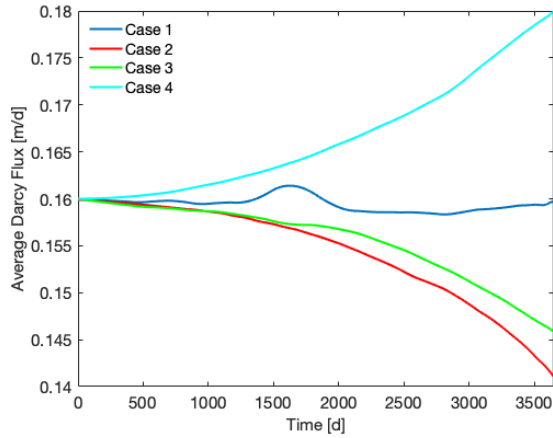


Figure 4.7 Temporal variation of the average Darcy flux within the Fe-PRB during the operation period for the four simulated cases.

The total groundwater flow rate through the Fe<sup>0</sup>-PRB over time was simulated to investigate the occurrence of groundwater by-passing. The temporal percentage of the flow rate loss for the four cases is depicted in Figure 4.8. The simulation shows that by-passing occurs instantly after the PRB installation for all cases. After 10 years of simulation, the total flow rate loss is 18.5%, 12.9%, 10.9%, and 4% for case 1, case 2, case 3, and case 4, respectively. The flow rate loss in case 1 is 30% and 41% larger than in case 2 and case 3, which means the by-passing flow loss may be underestimated when porosity heterogeneity of the barrier is improperly considered (case 2 and case 3). The flow rate loss in case 4 is remarkably smaller than that in case 1, which suggests that a pea gravel equalization zone can effectively minimize the amount of by-passing flow during long-term operation.

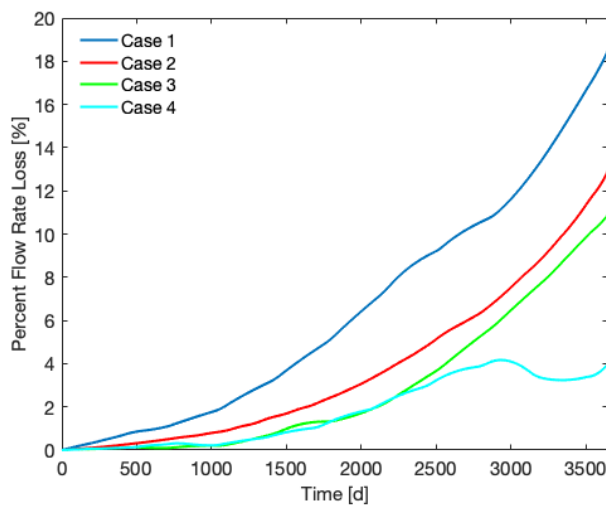


Figure 4.8 Percentage of flow rate loss within Fe-PRB over time for the four simulated cases.

### 4.3.3 Contaminant plume migration

Figure 4.9 illustrates the contaminant plume migration over time for all cases. For case 2, the homogeneous aquifer leads to a uniformly distributed groundwater flow, the contaminant plume is spatially evenly distributed around the source. Since the size of the PRB cannot cover the whole height of the model domain, contaminant leakage passing around the PRB occurs initially, especially at the bottom of the PRB. After 10 years of simulation, because of the reduction of hydraulic conductivity and porosity within the PRB, the untreated contaminant plume spreads along the direction of groundwater flow and migrates by-passing the PRB. As shown in Figure 9, for case 3, no significant contaminant plume can be detected after 10 years. In case 1, since the PRB covers the preferential flow paths caused by aquifer heterogeneity, for the initial condition, the PRB can completely remove the contaminant plume. Nonetheless, higher degrees of untreated contaminant plume spread and migration within the research domain can be seen after 10 years of operation in case 1, comparing to case 2 and case 3. For case 4, in which a pea gravel zone is added, no evidence of contaminant plume leakage down gradient of the PRB can be detected after ten years simulation.

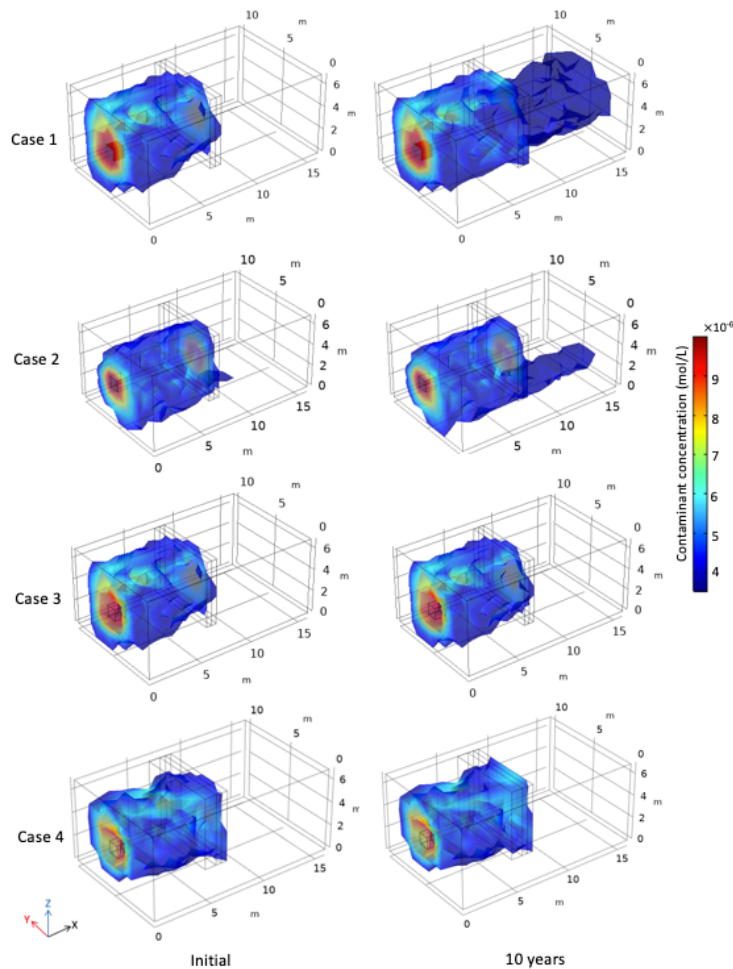


Figure 4.9 Contaminant plume distribution within the model domain for all cases. The four rows show the simulation results of case 1, case 2, case 3, and case 4, respectively. The first and second columns illustrate the initial contaminant plume and the contaminant plume migration after 10 years of operation, respectively.

#### 4.3.4 Groundwater residence time

Figure 10 illustrates particle advective transport results at the cross-section ( $y = 5\text{m}$ ) of the model domain for case 1 and case 2 within the first 6 days of spreading. Since case 1, case 3, and case 4 assumed a similar heterogeneous aquifer, the particle tracing results are identical within the first 6 days for those two cases. As evident from Figure 4.10, for case 1, the transport velocities of particles are significantly different. Particles with large velocity pass rapidly through the PRB, whereas those with low velocity scarcely migrate after 6 days. In case 2, except for the high velocity particles at the edge of the PRB, released particles have an almost uniform transport velocity.

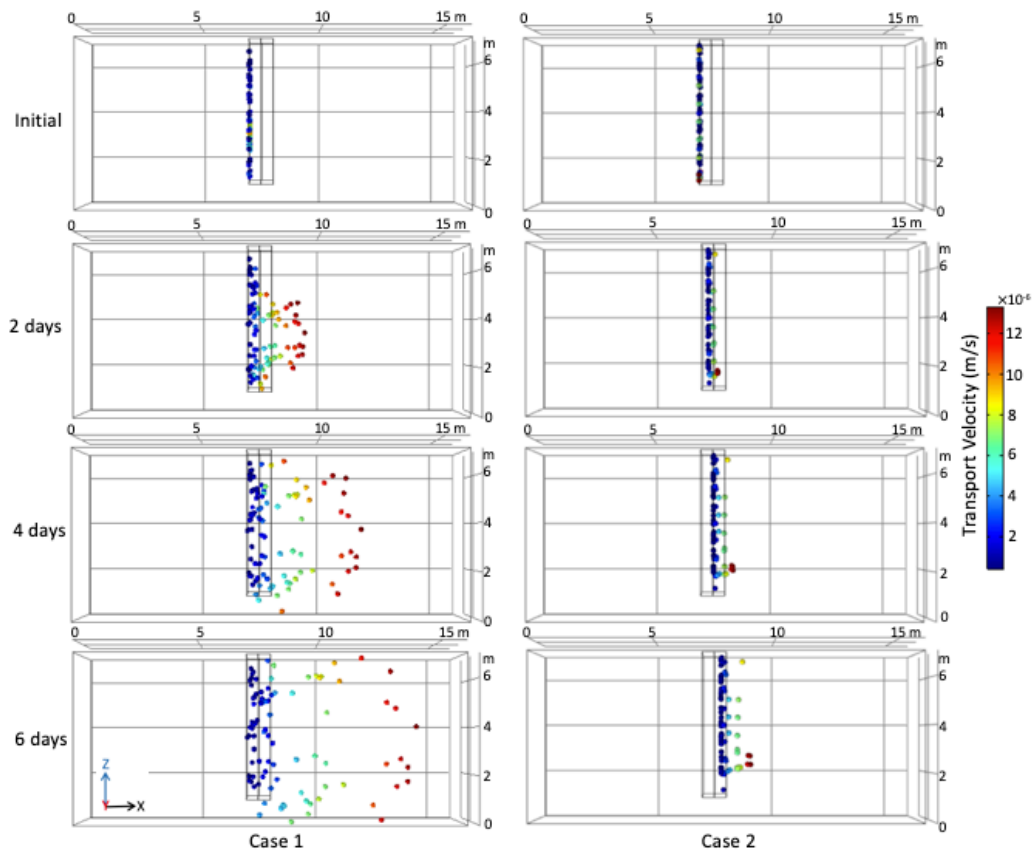


Figure 4.10. The positions of particles on the cross-section of the model domain for case 1 and case 2 within the first 6 days. The first and second columns show the simulation results of case 1 and case 2, respectively. The first row shows the initial positions of the particles. The second, third and fourth rows illustrate the distribution of particles after 2, 4 and 6 days of transport, respectively. Different colours represent different transport velocities of the particles. Since case 1, case 3, and case 4 assumed the same heterogeneous aquifer, the particle tracing results within the first 6 days for three cases are identical. Thus, the results of case 3, and case 4 are not shown.

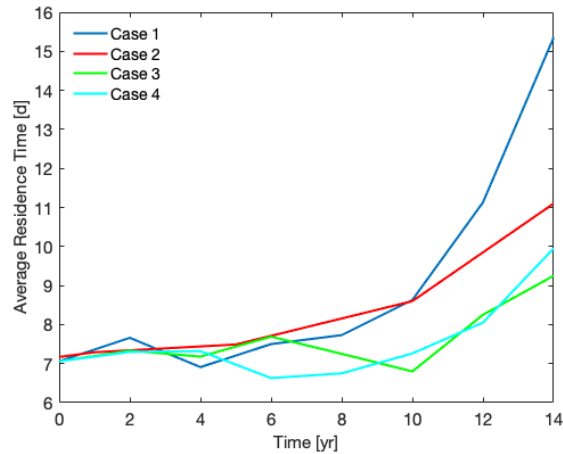


Figure 4.11. Average groundwater residence time within the Fe<sup>0</sup>-PRB over time for all cases.

The time when each water particle leaves the PRB was recorded, and the simulated average residence times of particles within the Fe<sup>0</sup>-PRB over time are shown in Figure 4.11 for the four cases. The average residence times increase continuously after the installation of Fe<sup>0</sup>-PRB for case 2. In case 1 and case 3, the groundwater residence time remains almost constant for the first 4 and 10 years, respectively, and then increases. No obvious reduction of groundwater residence time is observed for all cases, which means that, as long as the groundwater can flow through the PRB, there will be enough reaction time to remove the contaminant. This finding is consistent with the field observation by Wilkin et al. (Wilkin et al., 2018), who reported that a Fe<sup>0</sup>-PRB can continue to remove contaminants from groundwater after 22 years of operation. For case 4, when a pea gravel zone is added in the model, there is a minor decrease of average groundwater residence time between 4 and 6 years simulation, which may be caused by the accelerated average Darcy flux as shown in Figure 4.7. The simulated average groundwater residence time of case 4 is smaller than that of case 1.

#### 4.4 Summary and discussion

The physical and chemical processes of contaminants removal within the Fe<sup>0</sup>-PRB are very complex, and related parameters, such as porosity, mineral precipitation rates, are difficult to measure directly. Therefore, a model fully validated based on field observations is currently hard to approach. The model described in this study uses the well-documented partial differential equations to simulate the groundwater flow and contaminant transport within the Fe<sup>0</sup>-PRB and its surrounding aquifer. In order to make the model close to reality, a 3-D high resolution aquifer outcrop analogue was utilized to implement aquifer heterogeneity. We also set the parameters of the governing equations according to the literature, and calibrated the

values of constant head and precipitation rate in our model based on the field observations of (Sarr, 2001). Due to above considerations, we believe that the established model in this study can reasonably simulate the reality in the field.

The simulation results show significant differences among the spatial porosity distributions inside the Fe<sup>0</sup>-PRB over time for all cases. In case 1, the precipitation rate varies with the Darcy flux. The applied heterogeneous aquifer causes spatially variable fluxes within the Fe<sup>0</sup>-PRB, which results in a highly heterogeneous porosity distribution within the barrier medium. For case 2, the porosity of the barrier medium remains almost uniform over time, because the aquifer is homogeneous as well as the groundwater flux. The larger porosity reduction on the edge of the PRB is caused by the accelerated flux as the initial hydraulic conductivity of the PRB is higher than that of the aquifer. Higher fluxes lead to a larger precipitation rate, increasing the porosity reduction. For case 3, since a homogeneous porosity reduction is assumed, the porosity of the barrier medium is homogeneous over time.

The difference of porosity distributions between case 1, case 2, and case 3 results in a different behaviour of groundwater flow. For case 2 and case 3, the average Darcy flux decreases continuously over time within the PRB, while the average Darcy flux remains constant for case 1. The possible interpretation is that, in case 1, although the fluxes within the initially high flux zones reduce rapidly, fluxes within the areas with initially low fluxes increase over time. The Darcy flux distribution within the PRB and the aquifer shows that for case 1 and case 3 an accelerated flow appears gradually outside of the PRB, which indicates the by-passing of groundwater flow around the PRB. Case 1 shows a higher degree of by-passing compared to that of case 3. This implies an underestimation of by-passing of a PRB where the heterogeneity of the barrier medium is not taken into account. This finding is consistent with the simulation results of flow rate loss over time for the three cases, which show that if heterogeneity of the aquifer (case 2) or heterogeneity of the barrier medium (case 3) is not considered, 30% or 41% of flow rate loss (by-passing) in ten-years simulation are underestimated.

The simulation results of case 1 show a significantly higher degree of contaminant plume spreading and migration over time, compared to that of case 2 and case 3. Therefore, for the Fe<sup>0</sup>-PRB design and long-term evaluation, heterogeneity of the pore space is important for the evaluation of the long-term plume migration. Where only a homogeneous surrounding aquifer is simulated, or heterogeneous mineral precipitation is neglected, the untreated contaminant plume spread over time may be underestimated.

Particle tracing was applied to assess groundwater residence time within the PRB for all cases. The average residence time of particles tends to increase with time, and no evidence of

residence time reduction is observed in case 1, case 2, and case 3. Therefore, in this study, the reduction of water residence time is not a concern of PRB performance. Rather than the reduction of groundwater residence time, by-passing flow is the key factor influencing the long-term performance of a continuous-wall Fe<sup>0</sup>-PRB.

The effectiveness of a pea gravel equalization zone can be assessed by comparing the simulation results between case 1 and case 4. Identical surrounding aquifer and mineral precipitation rates are utilized in case 1 and case 4, and the only difference between the two case studies is the addition of 1-m-thick pea gravel equalization zone up gradient of the PRB in case 4. The simulation results show that the porosity and horizontal Darcy flux are more homogeneously distributed during operation in case 4 than in case 1 (Figure 4 and Figure 6). The average porosity loss, and the average Darcy flux within the PRB are larger when a pea gravel zone is considered. It is consistent with the finding of Li and Benson et al. 2010, who reported that pea gravel equalization zones result in an increasing average porosity reduction in their study. The possible explanation for the increasing Darcy flux and average porosity loss is that the highly permeable gravel zone can concentrate the groundwater flow in the surrounding area and constantly supply it to the PRB. Due to the effect of the permeable gravel zone and less heterogeneous distributed barrier, the simulation results show less flow rate loss and no contaminant plume leakage around the PRB over ten years operation in case 4. Thus, it can be found in this study that the addition of a pea gravel equalization zone can effectively improve the long-term performance of a continuous-wall Fe<sup>0</sup>-PRB by equalizing the groundwater flow into the PRB, reducing the heterogeneity of the barrier medium, and minimizing the by-passing flow that may exist during long-term operation. However, the particle tracking results show less average groundwater residence time within the PRB when a pea gravel zone is added, which may have a negative impact on contaminant removal.

In this case study, the predicted results and findings are specific to a Fe<sup>0</sup>-PRB with a continuous-wall design. Although the application of PRBs with continuous-wall design is the most common due to its low installation cost, the Fe<sup>0</sup>-PRBs with this design may face some problems during long-term operation, e.g. the issue of by-passing flow in this study. In field applications, a funnel-and-gate design can be utilized to eliminate the effect of by-passing flow. A funnel-and-gate design comprises funnels, i.e. cut-off walls around the barrier, which can converge the contaminant plume to the PRB (Thakur et al., 2020). The cut-off walls, such as sheet piles and slurry walls, have low permeability, and can prevent the occurrence of the by-passing flow around the PRB (Obiri-Nyarko et al., 2014; Smith et al., 2003). However, the funnel-and-gate construction is more expensive than a continuous-wall system, which

hampers its broad application prospects for projects with a limited budget. In a real world scenario, both the construction costs of a PRB and its long-term performance should be carefully considered in the design stage. In addition, the predicted effect described herein is based on case studies. A more general investigation on the impact of porosity heterogeneity of the barrier, considering statistics, should be conducted in the future.

#### 4.5 Conclusions

A series of simulations were conducted using a 3-D groundwater flow and transport model to evaluate how porosity heterogeneity of the barrier medium may affect the groundwater flow and influence the long-term performance of a continuous-wall Fe<sup>0</sup>-PRB. Four cases were simulated where each considered: (1) heterogeneous aquifer and heterogeneous mineral precipitation, (2) homogeneous aquifer and heterogeneous mineral precipitation, (3) heterogeneous aquifer and homogeneous mineral precipitation, and (4) heterogeneous aquifer and heterogeneous mineral precipitation with a pea gravel equalization zone up gradient of the PRB. A 3-D high resolution aquifer outcrop analogue was adopted to set the hydraulic properties of the heterogeneous aquifer. Results from this study reveal the following:

- Preferential flow in heterogeneous aquifers and heterogeneously distributed mineral precipitation can cause a significant porosity heterogeneity of the barrier medium over time, which results in a remarkable difference of groundwater flow behavior.
- For all cases, by-passing occurs instantly after beginning of the operation. If porosity heterogeneity of the barrier medium is not considered, 30%-41% of the by-passing flow rates are underestimated in ten-years simulation. By-passing is a key concern threatening the long-term performance of a continuous-wall Fe<sup>0</sup>-PRB.
- For the transport of contaminants, the long-term contaminant plume migration is underrated if porosity heterogeneity of the barrier medium is neglected.
- The residence time of groundwater within the Fe<sup>0</sup>-PRB increases over time. Obvious reduction of groundwater residence time is not observed in case studies.
- Installation of a pea gravel equalization zone can effectively improve the long-term performance of a continuous-wall Fe<sup>0</sup>-PRB by equalizing the groundwater flow into the PRB, reducing the heterogeneity of the barrier medium, and minimizing the by-passing flow that may exist during long-term operation. But the pea gravel equalization zone results in a smaller residence time that could have a negative effects on long-term performance of a PRB.

We recommend to properly consider the impact of porosity heterogeneity of the barrier on the prediction of a continuous-wall Fe<sup>0</sup>-PRB longevity, especially when the surrounding aquifer is highly heterogeneous. The heterogeneity of the aquifer could form an unevenly porosity loss within the PRB and cause a large amount of by-passing flow during long-term operation. In addition, the installation of a pea gravel equalization zone up gradient of the Fe<sup>0</sup>-PRB is recommended, due to its effect to reduce the heterogeneity of the barrier, and to minimize the by-passing flow.

## References

- Agrawal, A., Tratnyek, P.G., 1995. Reduction of nitro aromatic compounds by zero-valent iron metal. *Environmental Science & Technology*, 30(1): 153-160.
- Arnold, W.A., Roberts, A.L., 2000. Pathways and kinetics of chlorinated ethylene and chlorinated acetylene reaction with Fe (0) particles. *Environmental Science & Technology*, 34(9): 1794-1805
- Bayer, P., 2000. Aquifer-Analog-Studie in grobklastischen 'braided river' Ablagerungen: Sedimentäre/hydrogeologische Wandkartierung und Kalibrierung von Georadarmessungen—Diplomkartierung. Diplomkartierung, Universitaet Tuebingen.
- Bird, R.B., Stewart, W.E., Lightfoot, E.N., 2006. *Transport phenomena*, 1. John Wiley & Sons.
- Bryant, I.D., Flint, S.S., 2009. *The geological modelling of hydrocarbon reservoirs and outcrop analogues*, 37. John Wiley & Sons.
- Caré, S. et al., 2013. Modeling the permeability loss of metallic iron water filtration systems. *Clean–Soil, Air, Water*, 41(3): 275-282 %@ 1863-0650.
- Caré, S., Nguyen, Q.T., l'Hostis, V., Berthaud, Y., 2008. Mechanical properties of the rust layer induced by impressed current method in reinforced mortar. *Cement and Concrete Research*, 38(8-9): 1079-1091
- Carman, P.C., 1997. Fluid flow through granular beds. *Chemical Engineering Research and Design*, 75: S32-S48
- Gillham, R.W., 1999. In situ remediation of VOC-contaminated groundwater using zero-valent iron: Long-term performance, pp. 21-25.
- Henderson, A.D., Demond, A.H., 2007. Long-term performance of zero-valent iron permeable reactive barriers: a critical review. *Environmental Engineering Science*, 24(4): 401-423
- Hu, R., Brauchler, R., Herold, M., Bayer, P., 2011. Hydraulic tomography analog outcrop study: Combining travel time and steady shape inversion. *Journal of Hydrology*, 409(1-2): 350-362.
- Hu, R., Gwenz, W., Sipowo-Tala, V.R., Noubactep, C., 2019. Water treatment using metallic iron: A tutorial

- review. *Processes*, 7(9): 622.
- Hu, R.Y., H.; Tao, R.; Cui, X.; Xiao, M.; Amoah, B.K.; Cao, V.; Lufingo, M.; Soppa-Sangue, N.P.; Ndé-Tchoupé, A.I.; Gatcha-Bandjun, N.; Sipowo-Tala, V.R.; Gwenzi, W.; Noubactep, C., 2020. Metallic Iron for Environmental Remediation: Starting an Overdue Progress in Knowledge. *water*, 12(641).
- Huggenberger, P., Aigner, T., 1999. Introduction to the special issue on aquifer-sedimentology: problems, perspectives and modern approaches. *Sedimentary Geology*, 129(3-4): 179-186.
- Jeen, S.-W., Gillham, R.W., Przepiora, A., 2011. Predictions of long-term performance of granular iron permeable reactive barriers: Field-scale evaluation. *Journal of Contaminant Hydrology*, 123(1-2): 50-64.
- Jeen, S.-W., Mayer, K.U., Gillham, R.W., Blowes, D.W., 2007. Reactive transport modeling of trichloroethene treatment with declining reactivity of iron. *Environmental science & technology*, 41(4): 1432-1438.
- Jeen, S.-W., O, J.S., Gillham, R.W., 2008. Modeling Geochemical and Reactivity Changes of Different Iron Materials, *GeoCongress 2008: Geotechnics of Waste Management and Remediation*, pp. 595-602.
- Johnson, R.L., Tratnyek, P.G., Miehr, R., Thoms, R.B., Bandstra, J.Z., 2005. Reduction of hydraulic conductivity and reactivity in zero-valent iron columns by oxygen and TNT. *Groundwater Monitoring & Remediation*, 25(1): 129-136.
- Kamolpornwijit, W., Liang, L., 2006. Investigation of gas production and entrapment in granular iron medium. *Journal of contaminant hydrology*, 82(3-4): 338-356.
- Kamolpornwijit, W., Liang, L., Moline, G.R., Hart, T., West, O.R., 2004. Identification and quantification of mineral precipitation in Fe<sup>0</sup> filings from a column study. *Environmental science & technology*, 38(21): 5757-5765
- Keum, Y.-S., Li, Q.X., 2004. Reduction of nitroaromatic pesticides with zero-valent iron. *Chemosphere*, 54(3): 255-263
- Korson, L., Drost-Hansen, W., Millero, F.J., 1969. Viscosity of water at various temperatures. *The Journal of Physical Chemistry*, 73(1): 34-39.
- Landolt, D., 2007. *Corrosion and surface chemistry of metals*. CRC press.
- Li, L., Benson, C.H., 2010. Evaluation of five strategies to limit the impact of fouling in permeable reactive barriers. *Journal of Hazardous materials*, 181(1-3): 170-180
- Li, L., Benson, C.H., Lawson, E.M., 2005. Impact of mineral fouling on hydraulic behavior of permeable reactive barriers. *Groundwater*, 43(4): 582-596
- Li, L., Benson, C.H., Lawson, E.M., 2006. Modeling porosity reductions caused by mineral fouling in continuous-wall permeable reactive barriers. *Journal of Contaminant Hydrology*, 83(1-2): 89-121

- Liu, Q. et al., 2020. A Numerical Study of Slug Tests in a Three-Dimensional Heterogeneous Porous Aquifer Considering Well Inertial Effects. *Water Resources Research*, 56(11): e2020WR027155 %@ 0043-1397.
- Luo, P., Bailey, E.H., Mooney, S.J., 2013. Quantification of changes in zero valent iron morphology using X-ray computed tomography. *Journal of Environmental Sciences*, 25(11): 2344-2351
- Maji, R., Sudicky, E.A., 2008. Influence of mass transfer characteristics for DNAPL source depletion and contaminant flux in a highly characterized glaciofluvial aquifer. *Journal of contaminant hydrology*, 102(1-2): 105-119.
- Mayer, K.U., Blowes, D.W., Frind, E.O., 2001. Reactive transport modeling of an in situ reactive barrier for the treatment of hexavalent chromium and trichloroethylene in groundwater. *Water Resources Research*, 37(12): 3091-3103
- McMahon, P.B., Dennehy, K.F., Sandstrom, M.W., 1999. Hydraulic and geochemical performance of a permeable reactive barrier containing zero-valent iron, Denver Federal Center. *Groundwater*, 37(3): 396-404.
- Melchers, R.E., Petersen, R.B., 2018. A reinterpretation of the Romanoff NBS data for corrosion of steels in soils. *Corrosion Engineering, Science and Technology*, 53(2): 131-140
- Moraci, N., Ielo, D., Bilardi, S., Calabrò, P.S., 2016. Modelling long-term hydraulic conductivity behaviour of zero valent iron column tests for permeable reactive barrier design. *Canadian Geotechnical Journal*, 53(6): 946-961
- Morales, J., Hutcheson, R., Cheng, I.F., 2002. Dechlorination of chlorinated phenols by catalyzed and uncatalyzed Fe (0) and Mg (0) particles. *Journal of Hazardous materials*, 90(1): 97-108
- Multiphysics, C., 2012. *Comsol multiphysics user guide (version 4.3 a)*. COMSOL, AB, 992.
- Nam, S., Tratnyek, P.G., 2000. Reduction of azo dyes with zero-valent iron. *Water Research*, 34(6): 1837-1845.
- Neumann, A. et al., 2013. Arsenic removal with composite iron matrix filters in Bangladesh: a field and laboratory study. *Environmental science & technology*, 47(9): 4544-4554
- Nield, D.A., Bejan, A., 2006. *Convection in porous media*, 3. Springer.
- Noubactep, C., 2011. Review Aqueous contaminant removal by metallic iron: Is the paradigm shifting? *Water SA*, 37(3 ).
- Obiri-Nyarko, F., Grajales-Mesa, S.J., Malina, G., 2014. An overview of permeable reactive barriers for in situ sustainable groundwater remediation. *Chemosphere*, 111: 243-259
- Parbs, A., Ebert, M., Dahmke, A., 2007. Long-term effects of dissolved carbonate species on the degradation of trichloroethylene by zerovalent iron. *Environmental science & technology*, 41(1):

291-296.

- Phillips, D.H. et al., 2000. Performance evaluation of a zerovalent iron reactive barrier: mineralogical characteristics. *Environmental Science & Technology*, 34(19): 4169-4176.
- Phillips, D.H., Watson, D.B., Roh, Y., Gu, B., 2003. Mineralogical characteristics and transformations during long-term operation of a zerovalent iron reactive barrier. *Journal of Environmental Quality*, 32(6): 2033-2045
- Rangsvivek, R., Jekel, M.R., 2005. Removal of dissolved metals by zero-valent iron (ZVI): Kinetics, equilibria, processes and implications for stormwater runoff treatment. *Water Research*, 39(17): 4153-4163.
- Reardon, E.J., 1995. Anaerobic corrosion of granular iron: Measurement and interpretation of hydrogen evolution rates. *Environmental science & technology*, 29(12): 2936-2945.
- Sarr, D., 2001. Zero-Valent-Iron Permeable Reactive Barriers- How Long Will They Last? *Remediation*, 11(2): 1-18
- Smith, J.W.N., Boshoff, G., Bone, B.D., 2003. Good practice guidance on permeable reactive barriers for remediating polluted groundwater, and a review of their use in the UK. *Land Contamination & Reclamation*, 11(4): 411-418.
- Sorel, D., Warner, S.D., Longino, B.L., Honniball, J.H., Hamilton, L.A., 2003. Performance monitoring and dissolved hydrogen measurements at a permeable zero valent iron reactive barrier. ACS Publications.
- Thakur, A.K., Vithanage, M., Das, D.B., Kumar, M., 2020. A review on design, material selection, mechanism, and modelling of permeable reactive barrier for community-scale groundwater treatment. *Environmental Technology & Innovation*, 19: 2352-1864.
- Tratnyek, P.G., Miehr, R., Bandstra, J.Z., 2002. Kinetics of reduction of TNT by iron metal. IAHS PUBLICATION: 427-434
- Vikesland, P.J., Klausen, J., Zimmermann, H., Roberts, A.L., Ball, W.P., 2003. Longevity of granular iron in groundwater treatment processes: changes in solute transport properties over time. *Journal of Contaminant Hydrology*, 64(1-2): 3-33
- Weber, A., Ruhl, A.S., Amos, R.T., 2013. Investigating dominant processes in ZVI permeable reactive barriers using reactive transport modeling. *Journal of contaminant hydrology*, 151: 68-82.
- Wilkin, R.T. et al., 2018. Geochemical and isotope study of trichloroethene degradation in a zero-valent iron permeable reactive barrier: A twenty-two-year performance evaluation. *Environmental science & technology*, 53(1): 296-306
- Wilkin, R.T., Puls, R.W., Sewell, G.W., 2003. Long-term performance of permeable reactive barriers using

- zero-valent iron: geochemical and microbiological effects. *Ground Water*, 41(4): 493
- Wilkin, R.T., Su, C., Ford, R.G., Paul, C.J., 2005. Chromium-removal processes during groundwater remediation by a zerovalent iron permeable reactive barrier. *Environmental science & technology*, 39(12): 4599-4605
- Williams, R.L. et al., 2007. Using dissolved gas analysis to investigate the performance of an organic carbon permeable reactive barrier for the treatment of mine drainage. *Applied geochemistry*, 22(1): 90-108.
- Wu, Q., Zheng, C., Zhang, J., Zhang, F., 2017. Nitrate removal by a permeable reactive barrier of Fe 0: A model-based evaluation. *Journal of Earth Science*, 28(3): 447-456
- Yabusaki, S., Cantrell, K., Sass, B., Steefel, C., 2001. Multicomponent reactive transport in an in situ zero-valent iron cell. *Environmental Science & Technology*, 35(7): 1493-1503
- Yang, H., Hu, R., Ruppert, H., Noubactep, C., 2021. Modeling porosity loss in Fe0-based permeable reactive barriers with Faraday's law. *Scientific Reports*, 11(1): 1-13.
- Zhang, Y., Gillham, R.W., 2005. Effects of gas generation and precipitates on performance of Fe PRBs. *Groundwater*, 43(1): 113-121.

## Chapter 5

### 5. Significance of the study and summary of achieved results

This study was performed to contribute to the design of more efficient and sustainable Fe<sup>0</sup>-based filtration systems. This chapter summarizes the achieved results (Chapter 2 through Chapter 4) while underlining their significance for the further development of the Fe<sup>0</sup> remediation technology.

#### 5.1 Starting point and dynamic literature review

The literature review as presented in Chapter 2 reflects the starting point of this thesis which corresponds to the state-of-the-art knowledge in 2018. The literature review is completed to consider advances in knowledge during this work (Chapter 3 and Chapter 4). By 2018, the Fe<sup>0</sup>-PRB was already considered as an established technology for groundwater remediation (Naidu and Birke 2015, Wilkin et al. 2019). The major open question was how to design really sustainable Fe<sup>0</sup>-PRBs, and how to accurately assess the longevity of such systems,

To understand the importance of this issue, it should be recalled how the Fe<sup>0</sup>-PRB technology was introduced and developed until then. There is no better way than to consider overview articles by pioneers of the technology (Gillham 2008, Gillham et al. 2010), technical reports (ITRC 2011), and textbooks (Naidu and Birke 2015). For example, Gillham et al. (2010) considered that "historically, the development of the granular iron PRB technology rests on the recognition of two advances: first, that metallic iron degrades chlorinated organic compounds, and second, that the reactions can proceed in situ under ambient groundwater conditions." This statement corresponds to the popular state-of-the-art knowledge on the operating mode of Fe<sup>0</sup>-PRBs, as it is considered within the Fe<sup>0</sup> research community (Kang and Choi 2009, Hu et al. 2021, Cao et al. 2022). Unfortunately, this "historical consideration" has overlooked the evidence, that under environmental conditions, no single species other than protons (H<sup>+</sup>) can reach the Fe<sup>0</sup> surface or the Fe<sup>0</sup>/H<sub>2</sub>O interface (Whitney 1903). In other words, designing efforts for sustainable Fe<sup>0</sup>-PRBs were flawed by a wrong reaction mechanism having direct influence on the porosity loss estimation. In fact, at least twice more Fe<sup>0</sup> is needed to produce the amount of electrons necessary to reduce any contaminant ( $\text{Fe}^{2+} \leftrightarrow \text{Fe}^{3+} + \text{e}^-$ ) than would have been achieved by an electrochemical mechanism ( $\text{Fe}^0 \leftrightarrow \text{Fe}^{2+} + 2\text{e}^-$ ).

## 5.2 Context of the thesis

Around 2010, the research group of Dr. Noubactep published some seminal works aiming at redirecting the design of Fe<sup>0</sup>-based filtration systems for water treatment (Noubactep 2010, Noubactep and Caré 2010a, 2010b, Noubactep 2011, Noubactep et al. 2012). Not knowing Whitney (1903) and other works denying the reductive transformation concept (e.g. Khudenko 1985, 1987, 1991), Noubactep and colleagues thought that there were common underlying mechanisms for interreactions in Fe<sup>0</sup>/H<sub>2</sub>O systems that provide a confidence for their non-site-specific design. Because contaminants without redox affinity to Fe<sup>0</sup> (e.g. bacteria, Zn<sup>2+</sup>) were also quantitatively removed, reductive transformation could not be the fundamental removal mechanism (Noubactep 2007, 2008, 2009). Therefore, adsorption, co-precipitation and size-exclusion are the fundamental mechanisms of decontamination using the Fe<sup>0</sup>/H<sub>2</sub>O systems. This cognizance questioned the importance of case-to-case treatability studies while simplifying the design of Fe<sup>0</sup> filters (Noubactep 2011). In other words, instead of testing individual Fe<sup>0</sup>/H<sub>2</sub>O systems for the removal of selected contaminants, it is required to characterize the behavior of some model species (e.g. methylene blue, Orange II) while Fe<sup>0</sup> is corroded by an aqueous solution in the long-term (Miyajima 2012, Miyajima and Noubactep 2013). Certainly, site-specific research using relevant contaminants are still needed to fine-tune design criteria for the optimal performance of Fe<sup>0</sup> filters (McGeough et al. 2007).

The presentation until now recalls a clear starting point for the design of better pilot and field Fe<sup>0</sup>-based filtration systems for water remediation. Further work considering the unique nature of each Fe<sup>0</sup> specimen (intrinsic reactivity, corrosion rate), and changes in the porosity of the system was required to explore factors limiting or fixing the service life of Fe<sup>0</sup>-PRBs. This would provide sustainability and has therefore economic implications for Fe<sup>0</sup>-PRB technology.

## 5.3 The role of iron corrosion products (FeCPs)

Under environmental conditions, there is continuing aqueous iron corrosion in Fe<sup>0</sup>-PRBs. The generated iron corrosion products at the surface of Fe<sup>0</sup> are adsorbents, and are able to scavenge all classes of contaminants (Chaves, 2005, Guan et al., 2015). The chemical composition of the FeCPs depends upon the local pH-Eh conditions, and all possible corrosion products have much less density compared to the parent metal, which makes the iron corrosion a highly volumetric expansive process (Caré et al., 2008, 2013). The generated iron corrosion products can fill the pore space within the Fe<sup>0</sup>-PRBs and cause the porosity loss of the system (Li et al.,

2006). Therefore, the FeCPs are useful as contaminant scavengers but hamper the long-term hydraulic performance of Fe<sup>0</sup>-PRBs. The effect of generated FeCPs is vital when considering the long-term porosity loss of a Fe<sup>0</sup>-PRB, as well as the longevity estimation.

The fouling role of iron corrosion products has been overlooked for long-term porosity loss estimation in some previous studies. For instance, the porosity loss in the Copenhagen Freight Yard Fe<sup>0</sup>-PRB was calculated based on the change in calcium and carbonate concentrations across the barrier (Kiilerich et al., 2000). The effect of generated FeCPs were totally ignored in this stoichiometric calculation, and the actual porosity loss in this field was largely underrated. The too small iron corrosion rates used in previous numerical model studies on Fe<sup>0</sup>-PRBs resulted in an underestimation of the effect of FeCPs and cause inaccurate estimation of PRB longevity (Mayer et al., 2001, Li et al., 2005, 2006; Yang et al., 2021).

In order to properly estimate the longevity of a Fe<sup>0</sup>-PRB, it is essential to root the estimation of the long-term porosity loss on the inherent characteristics of iron corrosion. In Chapter 3, a fundamental quantitative relationship of redox partners in electrochemistry, known as Faraday's Law, was utilized to establish a new mathematical model approach, which can simulate the porosity change of a hypothetical Fe<sup>0</sup>-PRB caused by iron corrosion products as induced by deionized water. The simulations demonstrate that volume-expansion by FeCPs alone can cause a great extent of porosity loss. The simulated porosity loss after 1 year of this study and reported porosity loss of previous studies are summarized in Table 5.1. As shown in the table, the predicted porosity loss in this study is greatly larger than the simulated results from former studies, which implies the underestimation of FeCPs in the previous studies, and suggests a careful evaluation of the iron corrosion process in future studies.

Table 5.1 Comparison of porosity loss values after 1 year simulation

Study	This study	Mayer et al. 2001	Yabusaki et al. 2001	Li et al. 2005	Li et al. 2006
Simulated porosity loss after 1 year (%)	12.3	0.7	2.56	0.65	1.2

#### 5.4 Importance of a three-dimensional model approach

The emphasis of previous model studies was mostly on the contaminant mass removal over time within the PRB, and the long-term effectiveness of PRBs was estimated with one-dimensional or two-dimensional models (Mayer et al., 2001; Yang et al., 2022). However, a one-dimensional or two-dimensional model is not sufficient to simulate the change of complex groundwater flow patterns within and around the barrier and the heterogeneous porosity

variation of the barrier medium over time. It is known that natural aquifers are heterogeneous, and that aquifer heterogeneity causes preferential groundwater flow pathways, which can result in heterogeneously distributed groundwater fluxes within the Fe<sup>0</sup>-PRB. As shown in Chapter 2, the Darcy flux has the highest positive correlation with the porosity loss. Therefore, although the barrier medium is homogeneous when installed, spatially heterogeneous secondary mineral precipitation can cause a varying reduction of porosity. An increasing heterogeneity in porosity of the barrier medium over time can influence the groundwater flow patterns, which in turn will cause by-passing flow around the PRB. In order to simulate the by-passing flow around or beneath the PRB, and to better estimate the long-term effectiveness of a Fe<sup>0</sup>-PRB, a three-dimensional model approach is necessary.

A 3-D groundwater flow and transport model is presented in Chapter 4. The model successfully simulated the redistribution of groundwater flow over time caused by the porosity heterogeneity of the barrier medium, and estimate the long-term performance of a continuous-wall Fe<sup>0</sup>-PRB. A 3-D high resolution aquifer outcrop analogue was adopted to set the hydraulic properties of the aquifer. The simulation results highlight the potential impact of the heterogeneity of groundwater distribution and porosity heterogeneity of barrier medium on the longevity estimation of a Fe<sup>0</sup>-PRB, and give practical implications for the future design.

## 5.5 Summary of achieved results

The following results were obtained from the literature review in Chapter 2:

- The general estimation methods for porosity loss of Fe<sup>0</sup>-PRBs, which are based on core sample studies and stoichiometric calculations, can significantly underestimate the actual porosity loss of Fe<sup>0</sup>-PRBs in the field, and lead to incorrect estimates of the longevity.
- The porosity loss values calculated by stoichiometric calculations are remarkably smaller than those estimated by solid phase studies on core samples. The possible reason is the improper assumption of the stoichiometric calculations, which considers only foreign precipitates or mixed precipitates contributing to the porosity loss in Fe<sup>0</sup>-PRBs. The important effect of iron corrosion products should be properly considered and investigated.
- The results of short-term column tests using high Darcy flux are difficult to be compared with those from field installations. In order to investigate the long-term porosity loss of Fe<sup>0</sup>-PRB systems, short-term column tests with accelerated Darcy flux should be avoided.
- The numerical modelling studies on Fe<sup>0</sup>-PRBs applied the same iron corrosion rate under different individual geochemical conditions. A small iron corrosion rate may cause a small simulated porosity loss compared to field Fe<sup>0</sup>-PRBs. The proper iron corrosion rate,

which can be used to simulate more accurately the long-term porosity loss of Fe<sup>0</sup>-PRBs, is yet to be determined.

- The in-situ Darcy flux has the highest correlation with the long-term porosity loss. Thus, in order to accurately estimate the long-term porosity loss of Fe<sup>0</sup>-PRBs, the Darcy flux within the barrier should be well-considered.

Then, comparing the experimental findings from literature to the simulation results of the newly established mathematical model (Chapter 3), the following results can be summarized:

- The derived iron corrosion rates in the presented model (2.60 mmol/(kg·d), 2.07 mmol/(kg·d) and 1.77 mmol/(kg·d)) are significantly larger than the corrosion rate used in previous studies (0.4 mmol/(kg·d)). Higher iron corrosion rate means more porosity loss caused by larger amount of generated iron corrosion products. Thus, the previous simulations with low iron corrosion rate may underestimate the porosity loss in a PRB. Moreover, a uniform unit of iron corrosion rate (e.g. mm/y) for Fe<sup>0</sup>-based PRB systems in order to improve the comparability of the different studies is proposed.
- The assumption in previous modeling studies, which describes the iron corrosion rate (in mmol/(kg·d)) as a first-order dependency on iron surface area, is accurate only when iron passivation is neglected. When iron passivation is considered, such an assumption underestimates the corrosion rates especially at the beginning phase of operation.
- The modelled porosity loss in this study (0.12/y with assumptions that the corrosion rate is a constant and goethite is the only corrosion product) is larger than the simulation results from previous studies (average 0.02/y). Our study demonstrates that iron corrosion products can cause a large porosity loss in the filter. Iron passivation features and the nature of the corrosion products are responsible for large differences between the simulation results. Therefore, iron corrosion processes and products need to be properly considered in order to accurately estimate the long-term operation of Fe<sup>0</sup>-based PRB systems.

The simulation results of the 3-D groundwater flow and transport model (Chapter 4) revealed the following:

- By-passing occurs instantly after beginning of the operation of the Fe<sup>0</sup>-PRB. If porosity heterogeneity of the barrier medium is not considered, 30%-41% of the by-passing flow rates are underestimated in a ten-years simulation. By-passing is a key concern threatening the long-term performance of a continuous-wall Fe<sup>0</sup>-PRB.
- For the transport of contaminants, the long-term contaminant plume migration is underrated if the porosity heterogeneity of the barrier medium is neglected.

- The residence time of groundwater within the Fe<sup>0</sup>-PRB increases over time. Obvious reduction of groundwater residence time is not observed in case studies.
- Installation of a pea gravel equalization zone can effectively improve the long-term performance of a continuous-wall Fe<sup>0</sup>-PRB by equalizing the groundwater flow into the PRB, reducing the heterogeneity of the barrier medium, and minimizing the by-passing flow that may exist during long-term operation. However, the pea gravel equalization zone results in a smaller residence time that could have a negative effect on long-term performance of a PRB.

## References

- Cao V., Bakari O., Kenmogne-Tchidjo J.F., Gatcha-Bandjun N., Ndé-Tchoupé A.I., Gwenzi W., Njau K.N., Noubactep C. (2022): Conceptualizing the Fe<sup>0</sup>/H<sub>2</sub>O system: A call for collaboration to mark the 30th anniversary of the Fe<sup>0</sup> PRB technology. *Water* (submitted water-1926410).
- Caré, S., Crane, R., Calabrò, P. S., Ghauch, A., Temgoua, E., & Noubactep, C. (2013). Modeling the permeability loss of metallic iron water filtration systems. *Clean–Soil, Air, Water*, 41(3): 275-282
- Caré, S., Nguyen, Q.T., l'Hostis, V., Berthaud, Y., 2008. Mechanical properties of the rust layer induced by impressed current method in reinforced mortar. *Cement and Concrete Research*, 38(8-9): 1079-1091
- Chaves, L.H.G., 2005. The role of green rust in the environment: a review. *Revista Brasileira de Engenharia Agrícola e Ambiental*, 9(2): 284-288
- Gillham R W, Vogan J, Gui L, Duchene M, Son J (2010). Iron barrier walls for chlorinated solvent remediation. In: Stroo H F, Ward C H, eds. *In Situ Remediation of Chlorinated Solvent Plumes*. New York: Springer, 537–571
- Gillham R.W. (2008): Development of the granular iron permeable reactive barrier technology (good science or good fortune). In "Advances in environmental geotechnics: proceedings of the International Symposium on Geoenvironmental Engineering in Hangzhou, China, September 8-10, 2007"; Y. Chen, X. Tang, L. Zhan (Eds); Springer Berlin/London, pp. 5–15.
- Guan, X. et al., 2015. The limitations of applying zero-valent iron technology in contaminants sequestration and the corresponding countermeasures: the development in zero-valent iron technology in the last two decades (1994–2014). *Water research*, 75: 224-248
- Hu R., Gwenzi W., Sipowo Hu R., Ndé-Tchoupé A.I., Cao V., Gwenzi W., Noubactep C. (2021): Metallic iron for environmental remediation: The fallacy of the electron efficiency concept. *Frontiers Environ. Chem.* 2, 677813.

- ITRC (Interstate Technology & Regulatory Council). 2011. Permeable Reactive Barrier: Technology Update. PRB-5. Washington, D.C.: Interstate Technology & Regulatory Council, PRB: Technology Update Team. [www.itrcweb.org](http://www.itrcweb.org) (access: 09.03.2012).
- Kang S.-H., Choi W. (2009): Response to Comment on “Oxidative Degradation of Organic Compounds Using Zero-Valent Iron in the Presence of Natural Organic Matter Serving as an Electron Shuttle”. *Environ. Sci. Technol.* 43 (10), 3966–3967.
- Khudenko B.M. (1985): Mechanism and kinetics of cementation processes. *Water Sci. Technol.* 17, 719–731.
- Khudenko B.M. (1987): Mathematical models of cementation process. *J. Environ. Eng.* 113, 681–702.
- Khudenko B.M. (1991): Feasibility evaluation of a novel method for destruction of organics. *Water Sci. Technol.* 23, 1873–1881.
- Kiilerich, O., Larsen, J.W., Nielsen, C., Deigaard, L., 2000. Field results from the use of a permeable reactive wall, pp. 377-384.
- Li, L., Benson, C.H., Lawson, E.M., 2005. Impact of mineral fouling on hydraulic behavior of permeable reactive barriers. *Groundwater*, 43(4): 582-596
- Li, L., Benson, C.H., Lawson, E.M., 2006. Modeling porosity reductions caused by mineral fouling in continuous-wall permeable reactive barriers. *Journal of Contaminant Hydrology*, 83(1-2): 89-121
- Mayer, K.U., Blowes, D.W., Frind, E.O., 2001. Reactive transport modeling of an in situ reactive barrier for the treatment of hexavalent chromium and trichloroethylene in groundwater. *Water Resources Research*, 37(12): 3091-3103
- McGeough K.L., Kalin R.M., Myles P. (2007): Carbon disulfide removal by zero valent iron. *Environ. Sci. Technol.* 41, 4607–4612.
- Miyajima K. (2012): Optimizing the design of metallic iron filters for water treatment. *Freiberg Online Geosci.* 32, 1–60.
- Miyajima K., Noubactep C. (2013): Impact of Fe<sup>0</sup> amendment on methylene blue discoloration by sand columns. *Chem. Eng. J.* 217, 310–319.
- Naidu R., Birke V. (2015): *Permeable Reactive Barrier: Sustainable Groundwater Remediation*. CRC Press, ISBN: 978-1-4822-2447-4., 333 pp.
- Noubactep C. (2007): Processes of contaminant removal in “Fe<sup>0</sup>-H<sub>2</sub>O” systems revisited. The importance of co-precipitation. *Open Environ. Sci.* 1, 9–13.
- Noubactep C. (2008): A critical review on the mechanism of contaminant removal in Fe<sup>0</sup>-H<sub>2</sub>O systems. *Environ. Technol.* 29, 909–920.

- Noubactep C. (2009): An analysis of the evolution of reactive species in Fe<sup>0</sup>/H<sub>2</sub>O systems. *J. Hazard. Mater.* 168, 1626–1631.
- Noubactep C. (2010): Metallic iron for safe drinking water worldwide. *Chem. Eng. J.* 165, 740–749.
- Noubactep C. (2011): Metallic iron for safe drinking water production. *Freiberg Online Geosci.* 27, 1–38.
- Noubactep C., Caré S. (2010a): Enhancing sustainability of household water filters by mixing metallic iron with porous materials. *Chem. Eng. J.* 162, 635–642.
- Noubactep C., Caré S. (2010b): Dimensioning metallic iron beds for efficient contaminant removal. *Chem. Eng. J.* 163, 454–460.
- Noubactep C., Temgoua E., Rahman M.A. (2012): Designing iron-amended biosand filters for decentralized safe drinking water provision. *CLEAN – Soil, Air, Water* 40, 798–807.
- Whitney W.R. (1903): The corrosion of iron. *J. Am. Chem. Soc.* 25, 4, 394–406.
- Wilkin R.T., Lee T.R., Sexton M.R., Acree S.D., Puls R.W., Blowes D.W., Kalinowski C., Tilton J.M., Woods L.L. (2019): Geochemical and isotope study of trichloroethene degradation in a zero-valent iron permeable reactive barrier: A twenty-two-year performance evaluation. *Environ. Sci. Technol.* 53, 296–306.
- Yabusaki, S., Cantrell, K., Sass, B., Steefel, C., 2001. Multicomponent reactive transport in an in situ zero-valent iron cell. *Environmental Science & Technology*, 35(7): 1493-1503
- Yang, H., Hu, R., Ruppert, H., Noubactep, C., 2021. Modeling porosity loss in Fe<sup>0</sup>-based permeable reactive barriers with Faraday's law. *Scientific Reports*, 11(1): 1-13.

## Chapter 6

### 6. General conclusions and outlook

This work presented a new 3-D numerical mode to simulate the long-term porosity loss of a Fe<sup>0</sup>-PRB, and the change of groundwater flow pattern due to the porosity variation of the barrier medium. A comprehensive literature review was conducted to obtain a profound understanding of the principle of porosity loss of Fe<sup>0</sup>-PRBs and the inherent characteristics of iron corrosion. A new mathematic model approach was also developed to properly simulate the porosity loss caused by iron corrosion products. Some general conclusions can be drawn in this study as follows:

- The current estimation methods for porosity loss of Fe<sup>0</sup>-PRBs, which are based on core sample studies and stoichiometric calculations, can significantly underestimate the actual porosity loss of Fe<sup>0</sup>-PRBs in the field, and lead to incorrect estimates of the longevity.
- The small iron corrosion rate applied in previous model studies may cause a small simulated porosity loss compared to field Fe<sup>0</sup>-PRBs. The proper iron corrosion rate, which can be used to accurately simulate the long-term porosity loss of Fe<sup>0</sup>-PRBs, is yet to be determined.
- Iron corrosion products (FeCPs) alone can cause large porosity loss in the Fe<sup>0</sup>-PRBs. Therefore, iron corrosion processes need to be properly considered to accurately estimate the long-term operation of Fe<sup>0</sup>-based PRB systems.
- The in-situ Darcy flux has the highest correlation with the long-term porosity loss. Thus, in order to accurately estimate the long-term porosity loss of Fe<sup>0</sup>-PRBs, the hydrogeological conditions of surrounding aquifers and the Darcy flux should be well-considered.
- The by-passing flow is greatly underestimated if porosity heterogeneity of the barrier medium is overlooked. Thus, the porosity heterogeneity of the barrier should be carefully considered when the longevity of a Fe<sup>0</sup>-PRB is estimated.

In addition, some potential topics are suggested for future research to properly predict the long-term porosity loss of a Fe<sup>0</sup>-PRB. The first challenge is developing a method to evaluate the actual porosity loss of a field Fe<sup>0</sup>-PRB. As analyzed in Chapter 2, the current evaluation methods consider inappropriate assumptions and underestimate the porosity loss in the field. Application of hydrogeological tests, e.g. multi-level tracer tests, may provide a more accurate result of porosity variation in the field. The second challenge is to determine a correct iron

corrosion rate for  $\text{Fe}^0$  applied in the PRBs. The iron corrosion rate has a vital influence on the porosity loss prediction. The minor value of iron corrosion rate applied in current model studies can cause significant underestimation of long-term porosity loss. The third challenge is to accurately determine the nature and amount of iron corrosion products. The type and composition of the iron corrosion products can be very complex and may change over time. A method that can quantitatively describe the amount of iron corrosion products under various conditions will be essential for the design of  $\text{Fe}^0$ -PRBs in the future.

## Publication List

List of all journal articles are authored or co-authored by me and related to the presented work (latest update: September 2022).

### Journals:

Hu, R., Yang, H., Tao, R., Cui, X., Xiao, M., Amoah, B. K., ... & Noubactep, C. (2020). Metallic iron for environmental remediation: Starting an overdue progress in knowledge. *Water*, 12(3), 641.

Yang, H., Hu, R., Ndé-Tchoupé, A. I., Gwenzi, W., Ruppert, H., & Noubactep, C. (2020). Designing the next generation of Fe<sup>0</sup>-based filters for decentralized safe drinking water treatment: A conceptual framework. *Processes*, 8(6), 745.

Cao, V., Yang, H., Ndé-Tchoupé, A. I., Hu, R., Gwenzi, W., & Noubactep, C. (2020). Tracing the scientific history of Fe<sup>0</sup>-based environmental remediation prior to the advent of permeable reactive barriers. *Processes*, 8(8), 977.

Yang, H., Hu, R., Ruppert, H., & Noubactep, C. (2021). Modeling porosity loss in Fe<sup>0</sup>-based permeable reactive barriers with Faraday's law. *Scientific Reports*, 11(1), 1-13

Yang, H., Liu, Q., Hu, R., Ptak, T., Taherdangkoo, R., Liu, Y., & Noubactep, C. (2022). Numerical case studies on long-term effectiveness of metallic iron based permeable reactive barriers: Importance of porosity heterogeneity of the barrier. *Journal of Hydrology*, 612, 128148.

Konadu-Amoah, B., Hu, R., Cao, V., Tao, R., Yang, H., Ndé-Tchoupé, A. I., ... & Noubactep, C. (2022). Realizing the potential of metallic iron for the mitigation of toxics: flee or adapt?. *Applied Water Science*, 12(9), 1-11.

### In preparation for submission to journal

Yang, H., Tao, R., Liu, Q., Hu, R., Taherdangkoo, R., Liu, Y., Ruppert, H., & Noubactep, C. Porosity loss in iron-based permeable reactive barriers: a review